UNIVERSIDADE NOVA DE LISBOA

Universidade Nova de Lisboa

Instituto de Higiene e Medicina Tropical

CHARACTERIZATION OF *CLOSTRIDIOIDES DIFFICILE* BIOFILM MATRIX PROTEINS

Isabel Contreiras da Silva Roseiro

A THESIS SUBMITTED FOR THE DEGREE OF MASTER IN MEDICAL MICROBIOLOGY

SEPTEMBER, 2022

INSTITUTO DE HIGIENE E MEDICINA TROPICAL
DESDE 1902

itqb nova

NOVA SCHOOL OF SCIENCE & TECHNOLOGY

NOVA MEDICAL SCHOOL

Universidade Nova de Lisboa

Instituto de Higiene e Medicina Tropical

CHARACTERIZATION OF *CLOSTRIDIOIDES DIFFICILE* BIOFILM MATRIX PROTEINS

Author: Isabel Contreiras da Silva Roseiro

Supervisor: Dr. Mónica Serrano

Co-supervisor: Prof. Dr. Adriano O. Henriques

A thesis submitted to fulfill the requirements for completing the degree of Master in Medical Microbiology

This work was supported by the FCT (Fundação para a Ciência e a Tecnologia) through the award PTDC/BIA-MIC/29293/2017.

INSTITUTO DE HIGIENE E
MEDICINA TROPICAL
DESDE 1902

Acknowledgments

First, I would like to thank the Scientific Committee of the MSc in Medical Microbiology of Universiade Nova de Lisboa for the organization and planning of this master's course and to Instituto de Tecnologia Química e Biológica António Xavier for receiving me as a master student.

I would like to thank Prof. Dr. Adriano O. Henriques, my co-supervisor, for welcoming me into his laboratory and for his continuous help and support throughout this year. His enthusiasm for science during our master classes sparked my interest about spore-formers and it was a privilege to have shared his scientific knowledge during this year.

To my supervisor Dr. Mónica Serrano, I thank her for being a mentor in the true sense of the word. Ever since her first class on biofilms, I knew I had to take this project but I wasn't aware of how lucky I was to have her as my supervisor. I am deeply grateful for her guidance, patience and for her incessant availability and support. I thank her for always encouraging me and teaching me to have a positive attitude in life and for all the conversations and unique sense of humor.

I would like to thank Major Wilson Antunes from Laboratório de Bromatologia e Defesa Biológica do Exército of Centro de Investigação da Academia Militar, for the scanning electron microscopy images. I would also like to thank Dr. Américo Duarte from Bacterial Energy Metabolism Lab of ITQB-NOVA for teaching me how to perform clear-native-PAGE gels.

A special thanks to Mónica Louro, for being my "Mike" and helping me to take my first steps in the lab. I thank her for sharing with me her passion for science and for all the advice and suggestions throughout this work. To Diogo Martins, for being my other tutor and my lab partner. Every practical technique I learned throughout this work had in someway his help and he was my right-arm, and sometimes my left too, during this year. For our downstair breaks and all our brainstorm scientific moments and most importantly, for your friendship. To all my MDL colleagues, Constança Neves for being my lab sister and the "head-ache" I never thought I needed, Carmen Olivença, for her contagious energy, positivity and her friendship, Khira Amara for her kindness and encouragement and Filipa Teixeira, for always having a good word and constant availability to help. To Teresa Silva for teaching me how to prepare the solutions and for all the help in routinary tasks.

To all my friends, that encouraged me during this year and without whom this would be impossible. I must thank in particular the people who had the patience to deal with me, almost every day, in the good and bad moments. To, Filipa Esteves Dias, for her friendship and support. To Francisco Henriques, for his patience and for making me laugh during this year. A special thanks to Filipa Henriques, my best-friend, for being my biggest support through these years and for being there every step of the way.

For last, and most importantly, I would like to thank my family. To my dad, Luís Roseiro and my brother, Duarte Roseiro, for all the encouraging words and endless support, even without fully understanding what I was doing during this year. For always believing in me and giving me the freedom to pursue what I love. I hope I can make you (three) feel proud.

This work was supported by the FCT (Fundação para a Ciência e a Tecnologia) through the award PTDC/BIA-MIC/29293/2017.

Resumo

Clostridioides difficile é um importante agente patogénico, atualmente reconhecido como uma das principais causas de infeção nosocomial associada ao uso de antibióticos. No entanto, o aumento das infeções na comunidade e a possibilidade de transmissão zoonótica têm sido uma crescente fonte de preocupação. Cerca de 25% das infeções causadas por *C. difficile* originam episódios de recorrência. *C. difficile* é estritamente anaeróbico e capaz de diferenciar esporos. *C. difficile* forma ainda biofilmes, onde são também formados esporos. Tanto os biofilmes como os esporos conferem resistência aos antibióticos e ao sistema imunitário do hospedeiro. Esta combinação torna difícil a eliminação da bactéria. A matriz extracelular é uma componente crucial do biofilme, sendo geralmente composta por exopolissacarídeos, DNA extracelular e proteínas. A composição da matriz do biofilme em *C. difficile*, bem como os mecanismos subjacentes à sua formação ainda não são totalmente conhecidos.

Com o objetivo de caracterizar as proteínas da matriz do biofilme, foi identificada uma estirpe clínica que apresenta uma forte produção de biofilme, 1800 (RT126). Em comparação com a estirpe de referência, a estirpe 1800 apresentou uma maior taxa de crescimento e eficiência de esporulação, mas a mesma eficiência de germinação. Os esporos da estirpe 1800 apresentam um exósporo espesso, irregular e do qual emanam projecções de aparência fibrilar, em contraste com o manto e exósporo mais fino e uniforme da estirpe de referência. As proteínas da matriz do biofilme foram extraídas e a sua identificação por espectrometria de massa revelou serem maioritariamente enzimas citoplasmáticas. O presente trabalho focou-se no papel da desidrogenase do glutamato (GDH) e da enolase, duas proteínas *moonlight*. Foi anteriormente demonstrado que a presença da GDH extracelular é importante para a colonização por *C. difficile* e para a progressão da doença. Com o objetivo de compreender o papel da GDH no biofilme de *C. difficile,* procedeu-se à eliminação do gene *gluD*, codificante para a GDH. A mutação afetou drasticamente a produção de biofilme e a análise por microscopia de varrimento revelou um forte decréscimo na densidade da matriz, e na quantidade e dimensões das fibras que normalmente ligam as células.

Demonstrou-se que a GDH purificada é maioritariamente hexamérica, sendo ainda visíveis formas de ordem superior, todas cataliticamente ativas. Surpreendentemente, as mesmas formas de GDH acumulam na matriz, mas são largamente desprovidas de atividade. A complementação extracelular com a forma selvagem ou a forma cataliticamente inativa da GDH restaurou a capacidade de formação de biofilme ao mutante. Com o objetivo de entender o papel da enolase no biofilme, e uma vez que o gene codificante, *eno*, é essencial, foi construído um mutante condicional usando o sistema CRISPRi. Este é, tanto quanto sabemos, o primeiro mutante para a enolase descrito em *C. difficile*.

Globalmente, descobriu-se que a GDH possui um papel central na formação do biofilme de *C. difficile* e sugere-se que em vez de possuir um conjunto dedicado de proteínas da matriz, este organismo reutiliza proteínas citoplasmáticas que desempenham funções *moonlight* na matriz extracelular do biofilme.

Palavras-chave: *Clostridioides difficile*, Biofilme, Proteínas *moonlight*, Desidrogenase do glutamato, Enolase

Abstract

Clostridioides difficile is now recognized as a leading cause of nosocomial infections linked to antibiotic therapy. While historically connected to health-care settings, the rise in community-acquired *C. difficile* infections (CDI) and the possibility of zoonotic transmission are an increasing concern. About 25% of CDI infections lead to disease recurrence. This organism perseveres in the intestine as biofilms, spores or biofilm-associated spores. The convergence of antibiotic- and immune system resistant biofilms and spores poses a serious threat. The extracellular matrix, a central part of the biofilm, is generally composed of exopolysaccharides, extracellular DNA and proteins. The matrix composition of *C. difficile* biofilms as well as the mechanisms underlying its formation, are still poorly understood.

We selected a strong-biofilm producer, strain 1800 (of ribotype 126), to characterize the biofilm-matrix proteins. In comparison to the reference laboratory strain 630Δ*erm*, strain 1800 presented a higher growth rate and sporulation efficiency, while germination efficiencies were similar in both strains. Spores from strain 1800 present a thicker and irregular exosporium with hair-like projections, contrasting with the thinner coat and exosporium in the reference strain. The biofilm-matrix proteins were extracted and identified by mass spectrometry. The majority of these proteins were found to be cytoplasmic enzymes Here, we focused on the role of NAD-specific glutamate dehydrogenase (GDH) and enolase, two known moonlight proteins. Extracellular GDH was previously shown to have a role in promoting *C. difficile* colonization and disease progression. In order to understand the role of GDH in *C. difficile* biofilms, we constructed an in-frame deletion mutant of *gluD*, coding for GDH. Deletion of *gluD* drastically impaired biofilm formation and scanning electron microscopy analysis revealed a strong decrease in the matrix density and in the dimension and quantity of fibers interconnecting cells.

We demonstrated that purified GDH forms an hexamer but also assembles into higher order species, all of which are enzymatically active. Strikingly, the same forms of GDH accumulate in the biofilm-matrix but are mostly inactive. Extracellular complementation with the wild-type or a catalytic inactive form of GDH restored the wild-type biofilm ability to the *gluD* mutant. To begin studying the role of enolase in biofilms and since its encoding gene, *eno*, is essential, we constructed a conditional mutant using CRISPRi silencing. This is, to our knowledge, the first *eno* mutant described for *C. difficile.*

Overall, we discovered an important role for GDH in *C. difficile* biofilms and we suggest that instead of producing a set proteins with that specific purpose, this organism uses cytoplasmic moonlight proteins to form the extracellular matrix of biofilms.

Key-words: *Clostridioides difficile*, Biofilm, Moonlight proteins, Glutamate dehydrogenase, Enolase

Table of contents

Page

List of figures

Symbols and abbreviations

%	percentage
g	acceleration of gravity
g	gram
h	hour
h^{-1}	growth rate unit
kDa	kilodalton
L	litre
lb/in^2	pound-force per square inch M Molar
mA	milliampere
min	minute
mg	milligram
mL	millilitre
mM	micromolar
ms	millisecond
nm	nanometre
^oC	degree Celsius
V	volt
v/v	volume per volume
w/v	weight per volume
Δ	deletion
µL	microlitre
µm	micrometre
ACE	Allele-Coupled Exchange
BHI	Brain-heart infusion
BHISG-DOC	Brain-heart infusion supplemented with L-cystein hydrochloride, glucose and deoxycholate
CA	Cholate
CA-CDI	Community-Acquired CDI
CDC	Centers for Disease Control and Prevention
CDCA	Chenodyoxycholate
CDI	*Clostridioides difficile* infection
c-di-GMP	Cyclic diguanylate
CDMM	*C. difficile* minimal mediun
CDT	*C. difficile* transferase
CdtLoc	CDT locus
CFU	Colony-forming unit
CRISPRi	CRISPR interference
CV	Crystal-violet
DDM	n-dodecyl-β-D-maltoside
DOC	Deoxycholate
DTT	Dithiothreitol
eDNA	Extracellular DNA
EIA	Immunoassays
EPSs	Exopolysaccharide

ESCMID	European Society of Clinical Microbiology and Infectious Diseases
FMT	Faecal microbiota transplantation
FOA	5-fluorootic acid
GADPH	Glyceraldehyde-3-phosphate dehydrogenase
GDH	Glutamate dehydrogenase
HA-CDI	Hospital-Acquired CDI
HMW-SLP	High molecular weight S-layer protein
ICSP	International Committee on Systematics of Procaryotes
IDSA	Infectious Diseases Society of America
SHEA	Society for Healthcare Epidemiology of America
LMW-SLP	Low molecular weight S-layer protein
LB	Luria-Bertani medium
MRSA	Methicillin-resistant *Staphylococcus aureus*
ORF	Open reading frame
PaLoc	Pathogenicity locus
PBS	Phosphate-buffered saline solution
PBS-T	PBS- Tween
PCR	Polymerase chain reaction
PMC	Pseudomembranous colitis
PMSF	Phenylmethylsulfonyl fluoride
PVDF	Polyvinyldiene difluoride
SEM	Scanning electron microscopy
SDS	Sodium dodecyl sulphate
SDS-PAGE	Sodium dodecyl sulphate-polyacrylamide gel electrophoresis
TA	Sodium taurocholate
TEM	Transmission Electron Microscopy
TEMED	Tetramethylethylenediamine
TLR	Toll-like receptors

1. Introduction

1.1 *Clostridioides difficile*

Clostridioides difficile (formerly known as *Clostridium difficile*) is a Gram-positive, strict anaerobic organism, able to produce endospores; it produces toxins and biofilm and is able to colonize and proliferate in the intestinal tract of humans and animals (Martin, Monaghan and Wilcox, 2016).

C. difficile was initially isolated from the stool of healthy newborns in 1935 by Hall and O'Toole. Initially, it was named *Bacillus difficilis,* due to the difficulty of its isolation and growth (Hall and O'Toole, 1935). At that time, researchers found that it could induce disease in animals, probably through the production of a secreted toxin, but it wasn't until the late 1970s that the organism was discovered to be related to human disease. In 1978, *C. difficile* was associated for the first time with pseudomembranous colitis (PMC) and with previous antibiotic therapy (Larson, Prince and Borriello, 1978; Rodriguez *et al.*, 2016). During the 2000s there was a substantial increase in severe cases of *Clostridioides difficile* infection (CDI) in Canada, USA, and Europe, mainly driven by the emergence of hypervirulent strains with high-transmission rates that became responsible for worldwide outbreaks (Martin, Monaghan and Wilcox, 2016).

Technological advances in molecular biology revealed through a new 16s rDNA analysis that *C. difficile* was closely related to organism belonging to the *Peptostreptococcaceae* family leading to is classification as as *Peptoclostridium difficile* (Yutin and Galperin, 2013). However, this genus name was rejected since it did not follow the Bacteriological Code defined by the International Committee on Systematics of Prokaryotes (ICSP) and the International Code of Nomenclature of Bacteria. Furthermore, the proposed change would lead to inevitable confusion in the clinical setting and would certainly have a negative impact on patient care. In 2016, Lawson *et al.* proposed the name *Clostridioides difficile,* in order to maintain the "C" in the genus name so that common terms such as "C. diff" and CDI would be conserved and the organism was included in the family *Peptostreptococcaceae* (Lawson *et al.*, 2016).

CDI is an intestinal disease mediated by two main toxins which can result in mild diarrhea or, in more severe cases, pseudomembranous colitis, toxic megacolon, or death (Rupnik, Wilcox and Gerding, 2009). Previous exposure to antibiotics is still the main risk factor for the development of CDI, with other important risk factors being older age and hospitalization (Ananthakrishnan, 2011; Czepiel *et al.*, 2019). Disease development and CDI severity are dependent on both strain characteristics and the patient's immune response. Although hospital-acquired CDI (HA-CDI) has historically been the most relevant form of CDI, the incidence of community-acquired CDI (CA-CDI) has increased in the past decade. In recent years, advances in molecular typing methods have shed light on the wide diversity of sources and routes of transmission for *C. difficile*, including environmental reservoirs, animals, food, undiagnosed symptomatic cases, and asymptomatic carriers (Martin, Monaghan and Wilcox, 2016; Lim, Knight and Riley, 2020).

C. difficile is now recognized as the most important cause of infections in healthcare settings linked to antibiotic therapy, but the rise of CA-CDI and zoonotic transmission also increasing (Smits *et al.*, 2016). CDI imposes a huge economic burden on healthcare systems with costs estimated to be 796$ million in USA and €300 million in Europe, per year (Finn, Andersson and Madin-Warburton, 2021). Hospitalization, treatment of secondary complications including surgery, prolonged length of stay, and intensive care unit care are contributing factors to the high economic burden (Gupta and Ananthakrishnan, 2021). Adding to this burden is the challenge of recurrent CDI (rCDI), with rates estimated to be at 15-35% considering all CDI episodes. Recurrence results in significant morbidity and increased healthcare costs, becoming a concerning health issue (Singh *et al.*, 2019). A recurrent episode is defined as "a relapse of CDI symptoms within 2-8 weeks of successful treatment of the initial episode" (Singh *et al.*, 2019). Recent studies suggest that 25% of the patients will experience these recurrent episodes, an in at least 30% of those, more than once (Finn, Andersson and Madin-Warburton, 2021).

1.1.1 Epidemiology of CDI

Currently, CDI incidence rate ranges from 1-1-631.8 per 100,000 population per year globally (Finn, Andersson and Madin-Warburton, 2021). Besides the considerable incidence of initial CDI episodes, recurrence imposes a substantial challenge

During the last decade was observed a general decrease of CDI in both USA and Europe. This decrease is likely due to the success of the implemented measures to fight *C. difficile* in the healthcare centers (Gupta and Ananthakrishnan, 2021; Kelly *et al.*, 2021). In contrast, the rise of CDI cases occurring in patients outside the hospital setting has increased and is now a matter of global concern. CA-CDI is defined as a symptomatic case in the community if no admission to a health-care facility 12 weeks prior to diagnosis is verified (Martin, Monaghan and Wilcox, 2016; Thornton *et al.*, 2018). Community-acquired cases now account for 35%-48% of all CDI cases (Kelly *et al.*, 2021). This is becoming particularly concerning not only due to the rise of cases but also for the risk groups that change in comparison to the HA-CDI. CA-CDI has been reported in younger and healthier patients without exposure to healthcare settings, groups that were previously thought to be at low risk (Rupnik, Wilcox and Gerding, 2009; Kelly *et al.*, 2021).

Between 2001 and 2012 there was an increase in CDI cases raising concern within the healthcare community (Kelly *et al.*, 2021; Nazareth *et al.*, 2022). This increase is partially explained by the emergence of epidemic strains of ribotype 027 (RT027), often termed hypervirulent. PCR ribotyping is one of the most used typing methods for C. difficile. This technique discriminates strains based on differences in the target spacer regions between the 16S and 23S ribosomal RNA (Rupnik, Wilcox and Gerding, 2009). Strain RT027 was characterized by having increased pathogenicity, leading to high rates of transmission rates, more severe disease and higher mortality rates. These strains were responsible for large epidemic outbreaks around the world, as seen in Quebec and Canada between 2003-2007 (Valiente, Cairns and Wren, 2014). Genotyping methods revealed that a similar strain responsible for the Canada and Quebec outbreaks, had also been isolated in several regions of the USA and by 2007 it had also reached European countries. In 2008, RT027 reached the Asian continent and by 2009 it was reported in Australia. (Valiente, Cairns and Wren, 2014; Kelly *et al.*, 2021). The prevalence of

RT027 has been decreasing in the last years, particularly in Europe, but concomitantly with the expansion of other ribotypes (Nazareth *et al.*, 2022).

C. difficile strains of ribotype 078 has been in the spotlight in the last years, emerging as a significant epidemic RT with a mortality rate similar to RT027 (Zhang *et al.*, 2019). While RT027 is common among HA-CDI, RT078 has a higher prevalence in younger patients and is more associated with community-associated cases. It has been suggested that the reason why RT027 and 078 have become successful epidemic strains, relies on their ability to utilize low concentrations of the sugar trehalose. This type of sugar has been increasingly used in the food industry and the enhanced ability to utilize trehalose, may have provided a selective advantage for these strains (Roxas *et al.*, 2020). The antibiotic resistance profile is also important in the epidemic spread of these ribotypes. Strains from RT027 and RT078 were found to be highly resistant to fluoroquinolones and the emergence of these strains can be related to the high prescription rate of these antibiotics in certain countries (Martin, Monaghan and Wilcox, 2016).

Ribotype 078 strains are predominant in farm animal. Similar strains are found in colonized farm workers and patients suggesting possible zoonotic transmission. (Squire and Riley, 2012; Smits *et al.*, 2016; Krutova *et al.*, 2018). A study developed in Cleveland, USA demonstrated that more than 25% of hospital-associated CDI cases were in patients that were already colonized at the time of admissions (Gonzalez-Orta *et al.*, 2019). This suggests the origin of infection not to be truly in the hospital; instead there might be an ongoing transmission in the community. Important community reservoirs include food animals, retail food and the environment. While the relevance of foodborn transmission is unclear, common ribotypes found in these reservoirs are of RT078, 014, 126, 127, and 033 (Lim, Knight and Riley, 2020).

In Portugal, the prevalence of RT027 was found to be 18.5% among HA-CDI and CA-CDI isolates identified between 2010 and 2015 (Nazareth *et al.*, 2022). A nation surveillance study in 2016 reported RT027 as the most frequent ribotype overall and among HA-CDI, while RT014 was the most commonly associated to CA-CDI. Since the ribotypes associated with HA- and CA-CDI largely overlap, other routes of transmission seem likely, including zoonotic transmission. Overall, Portugal presents a heterogeneity

of ribotypes although the high frequency of hypervirulent ribotypes 078, 027, and 126 raises concern (Santos *et al.*, 2016).

1.1.2 Diagnosis and treatment

Effective prevention, first, then treatment of *C. difficile* infection relies heavily on an accurate and prompt diagnosis. *C. difficile* diagnosis is generally applied in hospitalized patients with diarrhea (≥ 3 unformed stools per 24h) or that test negative for enteropathogens and in whom other causes of diarrhea have been ruled out (Guery, Galperine and Barbut, 2019). The classical diagnosis methods for CDI target either the presence of *C. difficile*, the presence of free toxins in stools or the presence of toxigenic *C. difficile* (Gateau *et al.*, 2018). ESCMID recommends a two-step algorithm for *C. difficile* diagnosis. This algorithm includes a test for the presence of *C. difficile* followed by an assay for the detection of free toxins in stool samples (Smits *et al.*, 2016; Guery, Galperine and Barbut, 2019).

Immunoassays (EIA) are currently the most used tests for diagnostic since they have a low cost, provide rapid results, and are easy to perform. EIA can be used to detect toxins or glutamate dehyrogenase (Rodriguez *et al.*, 2016). The glutamate dehyrogenase assay is based on the detection of this metabolic enzyme which is produced in high amounts by all strains of *C. difficile*. The high sensitivity and predictive value presented by this method explains why it is now used most often as an initial step of the *C. difficile* diagnosis algorithm. However, it must be taken into account that this method identifies all *C. difficile* strains which indicate colonization rather than disease. This test is often complemented by an EIA for the TcdA and TcdB toxins.

Samples culturing is recognized as the most sensitive detection method for *C. difficile* detetion. However, application in the clinical practice diagnosis is difficult and has a slow turn-around time. Nonetheless, stool culture is still important since it allows strain typing and antibiotic susceptibility determination which provide important epidemiological data (Rodriguez *et al.*, 2016). A cytotoxicity assay is the gold standard for the identification of toxin-producing strains. This method is based on the observation of a cytopathic effect after inoculation of a stool filtrate on a cell culture followed by a confirmation using a toxin B antibody. The primary limitations of this method still are a

lack of standardization, a slow turn-around time, and the fact that it requires well-trained personnel (Guery, Galperine and Barbut, 2019; Kelly *et al.*, 2021). Nucleic acid amplification assays are based on real-time PCR, loop isothermal amplification, or microarray technology. Although these methods have shown to be highly sensitive, they may not be accessible in all situations. Moreover, amplification of the toxin-encoding genes does not necessary confirm that toxins are being produced, which can lead to overdiagnosis of CDI (Gateau *et al*., 2018; Guery, Galperine and Barbut, 2019).

The current standard antibiotics recommended for CDI treatment are metronidazole, vancomycin, and fidaxomicin (Smits *et al.*, 2016). Metronidazole and vancomycin were the first antibiotics used for *C. difficile* treatment; they have, however, a wide-spectrum, cause an impact on the microbiota and are related with high recurrence rates (Guery, Galperine and Barbut, 2019). Fidaxomicin came as an alternative narrow-spectrum antibiotic, highly selective against *C. difficile,* and showing lower recurrence rates (Isidro *et al.*, 2017). Fidaxomicin is able to inhibit spore outgrowth and to prevent entry into sporulation, which explains its success in treatment and performance in preventing recurrence. Vancomycin and fidaxomicin appear to be more effective in comparison to metronidazole which is the reason why the recent IDSA/SHEA guidelines recommend the use of fidaxomicin or vancomycin in mild cases and first occurrence cases of CDI (Johnson *et al.*, 2021). Besides antimicrobial therapy, bacteriotherapies are also valid options for CDI treatment. Fecal transplant microbiota (FMT) has been demonstrated to be one of the most successful CDI treatments (Baktash *et al.*, 2018). This procedure essentially involves the transfer of fecal material from healthy donors to patients, which gives rise to gut microbiota reconstitution and consequent inhibition of *C. difficile* growth; this can be of particular importance in patients with multiple recurrence episodes (Zhu, Sorg and Sun, 2018). However, reproducibility of FMT is often a problem, as is access to the material the patient acquiescence (Isidro *et al.*, 2017).

1.1.3 *C. difficile* life cycle

Transmission of *C. difficile* occurs via the oral-faecal route. Endospore (hereinafter spore for simplicity) formation plays a crucial role in *C. difficile* infection, as spores are the main vehicle of transmission for this obligate anaerobic organism, unlike

to survive in the environment (Smits *et al.*, 2016). Spores are a highly resistant cell type capable of resisting to extreme environmental conditions, to persist in the environment for long periods of time, and to resist to commonly used disinfectants and most antimicrobials. In the healthcare settings, transient hand carriage by healthcare workers and patients are important sources of environmental contamination, facilitating transmission of *C. difficile* (Fawley *et al.*, 2007).

Ingested spores survive the gastric barrier and reach the small intestine where they may complete germination in contact with the surface of epithelial cells (**Figure 1A**) (Isidro *et al.*, 2017). Bile salts play a significant role in the induction of spore germination, and this explains, in part, the importance of the host microbiota and its associated metabolome in CDI (Sorg and Sonenshein, 2008; Smits *et al.*, 2016). Primary bile salts, as cholate (CA) and chenodeoxycholic acid (CDCA), are produced in the liver from cholesterol and released into the small intestine to assist in digestion. After food intake, primary bile salts are secreted into the duodenum where 95% are reabsorbed. The remaining non-reabsorbed are passed into the colon where they undergo 7α-dehydroxylation by intestinal bacteria, transforming them into secondary bile acids, deoxycholic acid (DOC) and lithoic acid (Sorg and Sonenshein, 2008; Czepiel *et al.*, 2019). *Clostridium scindens*, is one of gut microbiota species that actively transports cholate and chenodeoxycholic acid into the cytosol and metabolizes them into deoxycholate and lithocolate (Sorg and Sonenshein, 2008). It was previously demonstrated that bile salts such as taurocholate, cholate and DOC stimulate germination while others such chenodeoxycholate inhibit germination (Wilson, Sheagren and Freter, 1985; Sorg and Sonenshein, 2008). Gut microbiota-derived secondary bile salts, such as DOC, inhibit vegetative growth (Sorg and Sonenshein, 2010; Paredes-Sabja, Shen and Sorg, 2014; Shen, 2015). Moreover, while the concentration of primary bile acid was higher in patients with recurrent CDI, the concentration of secondary bile acids was higher in the fecal content of healthy people (Allegretti *et al.*, 2016).

Following antibiotic exposure, gut dysbiosis leads to a decrease in the bacteria that converts primary to secondary bile acids. The depletion of secondary bile salts and other sub-products of bacterial metabolism, as well as the reduced bacterial competition for nutrients, results in the establishment of a *C. difficile* population and subsequently,

infection (Baktash *et al.*, 2018). Germination is completed in the anaerobic cecum and colon. The resulting vegetative cells adhere to the intestinal epithelium and will start growing and colonizing the cecum and the colon (Sorg and Sonenshein, 2008). Recently, it has been shown that *C. difficile* is capable of forming biofilms within which the production of toxins and spores takes place (Semenyuk *et al.*, 2014).

The clinical symptoms characteristic of CDI are mainly caused by the action of proinflammatory cytotoxins TcdA and TcdB. The secretion and then the receptor-mediated endocytosis of these toxins results in gross alterations in the cytoskeleton of epithelial cells, the disruption of tight junctions and loss of cell integrity (Kuehne *et al.*, 2010). The damaged colonic mucosa leads to diarrhea episodes, shedding spores to the environment and thus completing the cycle (Abt, McKenney and Pamer, 2016; Czepiel *et al.*, 2019). Nonetheless, disease recurrence is most likely linked to the ability of spores to endure in the host or in its close environment (Deakin *et al.,* 2012).

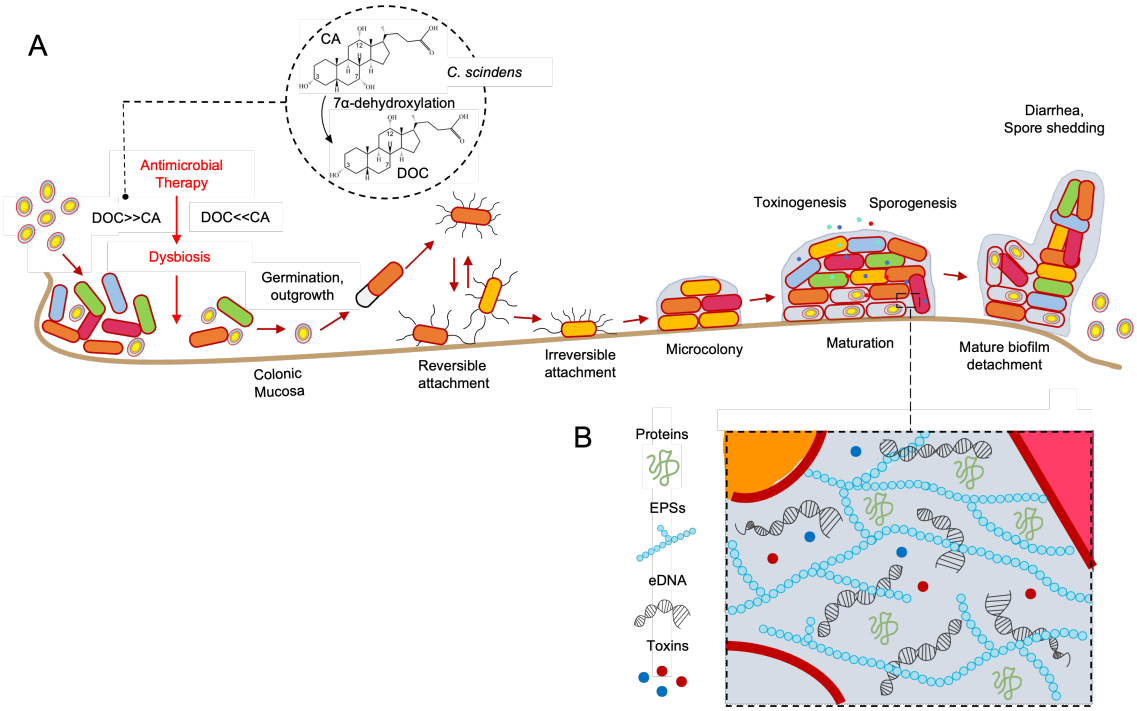

Figure 1. Schematic representation of the *C. difficile* infectious cycle. A) At the onset of infection, spores are ingested. These spores survive the gastric barrier and germinate in the intestine in response to primary bile salts. Antibiotic-triggered dysbiosis compromise the representation of commensal species, such as *C. scindens*, that convert primary bile salts such as cholate (CA) into secondary bile salts such as deoxycholate (DOC). Primary bile salts stimulate germination and outgrowth, whereas secondary bile salts inhibit vegetative growth. Upon dysbiosis, the ratio of CA/DOC increases thus stimulating spore germination and outgrowth. Vegetative cells will grow and establish a population of flagellated cells. The formation of a flagellum enhances cell motility and adherence to the gut mucosa. Adhesion of cells to a surface is the first step in biofilm formation. At first, this attachment can be reversible depending

on the environment conditions, but production of an extracellular matrix results in an irreversible attachment and subsequent microcolony formation. A mature biofilm contains subpopulations of cells with different functions (represented by different colors) such as sporulating cells. At last, cell death within the biofilm and physical disruption leads to dispersion of the biofilm, releasing single cells or spores. **B)** Within the biofilm, cells are encased in a matrix formed by proteins, exopolysaccharides (EPS) and eDNA. Inside these structures cells can initiate toxinogenesis and sporogenesis. Production of toxins will cause severe damage of the epithelium, leading to diarrhea episodes. Spores are then shed to the environment allowing infection of new hosts, completing the cycle. Adapted from Isidro *et al.,* 2017.

1.1.4 Virulence factors

When the host gut microbiota is unbalanced, *C. difficile* proliferates and colonizes the large intestine. However, not all patients will develop symptoms of CDI. Disease-causing ability depends not only on the host immune response but also on the expression of virulence factors which include the production of toxins, spores, flagella, cell-surface associated proteins and biofilm formation.

Toxin production

Toxin TcdA and TcdB are the main factors responsible for the pathogenic behavior of *C. difficile*. The *tcdA* gene, coding for TcdA and the *tcdB* gene, coding for TcdB, are both found in a pathogenicity locus known as PaLoc for short (Aktories, Schwan and Jank, 2017). Four other genes, *tcdR*, *tcdE, tcdL* and *tcdC* are also part of the PaLoc; TcdR codes for an alternative sigma factor that allows RNA polymerase to utilize promotors in the *tcdA*, *tcdB* and *tcdR* regulatory regions (Abt, McKenney and Pamer, 2016). TcdC was thought to be an anti-sigma factor responsible for modulating transcription of *tcdA* and *tcdB* by impairing binding of TcdR to RNA polymerase (Matamouros, England and Dupuy, 2007; Awad *et al.*, 2015). However, the function and relevance of TcdC in toxin production remains unclear (Hunt and Ballard, 2013; Janoir, 2016; Paiva *et al.*, 2020). TcdE shows features of a holin, and together with TcdL (a non-catalytic fragment of a peptidoglycan endolysin), might be involved in the export of TcdA and TcdB from the cell (Govind and Dupuy, 2012; Olling *et al.*, 2012; Mehner-Breitfeld *et al.*, 2018). The PaLoc can be mobilized from toxigenic to non-toxigenic strain (Mullany, Allan and Roberts, 2015) suggesting that the latter strains may become toxin producers through horizontal gene transfer (Brouwer *et al.*, 2013).

The toxins are released into the cell´s cytosol following internalized through receptor-mediated endocytosis; their N-terminal domain has glycosyltransferase activity

through which small GTP-binding proteins such as Rho, Rac and Cdc42, are inactivated (Awad *et al.*, 2015; Isidro *et al.*, 2017). Inactivation of Rho family GTPases affects various cellular pathways, resulting in loss of structural integrity and ultimately cellular apoptosis. The primary target of TcdA is the intestinal epithelium; TcdB, in turn, shows a broader specificity (Rodriguez *et al.*, 2016). Loss of epithelial integrity results from colonocyte death and the concurrent disassociation of tight junctions between intestinal cells (Awad *et al.*, 2015; Abt, McKenney and Pamer, 2016). Together, these effects increase intestinal permeability and fluid accumulation, which later manifests as diarrhea, the hallmark symptom of CDI. Additionally, TcdA and TcdB are known to activate the inflammasome and TLR-signaling pathways, resulting in an exacerbated inflammatory response that is likely to exarcebate host tissue damage. Sequence diversity within the *tcdA* and *tcdB* genes produces different toxin variants that may contribute to heterogeneity in virulence among strains (Abt, McKenney and Pamer, 2016). For instance, TcdB variants present in strains of RT027 could cause more severe tissue damage (Lanis *et al.*, 2013).

In addition to TcdA and TcdB, some *C. difficile* strains are able to produce a binary toxin known as CDT (*C. difficile* transferase). CDT is an actin-ADP-ribosylating protein encoded by the *cdtA* and *cdtB* genes in the CDT locus (CdtLoc). Additionally, the CdtLoc carries *cdtR*, coding for a response regulator of the LytTR family, required for *cdtAB* expression, and that at least in some ribotypes, also acts as a positive regulator of TcdA and TcdB production (Martínez-Meléndez *et al.*, 2022). CDT has two components: the enzymatic component (CDTa) that shows ADP ribosyltransferase activity and the binding/translocation component (CDTb) that enables translocation of the enzymatic component to the host cell cytosol (Awad *et al.*, 2015). Once in the cytosol of intestinal epithelial cells, CDT causes rearrangement of the microtubule network and the formation of surface protrusions (Martínez-Meléndez *et al.*, 2022). Although CDT is mainly found in RT027 and 078 strains, often linked to severe CDI, its role in pathogenesis is still not fully understood. Recent studies highlight the possibility of CDT acting as a colonization factor. Protrusions produced in response to CDT increase adherence of *C. difficile* at the surface of intestinal epithelial cells, thus enhancing colonization (Schwan *et al.*, 2009).

Sporulation

Upon exposure to as yet poorly characterized signals, that likely include nutritional and other stress factors, and quorum sensing, *C. difficile* cells enter sporulation, through which a metabolically dormant spore able to resist to extreme physical and chemical conditions is formed (Sonenshein, 2000; Edwards and Mcbride, 2014; Paredes-Sabja, Shen and Sorg, 2014). As a strict anaerobe, *C. difficile* virulence potential is largely dependent on sporulation. The production of highly infective spores that are excreted by infected patients, allows the oxygen-sensitive pathogen to persist outside the host and host-host transmission (Deakin *et al.,* 2012).

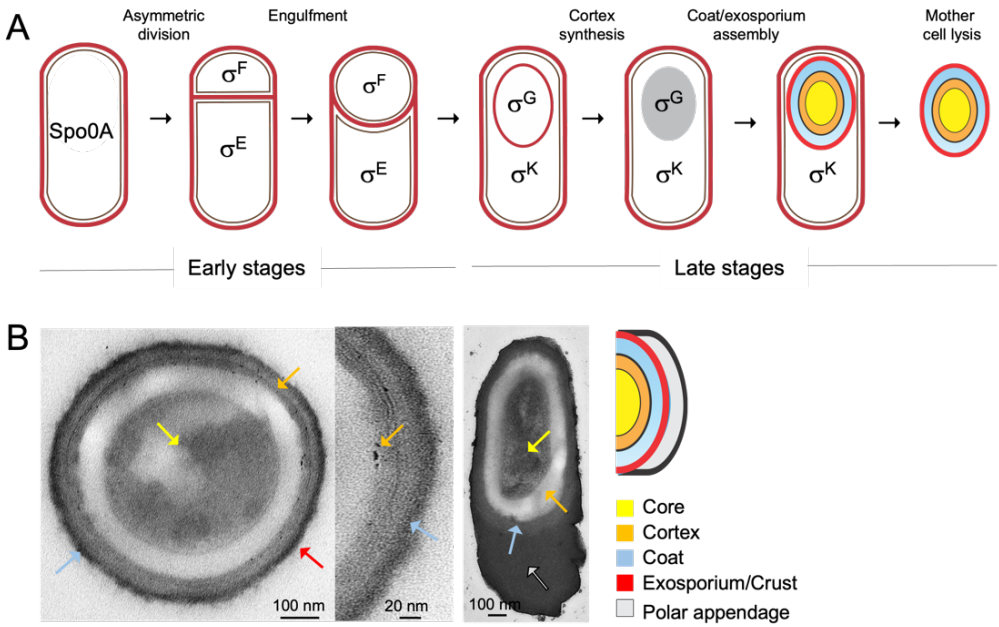

Figure 2. Morphological steps and activation of sigma factors during *C. difficile* sporulation. **A)** Sequence of the morphological events leading to spore differentiation: asymmetric division of the sporangial cell; engulfment of the forespore (which will become the mature spore) by the larger mother cell; after engulfment completion, the forespore is isolated from the surrounding medium; synthesis of the spore surface layers cortex, coat and exosporium; finally, the mother cell lysis, allowing the spore to be liberated into the surrounding medium. At the transcriptional level, the process is initiated upon Spo0A activation by phosphorylation and after asymmetric division controlled by four cell type-specific RNA polymerase sigma factors: σ^F in the forespore and σ^E in the mother cell, govern the first stages of sporulation, whereas σ^G and σ^K control the last stages in sporulation. **B)** transmission electron micrograph of a thin cross section of a *C. difficile* 630 spores. The visible structures of the spore are indicated: spore core (yellow arrow); spore cortex peptidoglycan layer (orange arrow); coat (blue arrow); exosporium/crust (red arrow) and appendage (black arrow). Adapted from Ramos-Silva, Serrano and Henriques, 2019.

The signals, environmental or others that elicit sporulation in *C. difficile* have not been identified, but the morphological stages of sporulation are well described (Pereira *et al.*, 2013) (**Figure 2**). An asymmetric division produces a smaller forespore and a larger

mother cell that will follow different programs of gene expression (Pereira *et al.*, 2013; Paredes-Sabja, Shen and Sorg, 2014; Ramos-Silva, Serrano and Henriques, 2019). The mother cell then surrounds the forespore, in a process termed engulfment that ears resemblances to phagocytosis which isolates the forespore from the external medium and releases it as a free cell inside the mother cell cytoplasm. Later in development, gene expression in the forespore prepares this cell for dormancy whereas the mother cell coordinates formation of the cortex, coat and exosporium layers. Lastly, auto-lysis of the mother cell releases the mature spore into the surrounding medium (Pereira *et al.*, 2013; Isidro *et al.*, 2017)

Phosphorylation of the response regulator Spo0A is required for sporulation (Abt, McKenney and Pamer, 2016). Spo0A is the master regulation of sporulation, conserved among spore formers and its phosphorylation drives the sporulation regulatory network by activating, among other genes, the expression of the genes encoding for the first sporulation specific sigma factors (Deakin *et al*., 2012; Ramos-Silva, Serrano and Henriques, 2019). Spo0A is also responsible for regulating other stationary phase responses, motility, carbon metabolism and toxin production, and it is also required for biofilm formation (Dawson *et al.*, 2012), (Mackin *et al*., 2013; Edwards and Mcbride, 2014; Pettit *et al*., 2014). Activation of the sporulation pathway results in sequential activation of cell-type specific RNA polymerase sigma factors. σ^F and σ^E in the forespore and the mother cell, respectively, control the early stages of sporulation. At later stages, these are replaced by σ^G and σ^K when the engulfment process is completed (Pereira *et al.*, 2013; Abt, McKenney and Pamer, 2016; Ramos-Silva, Serrano and Henriques, 2019). Forespore-mother cell signaling pathways operate at critical morphological stages of sporulation, to keep the two lines of gene expression in close synchronism with the morphological changes (Saujet *et al.*, 2013).

The overall spore architectural plan is conserved among spore-forming bacteria. The spore is composed by a core compartment that encases de DNA and is surrounded by a membrane and a thin peptidoglycan layer, that will serve as the cell wall of the outgrowing cell. This first layer of peptidoglycan is covered by a thick layer of modified peptidoglycan, the cortex, essential for heat resistance. The cortex is surrounded by a protein coat, which protects the spore from small toxic molecules and host lytic enzymes.

The spore is further enclosed in a glycosylated exosporium, a layer that mediates interactions of the spore with the environment, including the sensing of molecules that can induce germination (Pereira *et al.*, 2013; Antunes *et al.*, 2018).

C. difficile spores are able to interact with the intestinal mucosa and gain entry into the intestinal epithelial cells in a manner that depends on host fibronectin and vibronectin. The ability of spores to gain intracellular access to the intestinal barrier might contribute to disease recurrence (Castro-Córdova *et al.*, 2021). It has also been reported that *C. difficile* spores might contribute to virulence by surviving inside macrophages and even being able to produce cytotoxic effects in these cells (Paredes-Sabja *et al.*, 2012).

Cell-surface associated proteins

In *C. difficile* the surface layer mostly consists in two SLP subunits, the LMW-SLP (low-molecular weight S-layer protein) and the HMW-SLP (high-molecular weight S-layer protein). These forms derive from the proteolytic cleavage of precursor SlpA by the cysteine protease Cwp84 (Awad *et al.*, 2015; Janoir, 2016). S-layer proteins confer adherence of the cells to gut mucosa and can induce both inflammatory and antibody response in the host (Rupnik, Wilcox and Gerding, 2009). The cell wall proteins, Cwp, are a family of surface proteins that can mediate adherence to epithelial cells (Janoir *et al.*, 2007). These proteins can also be involved in degradation of host matrix proteins such as fibronectin, vitronectin or laminin and can therefore affect integrity of host tissues (Waligora *et al.*, 2001). There is a considerable variability among surface proteins such as SlpA and Cwp, possible as a consequence of selective pressure imposed by the host immune system, and thus contributing to avoid the host defense systems (Janoir, 2016).

Flagella

Production of peritrichous flagella confers motility to *C. difficile* cells. In *C. difficile*, the genes required for motility are thought to be expressed during early colonization stages and involved in colonization (El Meouche *et al*., 2013; Janoir, 2016). The role of flagella in colonization is supported by studies that highlight the ability of flagellar proteins to bind murine mucus and that non-flagellated strains show reduced adherence to the mouse caecum than their flagellated counterparts (Tasteyre *et al.*, 2001).

However, the importance of flagella to colonization is still contradictory with studies revealing that a flagellar mutant in the RT027 background is impaired in motility, adherence and colonization of the intestinal epithelium as compared to the congenic wild-type. The same study reported no differences in colonization capacity in RT012 parental strain (630Δ*erm*) and flagellar mutant (Baban *et al.,* 2013). The RNA polymerase sigma factor involved in the expression of late flagellar genes, σ^D, is also a positive regulator of the *tcdR* gene (see abobe; el Meouche *et al.*, 2013). Moreover, a flagellar switch in a phase variation-dependent production of flagella and toxins was found. Thus, the expression of specific virulence factors can confer different advantages and disadvantages during the course of infection (Anjuwon-Foster and Tamayo, 2017).

In recent years it was shown that *C. difficile* is able to form biofilms *in vitro* (Dawson *et al.*, 2012; Dapa *et al.*, 2013) and *in vivo* (Semenyuk *et al.*, 2015). Biofilm formation is emerging as in important virulence factor in *C. difficile* pathogenesis and will be discussed in more detail in the next chapters.

1.2 Biofilms

1.2.1 The role of biofilms in infection

The biofilm is one of the most widespread and successful modes of life, and it is arguably the predominant mode of growth for many microorganisms (Nobile and Johnson, 2015; Flemming *et al.*, 2016). Bacterial biofilms are defined as communities of bacteria, that grow attached to a surface and/or to each other and are embedded in a self-produced matrix composed of proteins, exopolysaccharides (EPSs) and eDNA (**Figure 1B**) (de Vos, 2015; Vestby *et al*., 2020).

Biofilm development goes through three main stages: attachment, maturation and dispersion (**Figure 1A**) (Rabin *et al.*, 2015). The first stage comprises an initial reversible attachment. Both the flagella and type IV-pili are important for initial adherence and cell aggregation (Percival *et al.*, 2011; Maldarelli *et al.*, 2016). Irreversible attachment is afterward achieved with the production of the biofilm matrix. Maturation of the biofilm occurs with recruitment of other cells, from the same or other species, that aggregate to form multiple layers. As the biofilm grows, more matrix components such as DNA and polysaccharides are incorporated into the biofilm. The last stage of the biofilm cycle is

dispersal. When environmental conditions are not favorable due to nutrient deprivation or intense competition the biofilm disperses and the release of planktonic bacteria or spores, in the case of sporeformers, allows spreading of the biofilm (Lister and Horswill, 2014; Rabin *et al.*, 2015)

Biofilms show a high level of organization. Cells interact intimately and influence each other's evolutionary fitness through cooperative and competitive interactions resulting in social phenotypes (Nadell, Drescher and Foster, 2016; Arnaouteli *et al.*, 2021). Spatial organization of these cells is fundamental to shape both competition and positive interactions in communities (Kim *et al.*, 2008). Heterogeneity within the biofilm offers advantages such as division of labor where the clonal population differentiates into subpopulations that perform specialized missions (Dragoš *et al.,* 2018).

Bacteria are able to interconvert between planktonic and biofilm-forming cells. In nature, however, biofilms may represent the prevalent mode of bacterial existence. Within the biofilm bacteria are protected from chemical and physical insults, exhibit increased tolerance to antibiotics and other antimicrobials, disinfection and innate and adaptive host immunity (Flemming *et al.*, 2016). The lack of success with antimicrobials in biofilms is explained by the difficulty of these substances penetrating and diffusing through the biofilm matrix (Stewart, 2002). Moreover, cells in biofilms are often characterized by an altered metabolism, gene expression and protein production. Biofilm cells have low metabolic rates and there can even be subpopulations of persister cells with growth rates close to zero (Lewis, 2010). These differences in bacterial physiology make biofilm bacteria insensitive to most of the common-use antibiotics that target processes relevant for cell growth or division. Additionally, horizontal gene transfer is common within the biofilm and can contribute to the dispersal of resistance to antibiotics and antimicrobials as well as virulence genes (Stewart, 2002; Rabin *et al.*, 2015).

In recent years, the study of biofilms has raised more interest in the scientific community, particularly in the biofilm formed by clinically relevant bacteria (Høiby *et al.*, 2011). It has been shown that the oral microbiome is predominantly located in biofilms that can be involved in the development of dental caries by species such as *Streptococcus sobrinus* and *S. mutans* (de Vos, 2015; Rabin *et al.*, 2015; Bowen *et al.*,

2018). Biofilms can also be found in the hospital setting, colonizing therapeutic devices such as implants, intravenous catheters or stents. Contamination of medical devices and equipment is a real health problem in particular, biofilm-associated infections caused by *Staphylococci*, including Methicillin-resistant *Staphylococcus aureus* (MRSA). When injected medical apparatuses are used, their removal may be the only treatment option (Lister and Horswill, 2014). Diseases such as cystic fibrosis or endocarditis are now known to be associated with microbial biofilms. Biofilm-associated infections, tend to be persistent, may not be dealt with by the immune system, and tend to be refractory to antibiotic and antimicrobial treatment (Høiby *et al.*, 2011; Rabin *et al.*, 2015; Vestby *et al.*, 2020; Motta *et al.*, 2021).

1.2.2 *C. difficile* biofilms

As mention above the high recurrence rates registered in CDI have become the current main clinical challenge in disease management. Recurrence was viewed as relying on spore production given the resilient nature of spores and their ability to invade epithelial cells; also, no relapse was observed in mice infected with a *spo0A* mutant (Deakin *et al.*, 2012; Castro-Córdova *et al*., 2021). A *spo0A* mutation, however, is pleiotropic affecting physiological processes such as motility, metabolic reprogramming during entry into stationary phase and biofilm-formation (Dawson *et al.*, 2012; Pettit *et al.*, 2014). In addition to spore formation, biofilm formation is hypothesized to play an important role in CDI and, in particular in disease recurrence (Tremblay and Dupuy, 2022).

C. difficile capacity to form biofilms *in vitro* and *in vivo* was demonstrated in recent years (Dawson *et al.*, 2012; Donelli *et al.*, 2012; Dapa *et al.*, 2013; Semenyuk *et al.*, 2014). Biofilm formation in *C. difficile* is mediated by multiple factors but seems to be triggered upon depletion of preferred energy sources, which leads to metabolic reprogramming orchestrated by global transcriptional regulators such as CodY, CcpA, SigL and Spo0A (Tremblay and Dupuy, 2022). Central to biofilm formation, is the shift to pathways such as glycine metabolism, Stickland fermentation, the Wood-Ljungdahl pathway, and of particular importance pyruvate production (Brauer *et al.*, 2021; Meza-Torres *et al.*, 2021; Tremblay *et al.*, 2021). In the host, this metabolic adaptation will

depend on the availability of nutrients such as sugars derived from the mucus layer or through the action of the microbiota (Tremblay and Dupuy, 2022). Recent studies revealed that bile salts such as the secondary bile salt DOC, in sub-lethal concentrations, together with a fermentable carbon source like glucose, induce formation of biofilm in *C. difficile* (Dubois *et al*., 2019).

The first reversible attachment is mediated by the flagellum, surface structures, and adhesins. c-di-GMP accumulation is induced by signal transduction systems, which decreases flagellar motility, enhances the production of type-IV-pill and of other surface proteins that increase adhesion (Mckee *et al.*, 2018; Dawson *et al.*, 2021; Tremblay and Dupuy, 2022). Microcolony formation and maturation is mediated by cell division, aggregate sedimentation and production of the biofilm matrix. Mother cell lysis during sporulation within the biofilm may contribute to the release of extracellular DNA (eDNA) that is incorporated into the biofilm matrix (Dawson *et al.*, 2021). Cell death is a property implanted in biofilm formation across species and in *C. difficile* this mechanism supports release of spores, eDNA and toxins into the matrix (Semenyuk *et al.*, 2014). As observed in other species, quorum sensing mechanisms contribute for the formation of biofilm communities (Li and Tian, 2012). As in other species, *C. difficile* biofilms is positively regulated by quorum sensing-based mechanisms (Dapa *et al.*, 2013). For instance, LuxS may play a role in mediating prophage induction, cell lysis and subsequent accumulation of eDNA (Slater *et al.*, 2019)*f*

Biofilm maturation leads to the production of subpopulations that are metabolically specialized creating, along time, spatial and functional heterogeneity within the biofilm. Sporulation is induced in a subpopulation of cells in the bottom of the biofilm, leading to recurrence (Meza-Torres *et al.*, 2021). Spores produced within the biofilm have specific characteristics which may be important during infection. As an example, Semenyuk *et al* 2014 reported the presence of a novel structure in the biofilm spores, named the shroud which is composed of fibers and granules. The shroud is possibly acquired after mother cell lysis and is most likely to be composed of dead cell debris. The function of this structure is not well understood but it might be involved in germination inhibition, binding the biofilm matrix and adhesion to the mucosa, as well as immune evasion (Semenyuk *et al.,* 2014). The final stages of biofilm in *C. difficile* include spore

production, a decrease in the concentration of c-di-GMP and eventually its dispersion (Tremblay and Dupuy, 2022). *C. difficile* biofilm is able to easily detach from the abiotic surface and form a free-floating aggregate, which may provide an insight into the dispersal capacity of the biofilm and consequently how it influences CDI treatment (Dawson *et al.*, 2012)

The dynamics of *C. difficile* biofilm formation *in vivo* probably include a multi-species biofilm as it was shown *in vitro* that *C. difficile* interacts with other intestinal species in a way that boosts biofilm formation (Dubois *et al.*, 2019). Moreover, the utilization of an *in vitro* gut model revealed that *C. difficile* is able to associate with colonic biofilm microbiota, and that neither the first line antibiotic vancomycin nor the otherwise highly successful FMT treatment were effective against the biofilm-associated *C. difficile* population (Normington *et al.*, 2021). *In vivo* studies showed that during CDI, the outer mucin layer contains *C. difficile* as well as other bacteria (Donelli *et al.*, 2012; Semenyuk *et al.*, 2015).

Spore formation within the biofilm along with its metabolic state and the protection conferred by the biofilm matrix, contributes to the reduced antibiotic sensitivity of *C. difficile* biofilms (Meza-Torres *et al.*, 2021; Rahmoun, Azrad and Peretz, 2021). Overall, the role of *C. difficile* biofilms in CDI remains unclear but is likely that they have an important role in colonization, persistence and disease recurrence (Semenyuk *et al.*, 2014; Normington *et al.*, 2021).

1.2.3 The extracellular matrix

The extracellular matrix is the most important feature of biofilms promoting adhesion to both biotic and abiotic surfaces and the close proximity of cells, which in turn promotes the coordination of behaviors through cell-cell signaling. It provides protection against environments insults, such as antibiotic therapy or the host immune system (Karygianni *et al.*, 2020; Brauer *et al.*, 2021). This matrix is generally composed of exopolysaccharides (EPSs), eDNA and proteins. The composition and structure of the biofilm matrix varies greatly according to species and the host environment (Flemming *et al.*, 2016).

Synthesis of EPSs can occur extracellularly or take place intracellularly followed by secretion to the matrix. In general, EPSs are not biofilm specific but their production is augmented during biofilm formation. EPSs are long linear or branched polymeric molecules, that can be fixed to the surface of the cell and forming an intricate network used as a scaffold for other matrix components, proteins and nucleic acids (Flemming and Wingender, 2010; Rabin *et al.*, 2015)

eDNA is an integral part of the matrix rather than just residual material released through cell lysis. Moreover, it has been shown that in some species DNA is even actively secreted (Ibáñez de Aldecoa, Zafra and González-Pastor, 2017). eDNA enhances adhesion and surface aggregation, strengthening the biofilm and contributing to matrix scaffolding (Das *et al.*, 2010; Karygianni *et al.*, 2020).

The matrix is also composed of proteins. Among those are enzymes involved in the degradation of EPS and other biopolymers, allowing the released compounds to be utilized (Bowen *et al.*, 2018). Pili, fimbria and flagella are also commonly found in the matrix. An important part of the matrix is also the networks formed by proteins that assemble into amyloids fibers; these are involved in bacterial adhesion, scaffolding and in maintaining biofilm integrity (Karygianni *et al.*, 2020). As an example, the TasA protein from *Bacillus subtilis* and the curli from *Escherichia coli*, increase the structural strength of biofilms by forming fibbers with amyloid-like properties (Erskine, MacPhee and Stanley-Wall, 2018). Other proteins from the host or the surrounding medium can also be incorporated in the biofilm matrix.

The precise composition of the biofilm matrix in *C. difficile* is difficult to determine, nonetheless, recent studies *in vitro* reveal possible components. For *C. difficile,* eDNA appears to be a crucial structural component (Dawson *et al.*, 2021). Autolysis is one of the sources of eDNA and it was previously shown that *C. difficile* Cwp19 is involved in cell autolysis; it could also be required for eDNA release to the matrix as the absence of Cwp19 impairs biofilm formation (Wydau-Dematteis *et al.*, 2018; Dubois *et al.*, 2019). EPSs are also present in *C. difficile* biofilms, however, no highly produced exopolysaccharide has been identified that is a specific component of

the *C. difficile* biofilm matrix (Dawson *et al.*, 2021). The theichoic-like acidic polysaccharide PSII, which also associates with the cell-wall, and a secreted polysaccharide formed by acetylated glucose monomers were detected in the biofilm matrix (Dapa *et al.*, 2013; Dannheim *et al.*, 2017; Dubois *et al.*, 2019). EPS does not appear to be an essential structural part of the biofilm matrix because treatment with $NaIO_4$, a compound that hydrolyzes polysaccharides, did not collapse pre-formed biofilms (Dubois *et al.*, 2019; Meza-Torres *et al.*, 2021). Proteins are also found in the biofilm matrix in *C. difficile*. Recent studies revealed that biofilm-matrix proteins in *C. difficile* are mostly intracellular and cell-wall proteins (Semenyuk *et al.*, 2014; Dawson *et al.*, 2021). Proteins can reach the biofilm matrix through secretion, release from the cell surface, cell lysis, a combination of these mechanisms or others as yet to be unraveled (Semenyuk *et al.*, 2014).

1.2.3.1 Moonlight proteins

Moonlight proteins are defined as "a subset of multifunction proteins that perform two or more biochemical functions that are not due to gene fusions, multiple splice variants, multiple proteolytic fragments with different functions, or promiscuous enzyme activities" (Jeffery, 2003). Moonlight proteins are usually cytosolic proteins, chaperones and metabolic enzymes that perform a second, unrelated function, outside of the cell (Jeffery, 2003; Amblee and Jeffery, 2015; C. Jeffery, 2018). However, how these second functions are acquired is still unknown. Also, how these proteins reach an external localization is puzzling, since most of them do not have a recognizable signal peptide for secretion. Secretion of these proteins may involve a specialized variety of a *bona fide* secretion system, a yet unknown secretion system or the production of membrane vesicles (Turnbull *et al.*, 2016; C. J. Jeffery, 2018). In pathogenic bacteria the extracellular function of these moonlight proteins often plays a role in infection. Some of these proteins can bind directly to host cells like fructose-1,6-biphosphate aldolase from *Neisseria meningitidis* or the Hsp60 chaperone from *C. difficile* (Hennequin *et al.*, 2001; Tunio *et al.*, 2010; C. Jeffery, 2018). Other proteins can bind to extracellular matrix or secreted mucins in the mucosal layer of the intestines such as the *Staphylococcus aureus* autolysin Aaa that binds matrix components like fibronectin (Heilmann *et al.*, 2005; C. Jeffery, 2018). Moonlight proteins can also aid infection by serving as receptors on the bacterial

cell surface to acquire nutrients, like glyceraldehyde-3-phosphate dehydrogenase (GADPH) from *Staphylococcus* sp. that also functions to acquire iron from the host by binding to transferrin (Modun and Williams, 1999; C. Jeffery, 2018).

Another well described example of moonlighting activity is that of the enzyme enolase. Enolase is responsible for the reversible conversion of 2-phosphoglyverate to phosphoenolpyruvate during glycolysis. At the cell-surface, enolase has been found to have various moonlight functions. Enolase binds plasminogen, fibronectin or laminin plays a decisive role in the pathogenesis of several bacterial species (Henderson and Martin, 2011). Glutamate dehydrogenase has also been identified as a moonlight protein. This enzyme catalyzes the oxidative deamination of glutamate to α-ketoglutarate and ammonia (Girinathan, Braun and Govind, 2014). In *B. subtillis*, glutamate dehydrogenase also shows a transcription factor binding activity and participates in the tight control of glutamate metabolism (Commichau *et al.*, 2007). In *C. difficile*, glutamate dehydrogenase (GDH) has been shown to play a role in colonization and disease progression. It is actively secreted to the extracellular medium, and secreted GDH appears to be important for rapid colonization *in vivo* (Girinathan, Braun and Govind, 2014; Girinathan *et al.*, 2016)

Moonlight proteins appear to play a title role in the formation of the biofilm matrix. As mentioned before, unlike *B. subtillis* or *E. coli*, which produce specific proteins to build the biofilm matrix, intracellular proteins appear to be the main protein component of the biofilm matrix in *C. difficile* (Dawson *et al.*, 2021). The protein content of the biofilm matrix formed by *S. aureus* is also mainly composed of cytoplasmic proteins (Foulston *et al.*, 2014). It can be hypothesized that as in *S. aureus*, *C. difficile* can recycle abundant metabolic and other cytoplasmic proteins released during the stationary phase that moonlight as components of the biofilm matrix.

1.3 Aims of this study

A previous study characterized the biofilm production in a panel of *C. difficile* clinical isolates using strain 630Δ*erm* (hereinafter 630 for simplicity) as the reference (**Figure 3**) (Louro, 2020). Robust biofilm-producing isolates were found mainly among live-stock associated ribotypes (RT014, 078, 126)

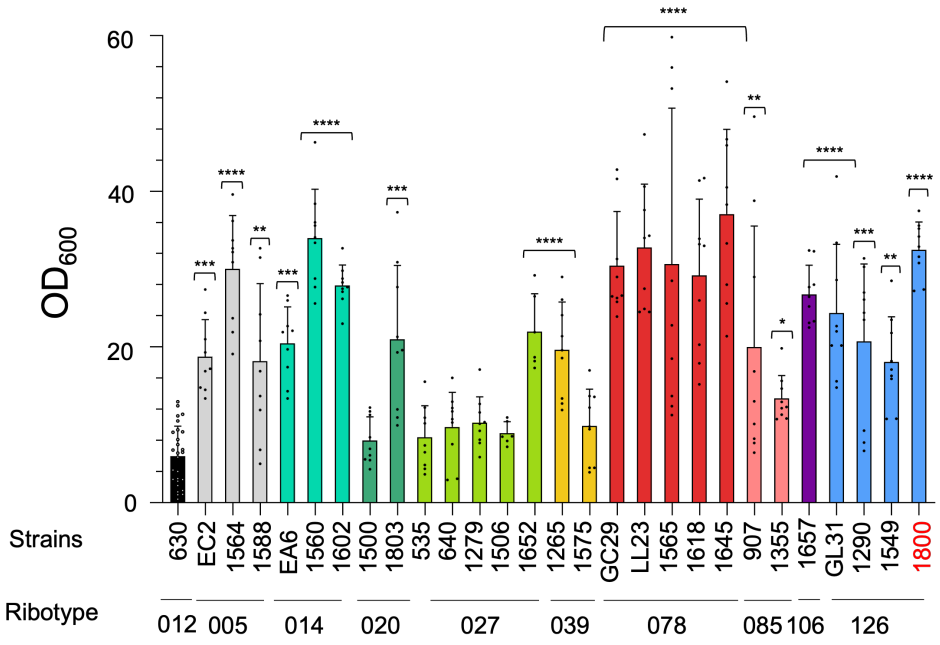

Figure 3. Biofilm formation by *C. difficile* isolates. Biofilm formation at 48 h was evaluated in a collection of 29 *C. difficile* strains isolated from animals and hospitalized patients (Louro, 2020). Biofilm formation was measured using a crystal violet assay (see Materials and Methods section). Asterisks indicate statistical significance determined with a Kruskal-Wallis test followed by an uncorrected Dunn's test (*p≤0.05, **p≤0.01, ***p≤0.001, ****≤0.0001 *vs* 630 at 48 h). Data shown indicate the mean, the exact measured values (dots) and the error bars represent the standard deviation.

From the group of isolates that was studied, we selected a robust biofilm producer, isolate 1800, to further characterize the biofilm matrix. Our main objectives throughout this work were:

1) the phenotypical characterization of strain 1800;

2) the identification of the biofilm matrix proteins from strain 1800;

3) To construct mutants with deletions of genes coding for the proteins identified in the matrix and to study the impact of these mutations on biofilm formation in *C. difficile* strain 630.

2. Materials and Methods

2.1 Microbiological techniques

2.1.1 Bacterial strains and growth conditions

All bacterial strains utilized in this work and their relevant properties are listed in Apppendix 1. Bacterial strains were stored at -80 ºC in 20% glycerol. All growth media are listed in Appendix 2.

Escherichia coli strains DH5α (Invitrogen), BL21 (DE3) (Novagen) and HB101(RP4) were used for molecular cloning, for protein overproduction and for *C. difficile* conjugation, respectively. Strains were grown in Luria-Bertani (LB) medium at 37 ºC and ampicillin (100 μg/ml) and/or chloramphenicol (20 μg/mL) were added when required.

C. difficile strain 630 was used throughout our work as a wild type reference strain. *C. difficile* cultures were incubated under anaerobic conditions (5% H_2, 15% CO_2, 80% N_2) at 37 ºC. Routinely strains were grown in brain heart infusion medium (BHI, from Oxoid). When required, cefoxitin (25mg/mL) and thiamphenicol (15 μg/ml) were added to growth media.

2.1.2 Biofilm production assays

Biofilm production assays were performed as described previously (Dubois *et al.,* 2019). For biofilm induction, a BHI overnight culture was diluted 1:100 in 1 mL per well of BHISG-DOC medium in 24-well polystyrene plates (from Greiner bio-one, Austria). The plates were incubated at 37 ºC in an anaerobic environment (as above) for 24 h and 48 h. To quantify biofilm production, media was removed and wells washed twice with phosphate-buffered saline (PBS; all buffers are listed in Appendix 3). Between each wash, the biofilms were air-dried for 10 min. Biofilms were then stained with crystal violet (CV; 0.2% w/v) for 30 min. Excess of CV was removed and wells washed two times with PBS. The biofilm-bound dye, corresponding to the biofilm mass, was dissolved with a 50:50 ethanol-acetone solution and the absorbance was measured at 600

nm with a spectrophotometer (Ultraspec2100 pro). To minimize measured errors, in high absorbances, the solubilized dye was diluted 1:100 in the ethanol-acetone solution.

2.1.3 Sporulation assays

Sporulation assays were performed as described previously (Serrano *et al.,* 2016). A BHI overnight culture (100 µL) was spread in 70:30 medium plates and incubated for 24 h. Afterwards, serial dilutions up to 10^{-5} were performed and plated in BHI agar supplemented with 0.1% of sodium taurocholate (TA, a germination inducer; from Roth), before and after incubation for 30 min at 70 ºC. Plates were incubated for 24 h and the colony forming units (CFU) were quantified. Sporulation efficiency was calculated using the formula below:

$$\text{Sporulation efficiency (\%)} = \frac{\text{CFU/mL of heat-treated cells}}{(\text{CFU/mL of non-treated cells} + \text{CFU/mL of heat treated cells})} \text{ x } 100$$

2.1.4 Spore production and purification

To induce sporulation, the strains were incubated in 70:30 medium for 48 h. The cells were rasped from the plates with cold ddH_2O, centrifuged at 4 ºC, 5752 x*g* 10 min, resuspended in cold ddH_20, and left at 4 ºC for 48 h to help cell lysis and spore release. The spores suspension was centrifuged at 4 ºC, 5752 x*g* 10 min, the sediment was resuspended in 1mL PBS-Tween 20 0.01% (PBS-T), layered on top of a 42% (v/v) solution of metrizoic acid (Gastrografin, from Bayer) and centrifuged at 4 ºC, 5752 x*g* 20 min. Purified spores, present in the sediment, were washed twice with ddH_2O and resuspended in a final volume of 500 µL of ddH_2O.

2.1.5 Germination assays

Germination assays were described previously (Antunes *et al.,* 2018). The spores were heat-shocked at 70 ºC for 10 min. Inside the anaerobic chamber, two sets of cuvettes were prepared, one with 1 mL of BHI and another with 950 µL BHI and 50 µL of TA 10%. The spores were added to each cuvette to an OD_{600} = 1 and the OD was measured at 5 min intervals for the first 30 min and thereafter for every 10 min. The efficiency of germination was calculated according to the formula:

$$\text{Germination efficiency (\%)} = \frac{OD_{600} \text{ at } t_n}{OD_{600} \text{ at } t_0} \text{ x } 100$$

2.1.6 Growth curves

To assess the growth rate in biofilm-forming conditions, BHISG-DOC was inoculated with a BHI overnight culture to an OD_{600}= 0.05. The OD_{600} was measured every two hours, until 14h of inoculation.

2.1.7 Protein over-production in *E. coli*

Protein over-production was performed using the auto-induction protocol described previously (Plácido et al., 2008). Briefly, *E. coli* BL21 (DE3) bearing the desired cells recombinant plasmids were grown in auto-induction medium supplemented with the required antibiotic(s) at 37 ºC, with orbital shaking, for 18 h. Cells were harvested by centrifugation at 4000 xg for 10 min.

2.2 Biochemical techniques

2.2.1 SDS-PAGE

Proteins were resolved on 12.5 % or 15 % SDS-PAGE gels. Loading buffer 10x was added to the samples and boiled for 5 min. The Precision Plus Protein ™ All Blue Ladder (from BioRad) was used as molecular weight standard. Gels were stained with Coomassie brilliant blue R-250 for 1 h followed by incubation in destaining solution until the protein bands were clearly seen against a clear background. InVision His-tag In-gel Stain (from ThermoFisher) was used to visualize His-tagged fusion proteins directly on polyacrylamide gels according to the manufacturer's instructions.

2.2.2 Clear-native PAGE

Proteins were separated on Clear-native PAGE gels with a 5-15% acrylamide gradient. Protein samples and the native marker were prepared by adding non-denaturing loading buffer, 0.05% DOC and 1.6 DDM 10%, and then incubated at 37ºC for 30 min. A native protein marker (high molecular weight, from GE Healthcare) was used in each run. Electrophoresis was performed with cathode and anode buffers, at 450V. The gel

was then either incubated for 1 h in Coomasie solution and transferred to a destaining solution, or used for the in-gel detection of GDH activity (see section 2.2.8).

2.2.3 Western Blot

SDS-PAGE resolved proteins were electrotransferred to nitrocellulose membranes (Supported Nitrocellulose, 0.45 μm; from BioRad) at 100 V for 90 min in electroblotting buffer for nitrocellulose membrane. Western blots of native-page gels were done using a polyvinylidene difluoride membrane (PVDF) membrane (from Millipore). Before transfer, the PVDF membrane was saturated in 100% methanol, followed by incubation for 5 min in electroblotting buffer for PVDF membrane. Proteins were transferred at 100 V for 90 min in electroblotting buffer for PVDF membrane. After transfer, the membrane was blocked in a solution consisting of 5 % milk in PBS-T for 1 h. Anti-GDH antibody (St John's Laboratory) was added at a 1:1000 dilution in PBS-T with 0.5 % milk, and incubated overnight at 4ºC. Before incubation with secondary antibody the membrane was washed in PBS-T. Mouse peroxidase-conjugated secondary antibody (Sigma-Aldrich) was used at a 1:5000 dilution in PBS-T with 0.5 % milk, for 30 min at room temperature. After three PBS-T washes the signal was developed using the SuperSignal West Pico Chemiluminescent reagents (from Thermo Scientific) and detected on an iBright Western Blot Imaging System.

2.2.4 Bradford protein assay

Protein concentrations were estimated spectrophotometrically using the Bradford method. The Bradford reagent (from BioRad) was diluted 1:5 in 1 mL of ddH_2O and 10 μL of protein was added. The OD_{595} was measured and protein concentration was estimated by comparison to a calibration curve prepared using BSA.

2.2.5 Protein purification by affinity chromatography

The cell sediments resulting from growth under auto-conditions (see above) were resuspended in 1 mL of French press buffer and lysed in french press cell (at 1800 lb/in^2). After clearing of the lysate by centrifugation, the supernatant was then used for protein purification. The His_6-Tagged fusion protein was purified by Ni^{2+} affinity

chromatography over a 1mL Ni^{2+} sepharose high performance column (GE healthcare) equilibrated with start buffer. The sample was slowly applied to the column, which was then washed with 10 mL of start buffer containing 10% (v/v) of glycerol. After another wash with 10 mL of start buffer, the protein was eluted with a step gradient of imidazole buffer (40, 100, 300 and 500 mM), and fractions of 1 mL were collected. The column was regenerated by washing again with start buffer, sealed to avoid dehydration, and finally stored at 4 ºC. Proteins in the fractions were analyzed by SDS-PAGE.

The purified protein was dialyzed overnight at 4 ºC in a SnakeSkin™ dialysis membrane with a molecular weight cut-off (MWCO) of 10 kDa (Thermo Scientific) in PBS buffer (pH 7). When needed, samples were concentrated in a Vivaspin column (MWCO of 3 kDa; GE Healthcare Biosciences AB).

2.2.6 Extraction and isolation of proteins from the matrix of *C. difficile* biofilm

Biofilm production was made as described in section 2.1.2 with an incubation period of 48 h in a 24-well plate. Biofilms were incubated in 1mL of PBS pH 7 and 50 µL of phenylmethylsulphonyl fluoride (PMSF) for 1 h inside the anaerobic chamber. The treated biofilms were then collected and centrifuged along with the medium at 5000 x*g* for 10 min. A 0.2 µm filter was used to remove remaining bacterial cells from the supernatant. The cellular sediment was resuspended in 500 µL of PBS pH 7. Cells were lysed in a French pressure cell (at 18000 lb/in^2), the lysate was directly collected to a microtube with 50 µL of PMSF, and subjected to centrifugation at 16200 x*g* for 5 min at 4 ºC and the supernatant kept for analysis. Samples were loaded on a 12.5 % SDS-PAGE and or loaded on a non-denaturing PAGE.

2.2.7 Zymogram

Purified glutamate dehydrogenase and matrix proteins extracts were assayed for GDH activity assays according to a published protocol (see 2.2.7; Girinathan *et al.,* 2013). Native gels were made with acrylamide concentrations of 3.5% in the stacking and 7.5% in the resolving gels. Samples were prepared by resuspension in a buffer lacking denaturing agents and proteins were resolved by non-deanturing PAGE, in tris-glycine buffer without SDS at 100V. For NAD-specific GDH activity detection, gels were

incubated in a 20 mM Tris-HCl (pH 8.0) solution containing 0.3 mg/mL nitro blue tetrazolium, 0.05 mg/mL phenazine methosulfate, 20 mM L-glutamate and 0.5 mM NAD. Enzyme activity appeared as purple bands in the gel.

2.2.8 Negative staining of protein samples for transmission electron microscopy

Purified protein at 0.2 mg/mL in PBS were adsorbed for 2 min to glow-discharged, 400 mesh carbon-coated grids. The grids were washed on 4 drops of ddH_2O and stained with 2% (w/v) uranyl acetate. Samples were imaged at the IGC electron microscopy facility on a Hitachi H-7650 Microscope equipped with an AMT digital camera operated at 120 keV.

2.3 Molecular biology techniques

2.3.1 Molecular cloning

DNA fragments were obtained by Polymerase Chain Reaction (PCR) with the high fidelity and processive Phusion DNA polymerase (from Thermo Fisher Scientific). The reaction conditions were settled according to the melting temperature of the primers, the expected size of the amplicon, and the manufacturer's specifications for Phusion. The DNA fragments obtained by PCR were purified using the NZYGelPure kit (NZYtech). All enzymes used for cloning were used accordingly to the manufacturer. The inserts in the various constructed plasmids were subjected to DNA sequencing. Plasmids and primers used in this work are listed in Appendix 4 and 5, respectively.

2.3.2 Plasmid DNA extraction

Restriction endonuclease cleavage of DNA isolated from minilysates was employed to identify *E. coli* harboring plasmids with the desired insert. Single colonies of *E. coli* were incubated overnight in LB supplemented with the appropriate antibiotic. Cultures were centrifuged for 5 min at 16 000 x*g* and the sediment was resuspended in 360 µL of STET buffer with 24 µL of lysozyme (10 mg/mL) and 10 µL of RNAse (10 mg/mL). The suspension was incubated at 37 ºC for 30 min and boiled for 10 min. Following centrifugation at 16000 *xg*, 70 % (v/v) of isopropanol was added to the supernatant. The DNA was sedimented by centrifugation at 16000 x*g* for 45 min at 4 ºC

and the sediment resuspended in 20 µL of ddH_2O. To isolate clean plasmid DNA the NZYMiniprep kit (NZYtech) was used in accordance with the instructions provided by the manufacturer.

2.3.3 Gel electrophoresis of nucleic acids

DNA fragments were resolved in 1% agarose gels in TAE buffer. Orange G loading buffer 10x was added to the sample before application in the gel. For DNA staining 0.001% (v/v) ethidium bromide was used. As molecular maker was used the 1 kilobase pair (kb) Plus DNA Ladder (from Invitrogen). Electrophoresis was performed at 120 V and DNA visualized using low wavelength UV light.

2.3.4 Production of competent *E. coli* cells and transformation

To prepare competent *E. coli* cells were grown in LB at 37ºC to an $0.3 \leq OD_{550nm} \leq 0.4$. After incubation for 15 min on ice, cells were centrifuged at 900 x*g* for 15 min at 4 ºC. The pellet was resuspended in RF1 buffer (30% of the culture initial volume) and incubated on ice for other 15 min. Following a centrifugation at 900 x*g* for 15 min at 4 ºC, the pellet was resuspended in RF2 buffer (8% of the culture initial volume). 200 µL aliquots were stored at -80 ºC.

Aliquots of *E. coli* competent cells were transformed with ligation mixtures (10 µL) or purified plasmid DNA (1 µL). After incubation for 40 minutes on ice, cells were incubated for 90 s at 42 ºC, followed by 2 min on ice. Cells were then incubated in 1 mL of LB at 37 ºC, with agitation. Cells were sediment by centrifugation for 2 min at 6000 *xg*, supernatant was discarded, and the pellet was resuspended in in 200 µL of LB and plated in LB agar supplemented with the required antibiotic and incubated overnight at 37 ºC.

2.3.5 *C. difficile* conjugation

Conjugation of *C. difficile* strains was performed as described previously (Purdy *et al.,* 2002). *E. coli* HB101 (RP4) carrying the recombinant plasmids was grown in LB to an $OD_{600} \sim 1$. Next 1 mL of the *E. coli* culture was centrifuged at 4 000 x*g* for 2 min, the supernatant discarded and the cell pellet washed gently with LB. After washing, the

cells were centrifuged at 4 000 x*g* for 2 min and the pellet was transferred to the anaerobic chamber. The pellet was resuspended in 300 µL of a BHI *C. difficile* culture and the cell suspension was spotted in a BHI plate. On the next day, spots were collected, resuspended in 1 mL of BHI and plated in five BHI plates with cefoxitin (25 µg/mL) and thiamphenicol (15 µg/mL). Thiamphenicol was used to select for plasmids of interest and cefoxitin was used to eliminate the growth of *E. coli*. Plates were incubated for 48 h.

2.3.6 Allele-Coupled Exchange (ACE) mutagenesis

The Allele-Coupled Exchange (ACE) technique allows the integration of a truncated version of a selected gene into the chromosome, replacing its wild-type counterpart (Ng *et al.,* 2013). Briefly: step 1**,** single colonies from the conjugation are re-streak to select for the first single cross-over that allows integration of the plasmid carrying the in-frame deletion of the selected gene into the chromosome; step 2, streaking single cross-over colonies in minimal medium (CDMM) supplemented with FOA (2 mg/mL) and uracil (5 µg/mL) to select for a second cross-over that will excise the plasmid containing the *pyrE* gene. The loss of the plasmid carrying the recombinant plasmid is confirmed by streaking in BHI and BHI with thiamphenicol. Integration of the truncated version of the gene into the chromosome was confirmed by PCR.

In order to create a mutant strain in a $pyrE^{+}$ background, the wild type *pyrE* gene should be restored. To do so, the *C. difficile* mutant strain in the Δ*pyrE* background (see above) is conjugated with pMTL-YN1 containing the *pyrE* gene. Conjugants able to grow in CDMM were selected and *pyrE* reversion confirmed by PCR. Loss of pMTL-YN1 is confirmed by streaking in BHI and BHI with thiamphenicol.

2.3.7 *C. difficile* chromossomal DNA extraction

Chromossomal DNA from single colony was extracted in 100 µL of 5% Chelex resin (Sigma-Aldrich). After incubation for 10 min at 95ºC the resin was pulldown by centrifugation at 10000 xg for 1 min, the supernatant recovered and used for PCR (see 2.3.1)

2.3.8 CRISPR interference (CRISPRi)

The utilization of CRISPR interference (CRISPRi) vectors with a xylose inducible defective Cas9 allows the construction of conditional mutants for essential genes, by allowing their expression in the absence of an inducer and their repression in its presence (Müh *et al.*, 2019). Seed region sequences (20-nucleotides) were obtained using the algorithm provided by Benchling set to default conditions and the protospacer adjacent motif (PAM) to NGG (Benchling, 2018).

2.3.9 Viability assays

Viability assays were performed as described previously (Müh *et al.*, 2019). A *C. difficile* overnight culture was serial diluted until 10^{-4} and spotted on BHI agar and BHI agar with 1% of xylose. After an overnight incubation, the plates were imaged.

2.4 Cell Biology

2.4.1 Transmission Electron Microscopy (TEM)

Spores from strains 630Δ*erm* and 1800 were purified as described above and were prepared for thin sectioning transmission electron microscopy, at the IGC electron microscopy facility. The grids were imaged on a Hitachi H-7650 electron microscope operated at 120 keV, and digital images collected with an AMT camera (Serrano *et al.*, 2016)

2.4.2 Immunofluorescence assays

Immunofluorescence assays of *C. difficile* biofilms were performed as described previously (Foulston *et al.,* 2014). Biofilms grown for 48 h in 24-well glass bottom plates were fixed for 30 min at room temperature in 45% formaldehyde. Fixation was stopped by adding 50 mM ammonium chloride. Next, biofilms were blocked with 3% BSA in PBS and then anti-GDH antibodies was added to a 1:500 dilution in PBS. The next day the plate was washed with PBS and anti-mouse IgG conjugated to Alexa Fluor 594 (Invitrogen) diluted 1:500 in PBS, was added. Plates were incubated for 1 h at room temperature and then washed three times with PBS. A Zeiss LSM 880 point scanning confocal microscope operated by the Zen 2.3 software (Zeiss, black edition), and coupled

to a 63x Plan-Apochromat 1.4NA DIC oil immersion objective (Zeiss) was used for image acquisition.

2.4.3 Scanning Electron Microscopy (SEM)

C. difficile biofilms were cultured as describe above for 48 h in 24-well plates with coverslips (Zeiss) in each well. Biofilms were fixed in fixing solution for 18 h at room temperature. Samples were washed 3 times with 0.1 M sodium cacodylate buffer (pH 7.4) with agitation. The last wash was kept for 18 h in buffer at room temperature. Samples were dehydrated in increasing steps of ethanol concentrations of up to 100% (v/v, for 10 min each, with agitation and at room temperature). The ethanol was removed, tert-butanol was added for 2 h at room temperature and the samples were frozen at -20 ºC followed by dehydration under vacuum. Lastly, the coverslips were gold sputtered with 10 nm golden in a Cressington 108 golden sputter. Samples were observed in a SU8010 Hitachi SEM, at 1.5 kV.

3. Results

3.1 Characterization of strain 1800

From a panel of clinical isolates that were previously characterized for their biofilm production (**Figure 3**) (Louro, 2020), we chose strain 1800, a robust biofilm-producer, to characterize the biofilm matrix proteins. Strain 1800 belongs to RT126 (*tcdAtcdB*$^{+}$, *cdtAB*$^{-}$), considered a hypervirulent ribotype closely related to RT078 (Baghani *et al.*, 2020). RT126 is predominant among livestock and is commonly associated with potential zoonotic transmission (Tsai *et al.*, 2016; Zhang *et al.*, 2020). We started by doing a general characterization of strain 1800 in which we evaluated the growth rate, sporulation and germination efficiency and spore morphology (**Figure 4**).

We started by characterizing the growth rate of strain 1800 in comparison to the reference, laboratory strain 630. Growth rates were calculated as described in section 2.1.6 (**Figure 4A**). Briefly, strains were grown in BHISG-DOC and the OD_{600} was measured every 2 hours for a period of 14h. We found a significant difference ($p \leq 0.01$) in the growth of strain 1800 compared with 630. Strain 1800 presents a higher growth rate when compared to the reference strain (0.594 h^{-1} and 0.415 h^{-1}, respectively) leading to an early entrance on stationary phase compared to the reference strain.

As a strict anaerobe, sporulation is a crucial process in the pathogenesis of *C. difficile*. We analyzed the strain´s ability to sporulate by measuring the titer of heat resistant spores after 24 h of incubation, as described in section 2.1.3 (**Figure 4B**). Strain 1800 presented an average sporulation efficiency of 86% compared to the reference strain with an efficiency of only 34%. Thus, strain 1800 was found to be a high spore producer. The spore morphology was analyzed by thin sectioning transmission electron microscopy (TEM) (**Figure 4D**). The main structural features previously described for spores of strain 630 (Paredes-Sabja, Shen and Sorg, 2014) included the spore core, the cortex peptidoglycan, and a lamellar coat surrounded by a thin, more electrondense, exosporium. We observed that spores from 1800 have a different organization of the outermost spore layer when compared to 630 spores. While spores from 630 present a compact, thin exosporium, 1800 spores have a thick exosporium layer with an irregular surface, from

which hair-like projections protruded. These morphological features have been described in the literature and both thin and thick exosporium morphologies have been found in spores from epidemic strains (Pizarro-Guajardo *et al.*, 2020). Spores produced by most clinical isolates, however, produce an exosporium that is thicker than that of the reference strain 630, with a bumpy appearance with hairy-like nap protrusions, similar to what we observed for 1800 spores (Paredes-Sabja, Shen and Sorg, 2014; Pizarro-Guajardo *et al.*, 2016; Antunes *et al*., 2018).

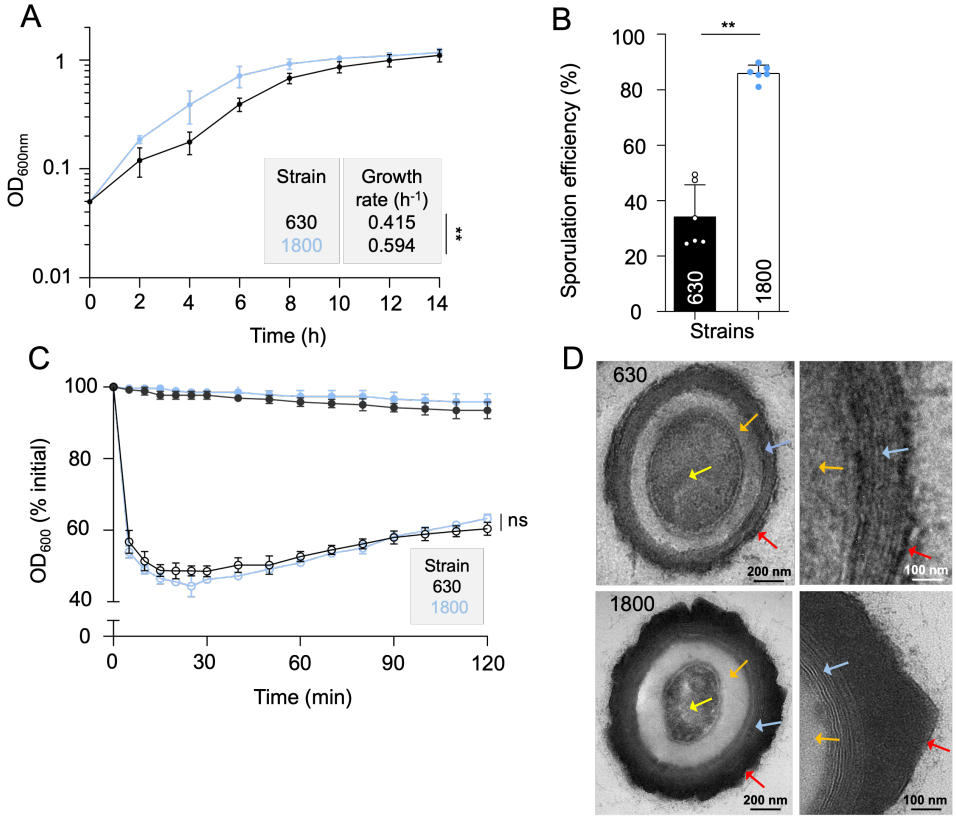

Figure 4. **Characterization of *C. difficile* strain 1800. A)** Growth curves of strains 630 and 1800**.** An overnight culture in BHI was used to inoculate 40 mL of BHISG-DOC to an OD_{600}= 0.05. The OD_{600} was measured every two hours, until 14 h of growth (see the Material and Methods section). **B)** Sporulation efficiency of strains 630 and 1800. Heat tests were performed to assess sporulation efficiency. After growing in 70:30 media for 24 h, the cells were diluted (10^0 to 10^{-6}) in 500 µL of BHI, 20 µL were inoculated in BHI agar plates supplemented with TA 0.1%. The remaining was heat treated (70 ºC) for 30 min and plated in the same medium. Spores of both conditions (the control and the heat treated) were incubated in anaerobic conditions for 24 h. Afterwards, CFUs were counted for both conditions, and the sporulation efficiency was calculated (see the Material and Methods section). **C)** Germination rates of strains 630 and 1800. Spores were heat-shocked at 70 ºC for 10 min. Inside the anaerobic chamber, two sets of cuvettes were prepared for each strain, one with 1 mL BHI (closed circles) and another with 950 µL of BHI and 50 µL of TA 10% (opened circles). OD_{600} was measured for 2 h (see the Material and Methods section). **D)** *C. difficile* 630 and 1800 spores imaged by thin sectioning transmission electron microscopy (TEM). Arrows indicate the different layers of the spore: yellow arrow, core; orange arrow, cortex; blue arrow, coat; red arrow, exosporium. The region encompassing the cortex, coat and exosporium is magnified on the images shown on the right. Asterisks indicate statistical significance determined with Mann-Whitney test (**p≤0.01) and "ns" (non-significant). Data shown indicate the mean (A to C), the exact measured values (dots) (B), and the error bars represent the standard deviation (A to C).

In order to cause disease, *C. difficile* spores must germinate and outgrow as vegetative cells. Spore germination is triggered by the interaction with small molecules, such as primary bile salts, whose receptors are located in the spore inner membrane (Sorg and Sonenshein, 2008). We evaluated spore germination, as described in section 2.1.5 (**Figure 4C**). Briefly, purified spores were induced to germinate by exposure to TA in BHI medium and the rate of germination was monitored by following the drop in the OD_{600} of the suspension. We observed a similar drop of about 50% in the OD_{600} in the first 30 min for spores of both strains, followed by spore outgrowth with similar kinetics. Although strain 1800 was found to produce more spores than the reference strain, germination efficiency was found to be similar in both strains.

3.2 Identification of biofilm matrix-associated proteins

We proceeded with the identification of the biofilm matrix-associated proteins in strain 1800. Extraction of the biofilm matrix proteins was done in previous work, by using a cell surface biotinylation and isolation kit (Louro, 2021). The extracted proteins were resolved in an SDS-PAGE gel, the gel stained with Coomassie (**Figure 5A**), and selected bands were sent for MALDI-TOF/TOF and TRIPLE-TOF analysis. Generated mass spectra were processed using Protein Pilot Software v. 5.0 (Sciex) for protein identification. The search was performed against the protein sequences database for strain 1800 and peptide identification was considered with >95% confidence. By analyzing the mass spectrometry date, we obtained a profile of predicted biofilm matrix-associated proteins in strain 1800.

The proteins with the highest score on the mass spectrometry analysis were selected, leading to the identification of 36 predicted biofilm matrix proteins (Appendix 6). These proteins were further divided into categories based on their functional assignement (**Figure 5B**). The majority of these proteins are cytoplasmic with a metabolic role. Our results are in agreement with previous findings who also reported that most of the biofilm matrix proteins in *C. difficile* are metabolic cytoplasmic proteins (Semenyuk *et al*. 2014; Dawson *et al*., 2021). In some examples, we were able to identify proteins involved in several energy metabolism pathways such as glycolysis (enolase, 6-phosphofructokinase) Stickland fermentation (NAD-specific glutamate dehydrogenase,

D-proline reductase) and other fermentation pathways (3-hydroxybutyryl-CoA dehydrogenase, acetaldehyde dehydrogenase). Surface proteins (ABC transporters, SlpA), chaperone proteins (DnaK, ClpB), proteins involved in environmental adaptation (SufB, Rubrerythrin) and in transcription/translation processes (YebC, Translation elongation factor Tu) were also identified as part of the biofilm matrix.

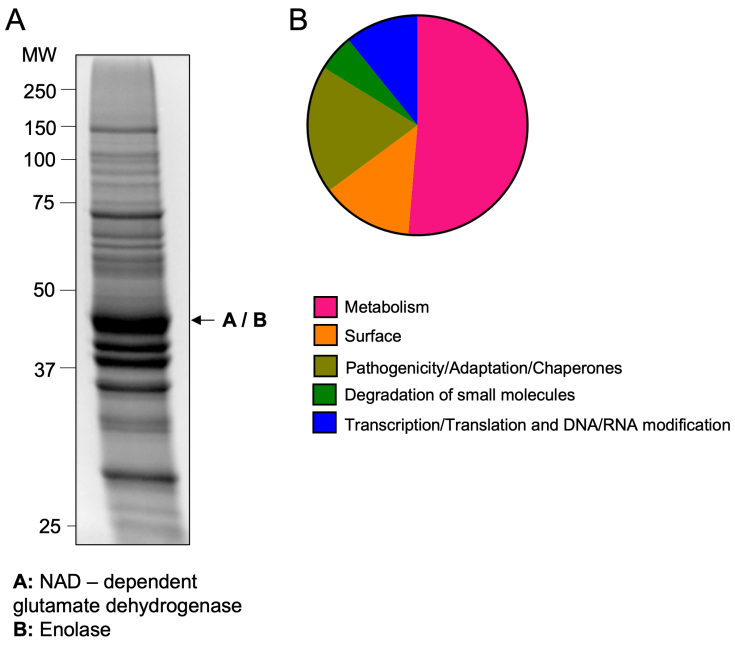

Figure 5. Analysis of the biofilm matrix proteins of strain 1800. A) SDS-PAGE electrophoresis of the biofilm matrix proteins. Extracted proteins were resolved in a 12.5% SDS-PAGE gel and stained with Coomassie brilliant blue 250. Bands were excised and sent for MALDI-TOF/TOF and TRIPLE-TOF analysis. Arrow indicates the band corresponding to the molecular weight of proteins NAD-specific glutamate dehydrogenase and Enolase**. B)** Functional protein classification of all 37 identified proteins is represented in the pie chart.

Of the 36 proteins identified, only five (3-hydroxybutyryl-CoA dehydrogenase, two ABC-transporter binding proteins, Oligopeptide ABC transporter, substrate-binding protein OppA and SlpA) had a recognizable signal peptide signal for secretion. Proposed mechanisms by which cytoplasmic proteins can reach the biofilm matrix include secretion systems, cell lysis or the formation of extracellular vesicles (Semenyuk *et al.*, 2014; Dawson *et al.*, 2021). Of the identified proteins, 17 have been described as having moonlight functions. As proposed for *S. aureus,* in which the biofilm matrix proteins are also mostly cytoplasmic, it seems that *C. difficile* may also recycle metabolic and other cytoplasmic proteins released during the stationary phase, that moonlight as components of the biofilm matrix (Foulston *et al.*, 2014). From the moonlight proteins identified,

NAD-specific glutamate dehydrogenase (46 kDa) and enolase (46 kDa), identified in the most abundant band of the SDS-PAGE gel of extracted proteins (**Figure 5A**), were chosen to further characterize their role in biofilm formation in *C. difficile*

3.2 Construction of an in-frame deletion mutant of *gluD*

NAD-specific glutamate dehydrogenase (GDH) is an enzyme responsible for the oxidative deamination of glutamate to α-ketoglutarate (Anderson *et al.*, 1993). This enzyme plays an important role in amino acid metabolism. GDH links amino acid metabolism to the tricarboxylic acid (TCA) cycle, by producing α-ketoglutarate, which is then incorporated into this metabolic pathway (Oliveira *et al.*, 2012). It is worth mentioning that *C. difficile* possesses a fragmented TCA cycle (Neumann-Schaal, Jahn and Schmidt-Hohagen, 2019). GDH is also involved in fermentation pathways such as the Stickland reaction, an important source of energy in *Clostridium* species (Sangavai and Chellapandi, 2017; Neumann-Schaal, Jahn and Schmidt-Hohagen, 2019). Glutamate is one of the most important nitrogen reservoirs and therefore GDH also plays an important role in bridging the carbon and nitrogen metabolism (Feehily and Karatzas, 2013; Jayaraman *et al.*, 2021). GDH is a cytoplasmic or cytoplasmic membrane-associated protein. In *C. difficile*, however, GDH is detected in the cytoplasm and in extracellular culture supernatants (Girinathan, Braun and Govind, 2014). A recent study demonstrated that GDH confers resistance to H_2O_2. Moreover, extracellular GDH improves *C. difficile* colonization and disease progression in a hamster model (Girinathan, Braun and Govind, 2014; Girinathan *et al.*, 2016). GDH was identified as a moonlight protein in *B. subtillis* (Commichau *et al.*, 2007), and the putative role of extracellular GDH in *C. difficile* pathogenesis suggests that this enzyme might have moonlight functions in *C. difficile* colonization. Among the repertoire of proteins identified in the biofilm matrix, we wanted to test whether GDH could have a moonlight function and act as an important structural and/or functional component of the biofilm matrix in C. *difficile*. To answer this question, we started by constructing a strain carrying an in-frame deletion of *gluD*, the GDH encoding gene (**Figure 6**).

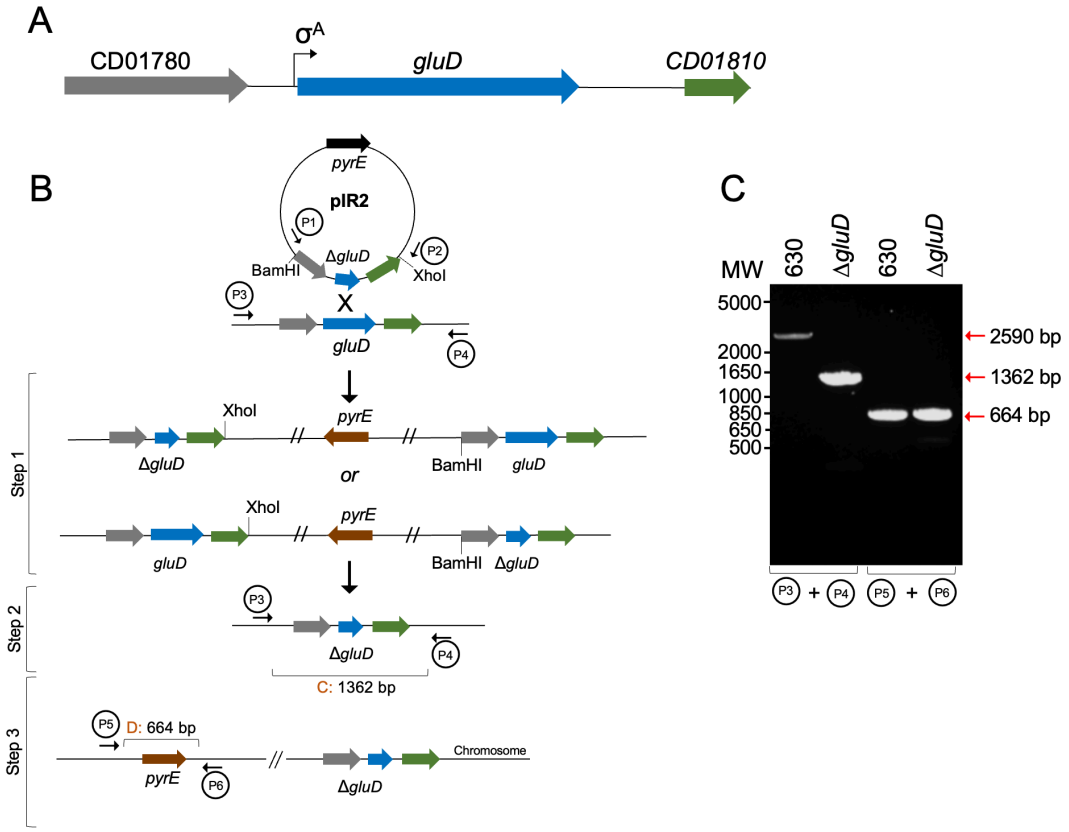

Figure 6. ACE-mediated in-frame deletion of the *gluD* gene in 630Δ*erm*Δ*pyrE* srain. A) Representation of the *gluD* region of *C. difficile* 630 chromosome where the broken arrow represents the σ^A-type promoter upstream of *gluD*. **B)** Plasmid pIR2 carries the *pyrE* gene and the in-frame deletion of base pairs 24 through 1246 of *gluD*. The plasmid integrates into the *gluD* locus by a single, reciprocal cross-over event (step1). After selection for plasmid excision (see Material and Methods; step 2) a strains carrying *gluD* in frame deletion was chosen for *pyrE* reversion (step 3). **C)** PCR analysis of the 630 strain in comparison with the *gluD* deletion mutant, to evaluate *gluD* deletion and *pyrE* reversion. Primers P3 and P4 were used for confirmation of the Δ*gluD* in frame deletion and primers P5 and P6 for *pyrE* reversion. The wild-type *gluD* gene has 2590 bp while the deletion allele has 1362 bp. The *pyrE* allele in the Δ*gluD* shows the same size as in 630 (664 bp) thus confirming *pyrE* reversion. P1: gluD_151F; P2: gluD_2691R; P3: gluD_127F; P4: gluD_2694R; P5: *pyrE*-vef-Fw; P6: *pyrE*-vef-Rev. The position and sizes of the expected products is shown by the red arrows. Molecular size markers (in bp) are also shown.

Inspection of *gluD* region of the chromosome reveals the presence of an upstream gene, coding for a putative ATPase, with an intergenic distance of 129 bp, and a downstream gene, coding for a putative membrane-associated metalloprotease of the M56 family, with an intergenic distance of 310 bp (**Figure 6A**). The ACE methodology (Ng *et al.*, 2013) (see section 2.3.6) was used to inactivate the *gluD* gene. An ACE cassette was assembled composed of a left-hand homology arm (LHA) and a right-hand homology arm (RHA) relative to *gluD*. The LHA (682 bp) was amplified by PCR using primers gluD_151F and gluD_2069R. The RHA (646 pb) was amplified by PCR using primers gluD_2075F and gluD_2691R. The two fragments were joined by splicing by overlap

extension (SOE) PCR and the resulting fragment of 1328 bp was cloned between BamHI and XhoI sites of pMTL-YN3 (Ng *et al.*, 2013) to produce pIR2 (**Figure 6B**). The fusion of the LHA with the RHA creates an in-frame deletion removing base pairs 24 to 1246 of *gluD* gene. pIR2 was introduced in *C. difficile* 630Δ*erm*Δ*pyrE* by conjugation from *E. coli* (see section 2.3.5).

gluD deletion was obtained as described before (see section 2.3.6) and verified using primers gluD_127F and gluD_2694R. The coding region of the wild-type allele is 2590 bp, while in the deletion allele the coding region is 1362 bp (**Figure 6 B-C**). At this point, a strain with deletion of *gluD* in a background Δ*pyrE* was constructed. To restore the *pyrE* gene, the plasmid pMTL-YN1 (Ng *et al.*, 2013) was introduced in the mutant strain 630Δ*erm*Δ*pyrE*Δ*gluD* by conjugation. The presence of the wild-type *pyrE* was verified by PCR using primers pyrE-vef-Fw and pyrE-vef-Rev, resulting in a fragment of 664 bp (**Figure 6 B-C**). At the end of this process, the desired construct, strain 630Δ*erm*Δ*gluD* (Δ*gluD*) was obtained.

Since there is not a strain carrying Δ*pyrE* in a 1800 background it was not possible to construct a *gluD* deletion in this strain.

3.3 Deletion of the *gluD* gene impairs biofilm formation

We started by evaluating the impact of *gluD* deletion on bacterial growth. To rule out that the differences observed in biofilm production came from differences during vegetative growth, growth rates were calculated as described in section 2.1.6 (**Figure 7A**). We observed similar growth rates in both strains and, after about 10 h following inoculation, both strains enter the stationary phase of growth. Therefore, deletion of *gluD* has no impact on the growth rate of *C. difficile,* at least under our culturing conditions.

To analyze the impact of *gluD* deletion on biofilm production we started by testing the ability of the mutant strain to form biofilm in BHISG-DOC, using the crystal violet assay, as described in section 2.1.2 **(Figure 7B)**. While there were no significant differences in the biofilm production at 24 h between strains, the *gluD* mutant produced significantly less biofilm at 48 h when compared to the wild-type, with a decrease of almost five times.

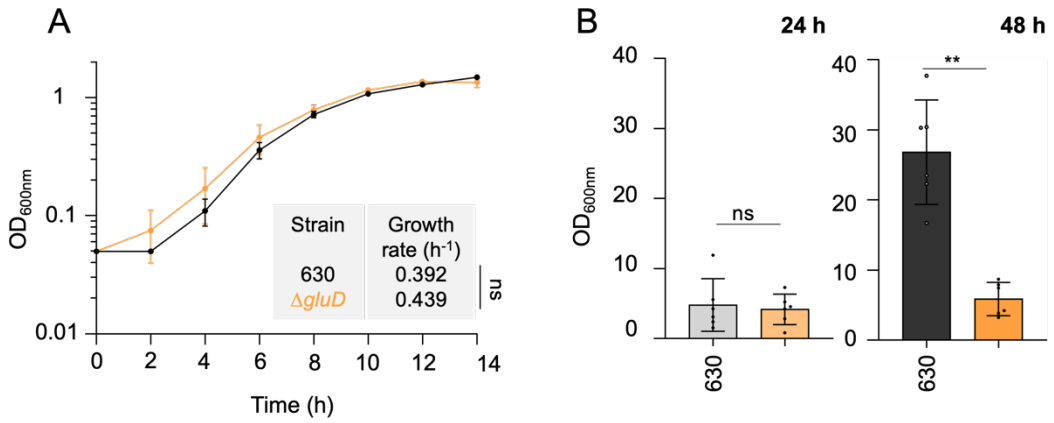

Figure 7. Analysis of the Δ*gluD* mutant biofilm production. A) Semi-logarithmic plots showing the growth of strains 630 and Δ*gluD*. A BHI overnight culture was used to inoculate 40 mL of BHISG-DOC to an OD_{600}= 0.05. OD_{600} was measured every two hours, until 14h of growth (see the Material and Methods section). **B)** Biofilm formation was measured at 24 h and 48 h after inoculation. Biofilm formation was measured using a crystal violet assay (see Materials and Methods section). Asterisks indicate statistical significance determined with with Mann-Whitney test (**p≤0.01) and "ns" (non-significant). Data shown indicate the mean, the exact measured values (dots); the error bars represent the standard deviation from the mean.

In order to observe the morphological and architectural differences of the biofilm formed by the *gluD* mutant strain, 48 h biofilms were imaged by scanning electron microscopy (SEM) as described in section 2.4.3 (**Figure 8A**).

In agreement with the biofilm production assays, SEM images revealed that less biofilm was formed by the *gluD* mutant strain when compared to the wild-type. The biofilm formed by the wild-type is characterized by extensive layers of *C. difficile* cells, interconnected by a network of extracellular material which we interpret to be the biofilm matrix (**Figure 8A, left panel**). Interestingly, the biofilm formed by the mutant strain lacked such dense matrix network. As a structural characteristic of both biofilms, we noticed the presence of fibers forming a web-like network connecting the cells (**Figure 8A, yellow arrows in right panels**). These fibers seemed to be longer and more robust in the biofilm formed by the wild-type strain. For a quantitative assessment of this feature,

we measured the length of fibers formed by the mutant strain and the wild-type using the Image J software package (**Figure 8B)**. A total of 100 fibers were measured per strain; the results revealed significant differences ($p \leq 0.0001$) in the fiber length between strains. Fibers present in the biofilm formed by the *gluD* mutant were shorter with an average length of 0.7 µm, while fibers from the wild-type biofilm could reach lengths of 6 µm and with an average length of 2 µm. Overall, these results suggest that GDH is an important structural determinant of the biofilm in *C. difficile* and that deletion of *gluD* impairs formation of the matrix network.

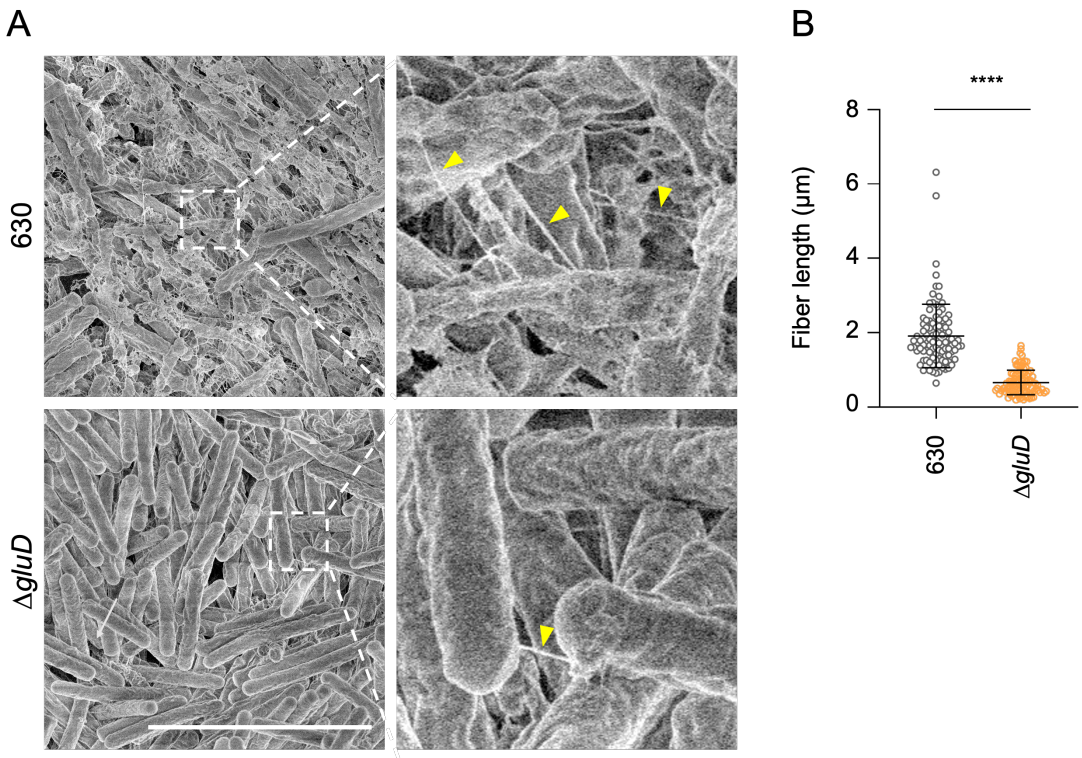

Figure 8. Scanning Electron Microscopy (SEM) images of 630 and Δ*gluD* biofilms. A) *C. difficile* biofilms were cultured for 48h in BHISG-DOC and samples were visualized by SEM (see Materials and Methods section). The right panels show a magnified image of the section indicated on the left panels. Yellow arrows, indicate fibers in the biofilm. Scale bar, 10 µm. **B)** Quantification of the biofilm fibers length in strains 630 and Δ*gluD*. SEM images of 630 and Δ*gluD* biofilms were analyzed and a total of 100 fibers per strain was measured using ImageJ. Asterisks indicate statistical significance determined with Mann-Whitney test (****$p \leq 0.0001$).

3.4 GDH accumulates within the extracellular matrix

To test how GDH accumulated in cellular and in the matrix extracts during biofilm growth, we used immunobloting with an anti-GDH antibody (**Figure 9B, upper panel**). Extraction of the biofilm matrix proteins was done as described in 2.2.7. Briefly, biofilms formed by the wild-type and the *gluD* mutant strain were grown for 24 h and 48 h. Afterwards, biofilms were incubated at pH 7, the pH at which matrix proteins are released from the cell surface (Louro, 2020). The treated biofilms were then collected, centrifuged, and the supernatant containing the biofilm matrix proteins was filtered. The sediments were lysed in a French press cell, centrifuged, and the supernatant was used as the cell extracts. The matrix and cell extracts were separated by SDS-PAGE. Immunoblot analysis confirmed the presence of *C. difficile* GDH in the matrix and cellular extracts of the wild-type strain and the absence of this protein in the *gluD* mutant strain. While GDH is present at similar levels in the cellular extracts at both time points tested, high levels of GDH were only found in the extracellular matrix in 48 h biofilms.

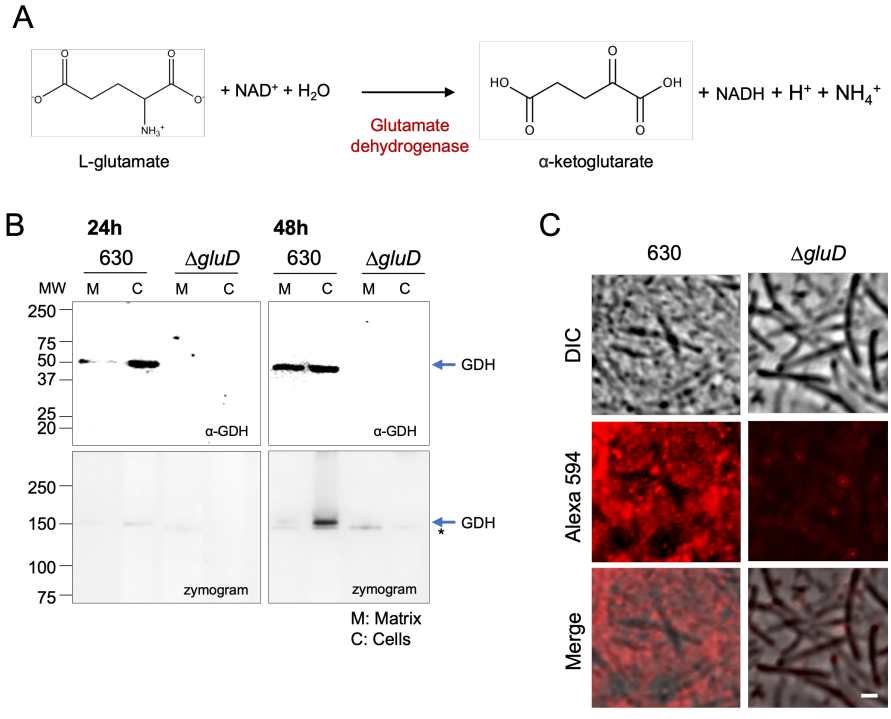

Figure 9. Analysis of glutamate dehydrogenase activity in the biofilm matrix in strains 630 and Δ*gluD*. A) Representation of the glutamate dehydrogenase enzymatic reaction. Glutamate dehydrogenase catalyzes the oxidative deamination of glutamate to α-ketoglutarate and ammonia. **B)** The presence of GDH in biofilm matrix and cellular extracts at 24 h and 48 h was assessed through a western blot (upper panel). Samples were resolved by SDS-PAGE (12.5%) and subjected to immunoblotting with an antibody raised against *C. difficile* GDH. Assessment of the GDH

activity (lower panel): an activity stain (zymogram) was used to detect NAD-specific GDH activity using NAD and glutamate as substrates (see the Materials and Methods section) in strains 630 and Δ*gluD* biofilm matrix (M) and cellular (C) extracts at 24 h and 48 h. Proteins in the samples were resolved by native PAGE (7.5%). Molecular weight markers (in kDa) are shown on the left side of the panels; the blue arrow on the right points to the position of GDH and the asterisks indicates a non-specific activity band. **C)** Immunofluorescence visualization of GDH in 48 h 630 and Δ*gluD* biofilms. Biofilms were probed with a mouse anti-GDH antibody, followed by a secondary anti-mouse antibody conjugated with Alexa Fluor 594 (red). Scale bar, 1 μm.

In order to localize GDH in the matrix of intact biofilms, we used immunofluorescence assays as described in 2.4.1 (**Figure 9C**). Biofilms were grown for 48 h, fixed, probed with anti-GDH antibody, and visualized using a secondary antibody conjugated to Alexa Fluor 594. Cells weren't permeabilized, so the proteins visualized in the biofilm were extracellular, *i.e.*, present in the matrix. The wild-type strain showed anti-GDH binding as a fluorescent signal localized between cells and surrounding cells, not overlapping with them, as observed in the merged images, thus confirming the presence of GDH in the matrix. No significant signal was detected in the *gluD* mutant strain. These results demonstrate that GDH is present in the matrix of mature biofilms.

3.5 GDH is enzymatically inactive in the biofilm matrix

While the abundance and the impact of *gluD* deletion on biofilm formation suggested an important structural role for GDH, we wanted to test whether the protein could have a functional role, linked to its enzymatic activity. As mentioned above, GDH catalyzes the oxidative deamination of glutamate to α-ketoglutarate and ammonia **(Figure 9A)**. We started by testing whether the matrix-associated GDH remained enzymatically active. To determine whether GDH present in the matrix was enzymatically active, we performed a zymogram assay as described in 2.2.8, in which the matrix and cell extracts (see above) were separated by non-denaturing PAGE and the gels incubated with L-glutamate as the substrate and NAD as the cofactor, to detect GDH enzymatic activity (**Figure 9B, Lower panel**). While in the biofilm grown for 24h we could only detect enzymatic activity as a fainted band present in the cellular extract of strain 630, at 48 h the presence of active GDH in the cellular extracts and, to a lesser extent, in the biofilm matrix of strain 630, was evident. The presence of enzymatically active GDH is shown by the appearance of a band of ~150 kDa in the zymogram. *C. difficile* GDH has a monomeric form of 46 kDa but the minimal active protein is most likely a trimer (Bolivar *et al.*, 2008), which is in agreement with the results obtained in the zymogram assay. As expected, active GDH is absent in the *gluD* mutant strain. The faint band indicated by the

asterisk (**Figure 9B, lower panel)** is thought to be non-specific activity and not to represent enzymatically active GDH, since is also present in the *gluD* mutant. Although intracellular and extracellular levels of GDH are similar at 48 h (**Figure 9B, lower panel**), in the zymogram, only a faint band was detected in the matrix extracts, indicating that extracellular GDH is largely enzymatically inactive. Overall, our results demonstrate that GDH is present in the biofilm matrix of *C. difficile,* mostly in an enzymatic inactive form.

3.6 Extracellular complementation of the *gluD* mutant phenotype

The results obtained led to us to believe the catalytic active form of GDH might not be crucial in the biofilm formed by *C. difficile*. The active site of GDH is composed of six important residues (**Figure 10**). In particular, aspartate (Asp) at position 147 is important for catalysis. The side-chain carboxyl group of Asp 147 is thought to interact with the amino group of the substrate. Based on previous evidence (Dean *et al.*, 1994), replacement of Asp 147 for a serine (D147S) allows the removal of negative charge and inhibits the interaction of the aspartate carboxyl with the substrate, thus creating a catalytically inactive protein.

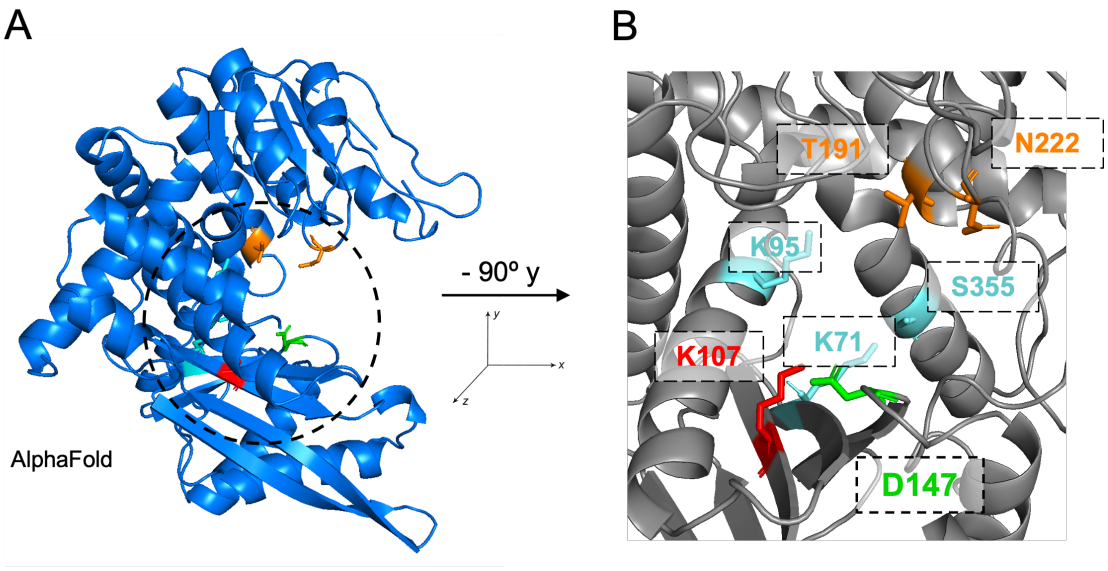

Figure 10. The AlphaFold structure of *C. difficile* glutamate dehydrogenase. A) Structural model of the *C. difficile* glutamate dehydrogenase (AlphaFold: AF-P27346-F1). The active site of GDH is highlighted in the circle and expanded on the right (**B**). Different colors represent amino acids important for GDH activity. Lysin residues on position 71 and 95 and serine on position 355 (blue) act as binding site for the substrate L-glutamate. Threonine on position 191 and asparagine on position 222 (orange) act as a binding site for the co-substrate NAD. Lysin on position 107 (red) is a proton donor. Aspartate on position 147 (green) is an important site for catalysis. The side-chain carboxyl group of Asp 147 is thought to interact with the amino group of the substrate. Based on previous evidence (Dean *et al.,*

1994), replacement of Asp 147 for a serine allows removal of negative charge and inhibits the interaction of the aspartate carboxyl with the substrate, thus allowing the creation of a catalytic inactive protein.

Deletion of *gluD* using the ACE system would enable complementation in *trans* concomitantly with restoration of the *pyrE* gene (Ng *et al.*, 2013). In trans complementation would be important to verify whether a wild-type phenotype would be restored and to understand to what extent the enzymatic activity of *C. difficile* GDH was important in biofilm formation. To allow this complementation analysis we tried to construct plasmids carrying a *gluD* wild type (WT) allele and an allele coding for a protein with the single amino acid substitution D147S. However we were not successful. In the impossibility to perform *in vivo* complementation in *trans* a different approach was taken, and extracellular complementation was attempted.

We started by overproducing and purifying the wild-type protein and the catalytic inactive form of GDH, with the single amino acid substitution D147S. We first constructed a plasmid for the overproduction and purification of the wild-type protein. Primers pET16b-gdhF with pET16b-gdhR were used to amplify by PCR the coding region of *gluD*. The resulting PCR product was digested with NcoI and XhoI and cloned between the same sites of pET-16b, to create pIR4 which contains an His_6-tag encoding sequence at the 3'-end of *gluD*. pIR4 was used as a template to perform the substitution D147S through QuickChange mutagenesis (Munteanu, Braun and Boonrod, 2012) using primers GDHAspSer_F and GDHAspSer_R, yielding pIR5. Plasmids were transformed into *E. coli* strain BL21 and His_6-GDH and His_6-GDH^{D147S} production and purification was done as described in 2.1.7. Samples from each step of the production and purification were analyzed by SDS-PAGE **(Figure 11A)**. Both His_6-GDH and His_6-GDH^{D147S} were overproduced and present in all fractions **(Figure 11A, upper panel, lanes: ET, P, S)**. The soluble fraction, the supernatant, was applied to a Ni^{2+} affinity column and the protein was purified. Most of His_6-GDH and His_6-GDH^{D147S} was eluted at an imidazole concentration of 100 mM (**Figure 11A, upper panel, lane: GDH**). The presence of the proteins was further verified by staining the SDS-page gel with InVision His-tag In-gel stain which allows the direct visualization of His-tagged fusion proteins (**Figure 11A, medium panel**). Coommasie and InVision His-tag In-gel staining confirmed the presence of His_6-GDH and His_6-GDH^{D147S} in the total cellular extracts and in both the soluble and insoluble fractions and the presence of the purified protein as a band of approximately 46

kDa, as expected from the deduced mass of the protein. The same samples analyzed by SDS-PAGE were also submitted to a zymogram assay as described above (**Figure 11A, lower panel**). As expected, we could detect GDH activity in all lanes corresponding to the His_6-GDH as shown by the presence of a band of approximately 150 kDa, the active trimer species (see above). No enzymatic activity was detected in His_6-GDH^{D147S}, thus confirming it to be a catalytic inactive form of GDH.

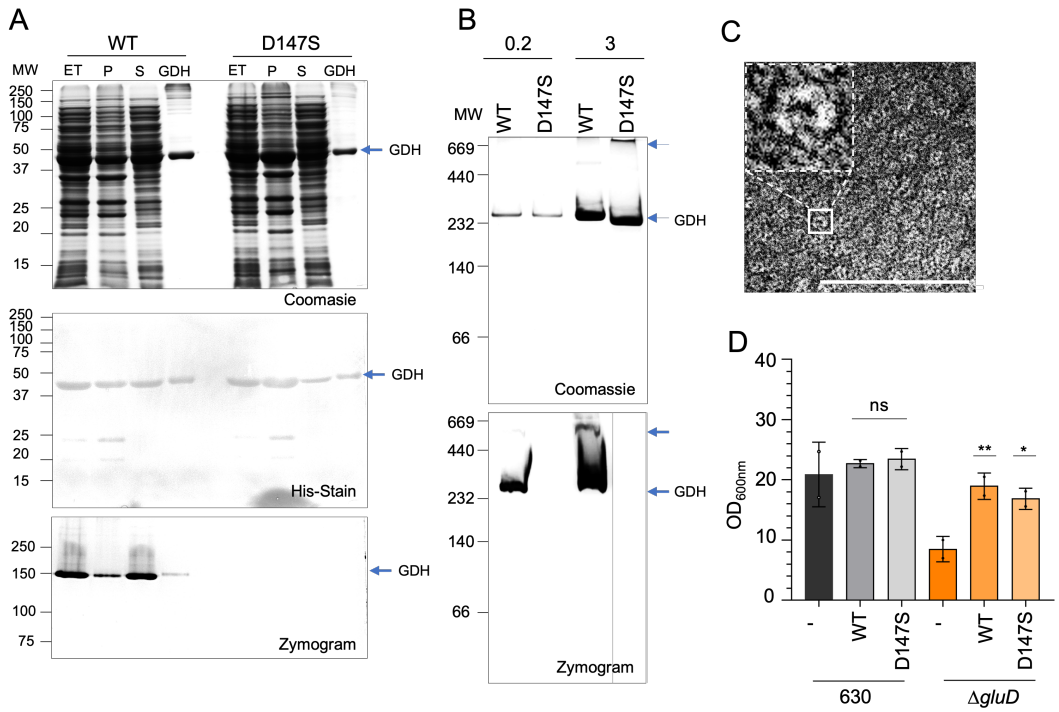

Figure 11. Purification of *C. difficile* GDH and GDH^{D147S} and assessment of enzymatic activity. A) SDS-PAGE (12.5%) representative of the purification of GDH^{WT} (WT) and GDH^{D147S} (D147S). Gels were stained with Coomassie brilliant blue (top panel) or subjected to His-Tag stain (middle panel). An activity stain (zymogram) was used to detect NAD-specific GDH activity using NAD and glutamate as substrates (bottom panel; see the Materials and Methods section). activity. Proteins in the samples were resolved by native PAGE (7.5%). ET – total cellular extract after cell disruption; P – insoluble fraction of the extract; S – soluble fraction of the extract; GDH – purified protein. **B)** Clear-native PAGE of purified GDH (WT) and GDH^{D147S} (D147S). Gels were stained with Coomassie brilliant blue (top panel) or used for the in-gel detection of GDH activity (bottom panel). In A and B, molecular weight markers (in kDa) are shown on the left side of the panels and the blue arrow on the right indicates the position of GDH. **C)** Negative staining electron micrographs of purified GDH. The upper left inserted panel shows a magnification of one of the particles. Scale bar, 100 µm. **D)** Extracellular complementation of Δ*gluD* with purified GDH**.** Biofilm formation was evaluated at 48 h after inoculation. Biofilms of strains 630 and Δ*gluD* were grown in BHIS-DOC supplemented with PBS (-), 40 µg per well of purified protein GDH^{WT} (WT) or GDH^{D147S} (D147S). Biofilm formation was measured using a crystal violet assay (see Materials and Methods section). Asterisks indicate statistical significance determined with an ANOVA test followed by an uncorrected Fisher's LSD test (*p≤0.05, **p≤0.01) and "ns" (non-significant). Data shown indicate the mean, the exact measured values (dots); the error bars represent the standard deviation from the mean.

To test if GDH present in the extracellular medium could restore the wild-type biofilm phenotype to the *gluD* mutant and if enzymatic activity is required for phenotypic

restoration we performed extracellular complementation assays with the purified proteins. Biofilms were grown for 48h in BHISG-DOC supplemented with 40 μg per well of purified His_6-GDH, His_6-GDH^{D147S} or the same volume of sample buffer as a negative control (**Figure 11D**). Biofilm production was quantified as described in 2.2.2. While in the biofilm formed by the wild-type strain no significant differences were registered with or without both extracellular proteins, the biofilm formed by the *gluD* mutant strain was significantly increased when grown in the presence of both wild-type or catalytic inactive forms GDH. Although the wild-type GDH had the most significant impact on increased biofilm production, the addition of both purified proteins was able to partially restore the wild-type biofilm forming ability to the *gluD* mutant.

3.7 *C. difficile* GDH behaves as an hexamer

While we were only able to detect the trimer conformation of GDH, *C. difficile* and other bacterial GDHs have been described as hexameric (Anderson *et al.*, 1993; Oliveira *et al.*, 2012). In order to confirm the oligomeric state of GDH, purified His_6-GDH and His_6-GDH^{D147S} were resolved in a Clear-Native PAGE as described in 2.2.2 (**Figure 11 B, upper panel**). In Clear-Native PAGE proteins are not separated according to their size and charge, as in non-denaturing PAGE used in the previous zymograms, but rather as a function of their size only. This is a valuable technique to isolate and preserve physiological oligomeric states and offers advantages for in-gel catalytic activity assays (Wittig, Karas and Schägger, 2007). Purified His_6-GDH and His_6-GDH^{D147S} were resolved in Clear-Native PAGE gels at concentrations of 0.2 and 3 mg/mL. At both concentrations, we found, for the wild-type and the catalytic inactive form of GDH, a band of approximately 295 kDa, similar to the expected size for the hexamer (276 kDa). Moreover, at higher concentrations, high-order aggregates could be observed with a molecular weight higher than 669 kDa. To analyze the catalytic activity of the different oligomeric states observed, samples were resolved as described above in a Clear-Native-PAGE, and GDH activity was assessed by performing a zymogram assay as described previously 2.2.3 (**Figure 11B, lower panel**). Enzymatic activity was detected in both concentrations of the wild-type protein while no GDH activity was detected in the catalytic inactive form. While in the previous assays we could only detect GDH activity in one band, the zymogram performed in Clear-Native PAGE revealed the presence of

catalytically active higher forms with the same molecular weights seen with Coomassie staining. From this, we conclude that both His_6-GDH and His_6-GDH^{D147S} are present in solution as hexamers and high molecular forms, and in the case of the wild-type allele both forms are catalytically active.

To gain insight into the protein conformation, purified His_6-GDH at 0.2 mg/mL was negatively stained and imaged by transmission electron microscopy as described in 2.2.9 (**Figure 11C**). Electron micrographs show small monodisperse particles of GDH in a variety of orientations with an average diameter of 8 nm. While it is difficult, based on these images, to infer protein structure, examination of individual particles reveals doughnut-shaped structures (**Figure 11C, expanded panel**). We can therefore hypothesize that this doughnut-shaped particles might correspond to hexameric assemblies.

3.8 Construction of CRISPRi vector for silencing *eno* expression in *C. difficile*.

Enolase is a glycolytic enzyme responsible for the reversible conversion of 2-phosphoglycerate to phosphoenolpyruvate (Paludo *et al.*, 2015). Enolase is a classic example of a moonlight protein, being described as having moonlight functions in several bacterial species including as an adhesin (Amblee and Jeffery, 2015; C. Jeffery, 2018). Enolase was also found in our repertoire of identified matrix proteins and we hypothesize that in a similar way to what happens in other bacterial species, this enzyme could be recycled and moonlight as a component of the extracellular matrix (Foulston *et al.,* 2014; Silva *et al*., 2014). Enolase is codified by the *eno* gene, which is an essential gene in *C. difficile* (Dembek *et al*., 2015). For this reason, to analyze the impact of enolase in *C. difficile* biofilms we started by constructing a CRISPRi vector targeting *eno* expression as described in 2.6.7. CRISPRi allows the construction of conditional mutants for essential genes by repressing their expression with an inducible defective Cas9 (Müh *et al.*, 2019). The CRISPRi vector pIA33, carries an *rfp*-targeting sgRNA under the control of the constitutive promotor P_{gdh} and nuclease-deactivated mutant of Cas9 (dCas9) under the control of xylose inducible promotor, P_{xyl}. The sgRNA targeting the *eno* gene (+458 bp relative to start codon in positive strand) was obtained by PCR amplification using primers sgRNA2 and ReverseSgRNA. The resulting fragment was digested with MscI

and NotI and inserted between the same sites of pIA33 to create pIR3, a CRISPRi vector targeting the *eno* gene (**Figure 12A**). pIR3 was introduced in *C. difficile* 630 by conjugation (see section 2.3.5). pIA33 was also conjugated into *C. difficile* 630 to serve as a negative control. Several attempts to construct a derivative of strain 1800 carrying pIA33 or pIR3 were unsuccessful.

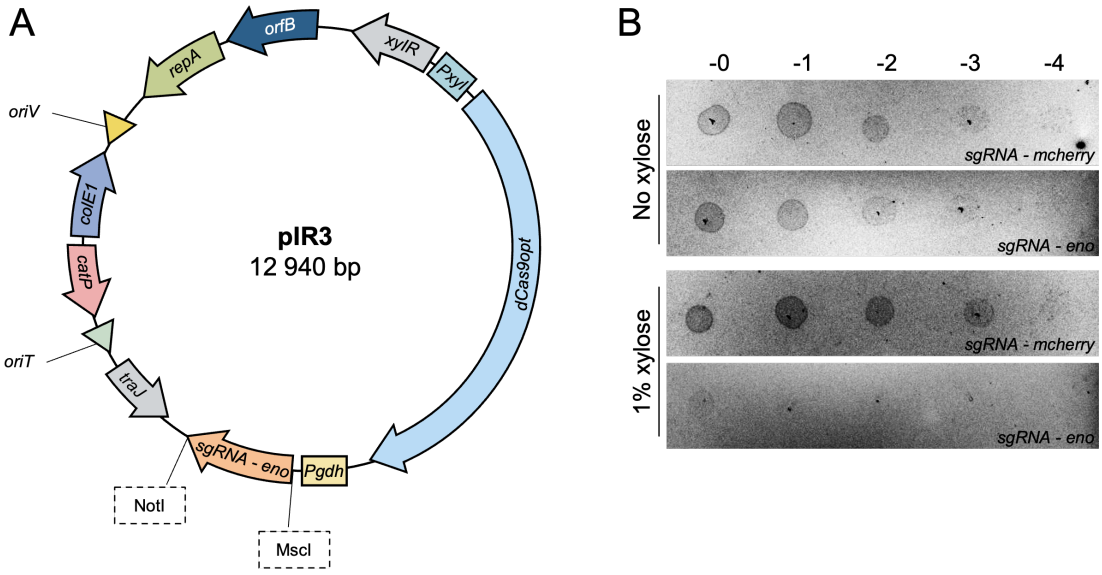

Figure 12. Construction of an enolase conditional mutant using the CRISPRi system. A) CRISPRi plasmid pIR3 carries a single guide RNA (sgRNA) targeting *eno*, expressed from the P*gdh* promoter, whereas P*xyl* drives expression of *dCas9*. SgRNA was amplified by PCR and inserted between the MscI and NotI sites of the backbone plasmid pIA33 (Müh *et al.*, 2019). *dCas9* codes for an inactive Cas9 codon-usage optimized (dCas9-opt) for expression in low-GC-content bacteria. Other genes are as follows: *orfB* and *repA* code for replication proteins; *catP* is a determinant of thiamphenicol or chloramphenicol resistance in *C. difficile* and in *E. coli,* respectively; *traJ* codes for a conjugation transfer protein. Origins of replication: from *E. coli* pBR322, *colE1* with a mutation increasing the copy number of the plasmid; *oriT*, functional in *C. difficile*. **B)** Viability assays. Strain 630 harboring CRISPRi plasmids pIA33 (negative control, targeting *mcherry)* and pIR3 (targeting *eno*) were grown overnight in BHI supplemented with thiamphenicol (see Materials and Methods section). Samples were serially diluted and 5 µL of each dilution spotted onto BHI plates supplemented with thiamphenicol and with or without 1% xylose to induce the expression of *dCas9-opt*. Plates were incubated overnight and imaged

Evaluation of the CRISPRi targeting *eno* was done by performing viability assays as described 2.6.8 (**Figure 12B**). Overnight cultures of strain 630 carrying plasmids pIR3 or pIA33 were serial diluted and spotted on plates with and without 1% xylose. On the absence of xylose, both strains showed the same viability pattern. However, in the 1% xylose plate, the strain carrying plasmid pIR3 showed a strong loss in viability with almost no growth even in the non-diluted spot. These results demonstrate that the CRISPRi vector is functioning as expected, since the strain grows normally without the

inducer and when exposed to 1% xylose, dCas9 expression is induced and targets the *eno* gene thus resulting in the loss of cell viability.

4. Discussion and Conclusions

The ability of bacteria to form biofilms has been associated with the chronic nature of several infections (Vestby *et al.,* 2020). One of the current main challenges in managing CDI is the high recurrence rate. About 25% of *C. difficile* infections lead to disease recurrence, with an increasing probability of further relapses thereafter (Finn, Andersson and Madin-Warburton, 2021). In recent years the capacity of *C. difficile* to form biofilm has been demonstrated and studies of its contribution to disease recurrence is now an important subject of research (Dawson *et al.*, 2012; Dapa *et al.*, 2013; Semenyuk *et al.*, 2014). The mechanisms underlying biofilm formation in *C. difficile,* as well as the biofilm composition*,* are still poorly understood. The identification of key components of *C. difficile* biofilms is crucial for understanding the basis of biofilm formation in this organism, and therefore the mechanisms underlying its persistence. In the present work, we identified the biofilm matrix proteins from a clinical isolate and chose two of those proteins to further characterize their role in the formation and structure of the *C. difficile* biofilm.

The use of strains isolated from their natural environment has proven to be more useful for understanding the behavior of naturally occurring biofilms than reference laboratory strains (McLoon *et al.*, 2011; Barreto *et al.*, 2020). In this sense, strain 1800 was selected among a group of previously characterized clinical isolates (**Figure 3**) (Louro, 2020) because it proved to be a robust biofilm producer. A general characterization of strain 1800 demonstrated a higher growth rate and sporulation efficiency when compared to the reference laboratory strain (630) (**Figure 4 A, B**). TEM images of 1800 spores revealed several structural differences compared to the reference strain (**Figure 4 D**). In strain 1800, the outermost layer of spores, the exosporium, appears as a thick and irregular electrondense layer with hair-like projections while spores from the reference strain present a compact coat and exosporium. The morphology of 1800 spores is consistent with reports from purified spores of hypervirulent strains (Pizarro-Guajardo *et al.*, 2016). The exosporium confers resistance to chemicals and enzymes while providing a hydrophobic surface that enhances spore adhesion to cells and abiotic surfaces (Henriques and Moran, 2007; Paredes-Sabja, Shen and Sorg, 2014). The exosporium thus appears to be an important layer in pathogenesis since it represents the

first line of contact of spores with host cells and the immune system. The stability and function of this layer, however, is still controversial. Some studies suggest that the exosporium can be easily lost or even absent in spores developed during biofilm formation (Paredes-Sabja, Shen and Sorg, 2014; Semenyuk *et al.*, 2014). Moreover, studies reveal that *C. difficile* spores that lack an exosporium are not only able to adhere better to colonic surfaces but also to germinate more efficiently (Escobar-Cortés, Barra-Carrasco and Paredes-Sabja, 2013; Antunes). In our conditions, however, strain 1800 and the reference strain did not exhibit significant differences in germination efficiency (**Figure 4C**). Evidence suggests that variation in the regulatory mechanisms that govern the assembly of the spore surface layers might occur during biofilm formation and that spores within biofilms exhibit structural differences (Semenyuk *et al.*, 2015; Pizarro-Guajardo, Calderón-Romero and Paredes-Sabja, 2016). Although we were not able to purify spores directly from the biofilm, future work will aim at the structural characterization of spores produced within the biofilm in comparison to those formed by planktonic cultures.

In analyzing the biofilm matrix-associated proteins from strain 1800 we identified 36 proteins (**Figure 5**). We were able to identify proteins involved in glycolysis, Stickland reactions, fermentation pathways such as those leading to butyrate and ethanol production, and the metabolism of amino acids such as proline and glycine. Besides proteins involved in metabolic pathways we also identified cell surface proteins, chaperones, proteins related to stress tolerance and transcription and translational regulators. There are several similarities between our repertoire of matrix-associated proteins and the proteins identified by Dawson and co-authors (Dawson *et al.* 2021). Likewise, some of the proteins identified herein overlapped with those associated with pathways shown to be up-regulated during biofilm formation by *C. difficile* (Poquet *et al.* 2018, Dubois *et al* 2019; Tremblay *et al* 2021). In contrast to *B. subtillis* or *E. coli*, which produce specific proteins to build the biofilm matrix (Barnhart and Chapman, 2006; Romero *et al.*, 2010), no protein with that specific function has yet been identified in *C. difficile*. Instead, our results indicate that *C. difficile* has a biofilm matrix mostly composed of cytoplasmic proteins, in agreement with previous findings (Semenyuk *et al.*, 2014; Dawson *et al.*, 2021).

eDNA is an essential structural component of the biofilm in *C. difficile* (Dawson *et al.*, 2021). It has been proposed that in *S. aureus*, positively charged cytoplasmic proteins make electrostatic interactions with the negatively charged cell-surface and with eDNA forming an electrostatic network providing physical strength and stability to the biofilm (Foulston *et al.,* 2014; Dengler *et al*., 2015; Graf et al., 2019; Kavanaugh *et al*., 2019). Among the biofilm-matrix proteins that we identified, 5 proteins (Inosine-5'-monophosphate dehydrogenase, transcriptional regulatory protein YebC and 3 different Translation elongation factor Tu) were shown before to be capable of binding DNA (Mclean *et al.*, 2004; Brown *et al.*, 2017; Kavanaugh *et al.*, 2019). We also identified 28 basic proteins, with an isoelectric point (pI) above 5, and among these, 7 present a pI greater than 6. Dubois and co-authors suggested that due to the catabolism of fermentable lower sugars during biofilm formation, the pH of the medium decreases to values between 5-6 (Dubois *et al.,* 2019). Possibly, in this acidic environment, a subset of matrix proteins becomes positively charged and interact with the negatively charged eDNA and cell surface creating a cohesive network.

The reuse of cytoplasmic proteins as matrix components might be an advantageous energy-strategy as it eliminates the need to invest resources in the production of specialized matrix proteins. From our analysis, only five proteins showed a recognizable signal peptide for secretion. How intracellular proteins lacking secretory signals reach the biofilm matrix is still unclear. Cell lysis is a common feature in biofilms that can be mediated by prophages, sporulation or autolysis (Meza-Torres *et al.*, 2021). In some bacterial species, cell lysis within biofilms was shown to be a coordinated process (Mann *et al.,* 2009; Turnbull *et al*., 2016). In *C. difficile* the autolysin Cwp19, and quorum-sensing mechanisms involved in prophage induction have been suggested to have a role in biofilm formation (Wydau-Dematteis *et al.*, 2018; Dubois *et al.*, 2019; Slater *et al.*, 2019). Cell lysis could therefore be an effective mechanism by which cytoplasmic proteins reach the biofilm matrix. Several reports, however, have shown that the release of cytoplasmic proteins during stationary phase is not due to cell lysis but rather dependent on non-classical secretion systems (Recchi *et al.*, 2002; Bendtsen *et al.*, 2005; Yang *et al.*, 2011; Zhao *et al.*, 2017). Other mechanisms such as the contribution of membrane vesicles have also been proposed and implicated in biofilm formation in species such as *Pseudomonas aeruginosa*, *Streptococcus mutans* or *Mycobacterium*

ulceris (Turnbull *et al.,* 2016; Cao and Lin, 2021). Interestingly, some of these cytoplasmic proteins are detected in the extracellular medium in many bacterial species which suggests that excretion is somehow protein-specific. Moreover, most of the cytoplasmic proteins that are secreted to the exterior have been identified as having moonlight functions (Henderson and Martin, 2011). Among our repertoire of biofilm-matrix proteins, 17 were identified as moonlight proteins such as Glucose-6-phosphate isomerase, NAD-specific glutamate dehydrogenase and Enolase (see also below). In *S. aureus*, it was discovered that the biofilm matrix is also largely composed of cytoplasmic proteins that are released during stationary phase and associate with the cell surface in a pH-dependent manner (Foulston *et al*., 2014).

Besides an effective strategy for saving resources, the use of cytoplasmic proteins in the biofilm matrix can bring advantages in building multi-species biofilms. Not needing to recognize specific proteins *C. difficile* may utilize proteins produced by other species. This strategy might be relevant considering the dynamics of *C. difficile* biofilm formation in the gut, which is most likely a multi-species biofilm (Donelli *et al.*, 2012; Semenyuk *et al.*, 2015; Dubois *et al.*, 2019). In order to shed a light on the role of moonlight proteins in the formation and properties of the biofilm matrix in *C. difficile*, we further characterized NAD-specific glutamate dehydrogenase (GDH) and enolase.

GDH catalysis the oxidative deamination of L-glutamate to produce α-ketoglutarate and ammonia using NAD as a co-factor (Anderson *et al.*, 1993). This enzyme plays a central role in amino acid metabolism, in particular in important fermentation pathways such as Stickland reactions (Oliveira *et al.*, 2012). Moreover, glutamate is a crucial reservoir of nitrogen in the cell (Feehily and Karatzas, 2013; Jayaraman *et al.*, 2021). Previous studies have revealed that in *C. difficile* GDH is actively secreted to the extracellular medium where it plays a role in colonization and disease progression *in vivo* (Girinathan, Braun and Govind, 2014; Girinathan *et al.*, 2016). In *B. subtilis,* apart from the role as a metabolic enzyme, GDH was found to have a moonlight function by binding to a transcription factor, regulating glutamate metabolism (Commichau *et al.*, 2007). The fact that GDH is an important metabolic protein identified as having moonlight functions, together with the apparent importance of extracellular

GDH in colonization by *C. difficile*, underlies our rationale for choosing this protein as an interesting target to evaluate its role in the biofilm-matrix.

To understand the importance of GDH in the *C. difficile* biofilm, we used ACE mutagenesis to construct a mutant strain bearing an in-frame deletion mutation of the *gluD* gene coding for GDH (**Figure 6**). We demonstrated that deletion of *gluD* impairs biofilm formation *in vitro*. Quantification of biofilm production by the *gluD* mutant did not reveal significant differences to the wild-type in biofilms grown for 24 h grown; at 48 h, however, the *gluD* mutant produced almost five times less biofilm than the wild-type strain (**Figure 7B**). Growth curves of the *gluD* mutant and the wild-type strain showed no significant differences and therefore the differences observed in biofilm production do not arise from perturbations during vegetative growth (**Figure 7A**). A previous study reported a growth defect for a *gluD* insertional mutant (Girinathan, Braun and Govind, 2014). However, this phenotype was observed using a different parental strain (JIR8094) and growth media (TY). Previous work revealed that DNAse I treatment had a profound effect on 24 h and 48 h grown *C. difficile* biofilms, while in proteinase K-treated biofilms the morphological impact was only notorious at 48h (Louro, 2021). This leads us to hypothesize that eDNA might have an important role in early stage biofilm development while proteins such as GDH may be important for biofilm stabilization at a later stage (**Figure 13**). The importance of eDNA in the early stages of biofilm formation and the major structural role played by proteins at later stages has been reported for other species (Whitchurch *et al*., 2002; Li *et al*., 2020; Peng *et al*., 2020). If indeed in *C. difficile* eDNA is important in early stages for initial cell attachment and proteins are afterwards more important for stability, this explains the absence of differences between the *gluD* mutant and the wild-type at 24h and the defective biofilm-production observed at 48h. While it is beyond the scope of this study to understand the role of eDNA in *C. difficile* biofilms, future work should aim at a deeper understating of how eDNA and matrix-proteins interact to form the biofilm-matrix and when in the time-line of biofilm formation these interactions take place.

SEM images show that the biofilm formed by the wild-type strain is composed by a mesh of *C. difficile* cells linked by an extracellular matrix (**Figure 8A**). Not only did the *gluD* mutant strain produce less biofilm, it also lacked the dense matrix network

present in the wild-type. The biofilm formed by both strains exhibited cells with an increased length relative to cells undergoing planktonic growth. This phenotype has been previously described in DOC-induced biofilms (Dubois *et al.*, 2019). Moreover, in both strains, we were not able to observe sporulating cells or spores within the biofilm. Spore formation has been described to occur within the biofilm and spores encased in the biofilm-matrix are considered a major contributor to bacterial persistence (Dawson *et al.*, 2012; Semenyuk *et al.*, 2014). The absence of spores in our biofilms could be explained by the presence of glucose in growth media, which is known to suppress sporulation (Antunes *et al.*, 2012). Dubois *et al.,* have also reported low sporulation efficiencies in DOC-induced biofilms and concluded that besides glucose, DOC also represses sporulation (Dubois *et al.*, 2019). Future work on the analysis of spore formation within the biofilm should include not only the absence of sporulation-inhibitory components in the growth media but also an increase in the biofilm growth-time from 48 h up to 6 days as described in other studies (Dawson *et al.*, 2012; Semenyuk *et al.*, 2014; Pizarro-Guajardo, Calderón-Romero and Paredes-Sabja, 2016).

Looking deeper into the architecture of the biofilms we noticed the presence of fibers forming a web-like network connecting cells. These fibers were more abundant in the wild-type strain and shown to be significatively longer when compared to those found for the *gluD* mutant (**Figure 8B**). While the nature of these fibers is unclear, we believe that these could be composed of cellular debris, cell appendages like pili or have a proteinaceous component. Since the *gluD* mutant strain presents fewer and smaller fibers, it would be interesting to test whether GDH could be involved in the formation of these structures. Future work involves immunogold labeling assays using an anti-GDH antibody to understand the precise location of this protein in the biofilm.

The finding that GDH is part of the matrix results from the identification of matrix-associated proteins in strain 1800. We were also able to demonstrate that GDH accumulates in the biofilm matrix of the 630 strain through immunoblots and immunofluorescence assays using an anti-GDH (**Figure 9 B, C**), in agreement with previous reports (Dawson *et al.,* 2021). As mentioned previously, strain 1800 belongs to the hypervirulent RT126 while the reference strain belongs to RT012. The presence of GDH in the biofilm-matrix formed by strains of these very different ribotypes leads us to

suspect that GDH may be a universal biofilm-matrix protein in *C. difficile*. To answer this question, future work involves the assessment of GDH presence in the matrix of strains from different ribotypes.

We showed that intracellular and extracellular levels of GDH are similar at 48 h biofilms; in zymogram assays, however, the GDH present in the biofilm-matrix is mostly enzymatically inactive (**Figure 9B**). As it happens with the vast majority of the identified matrix-associated proteins, GDH does not possess a signal-peptide sequence for secretion and the mechanism through which it reaches the biofilm-matrix remains unknown. Through SEM imaging of biofilms and in immunofluorescence assays, we were able to observe areas of several damaged cells within the biofilm which is in agreement with the cellular lysis process that is naturally associated to biofilm formation. In this sense, we cannot exclude cell lysis and possibly also coordinated autolysis as an important mechanism by which GDH might be secreted to the biofilm-matrix. However, Girinthian and co-authors have shown that in *C. difficile* GDH is actively secreted during growth and that this secretion is lysis independent (Girinthian *et al.* 2014). Later studies by the same group complemented a *C. difficile gluD* mutant with *gluD* homologues from *B. subtilis*, *C. sordellii*, and *C. perfringens* and demonstrated that *C. difficile* is only capable of secreting its-own GDH (Girinathan *et al.*, 2016). These results suggest that GDH is secreted in an independent lysis way and through a specific secretion mechanism. Neither of these studies, however, have evaluated GDH secretion in a biofilm background. In this sense, further investigations are needed to identify the non-classical secretion system responsible for GDH export and to understand which secretion mechanism occurs during biofilm development.

A transcriptomic analysis revealed that *gluD* is up-regulated at 14h and 24h in biofilms grown in the presence of DOC (Tremblay *et al.*, 2021). This up-regulation is in agreement with the metabolic rearrangement associated with the biofilm formation process itself and in particular in DOC-induced biofilms. Biofilms grown in the presence of glucose and DOC have shown to present a remodeled metabolic profile resembling a stationary phase cell, in which enzymes involved in Stickland reactions such as GDH are favored (Poquet *et al.*, 2018; Dubois *et al.*, 2019; Tremblay *et al.*, 2021). Intracellularly, GDH may play an important role in the metabolic shift that underlies biofilm-formation

in DOC-induced biofilms. Although the role of extracellular GDH is unclear, we have shown that in the biofilm-matrix this enzyme is mostly present in an enzymatically inactive form. It follows that its role is not catalytic.

Heterogeneity in gene expression within the cell population is a common characteristic in biofilms (Nadell, Drescher and Foster, 2016; Arnaouteli *et al.*, 2021). This phenotypic and genetic diversity is observed due to the presence of chemical and nutrient gradients within the biofilm. This phenomenon, known as divison of labour, has been well described in several species and allows specialization of different tasks during cooperative or competitive interactions (Meza-Torres *et al*., 2021). In *B. subtillis* the phenotypic segregation of three subpoulations composed of matrix-non-producers, EPSs producers and producers of EPSs and TasA, has been well-described and allows maximum group productivity (Dragoš *et al.*, 2018). In *C. difficile* there are currently no studies regarding the differential expression of biofilm-matrix proteins. In this sense, it would be interesting to assess whether there is a differential expression or secretion of GDH in the biofilm and if this expression is somehow coordinated in time and space.

The wild-type protein and the catalytic inactive form of GDH (D147S, **Figure 10**), were overproduced as a fusion to a C-terminal His_6-tag in *E. coli* BL21 and purified. Zymogram assays confirmed the His_6-GDH to be enzymatically active and His_6-GDH^{D147S} a catalytic inactive form of GDH (**Figure 11A**). Extracellular complementation assays were performed by growing wild-type and *gluD* mutant biofilms for 48h in the presence of purified His_6-GDH or His_6-GDH^{D147S} (**Figure 11D**). Our results reveal that the addition of both purified forms of GDH significatively increased biofilm formation by the *gluD* mutant, partially restoring the wild-type biofilm phenotype. Even though complementation with His_6-GDH achieved increased values of biofilm formation in the *gluD* mutant, it appears that when present in the extracellular medium, both catalytic active and inactive forms of GDH contribute to the increase in biofilm formation. Interestingly, in the wild-type strain the addition of both forms of purified GDH did not enhance biofilm production. These results suggest that the presence of extracellular GDH during biofilm formation in the *gluD* mutant strain compensates for the absence of *gluD* expression. Moreover, the fact that phenotype restoration was achieved with the extracellular presence of GDH suggests that an important role for GDH during biofilm-

formation is dependent on the presence of this enzyme in the extracellular medium, most likely through the incorporation of this enzyme in the biofilm-matrix. This would explain the increase biofilm production in *gluD* mutant strain and the absence of effect in the wild-type strain.

Zymogram assays performed on non-SDS PAGE gels either with the cellular and biofilm-matrix extracts or with purified His_6-GDH showed the presence of a band of approximately 150 kDa. This size corresponds to a trimer, the minimal active form of the enzyme (Bolivar *et al.*, 2008). However, *C. difficile* and other bacterial GDHs were described as hexameric (Anderson *et al.*, 1993; Oliveira *et al.*, 2012). By resolving purified His_6-GDH and His_6-GDH^{D147S} in a Clear-Native PAGE in which the proteins are separated according to their size only, we were able to confirm the oligomeric state of GDH (**Figure 11B**). We concluded that both wild-type and catalytic inactive forms of GDH behave as hexamers (~295 kDa) but also exhibit other higher molecular weight forms. For the wild-type protein, both the hexamer and the higher order structures are catalytically active. Negative stain TEM imagens of purified His_6-GDH showed the presence of monodisperse particles with doughnut-shaped structures, which might correspond to the hexameric structure (**Figure 11C**). While we have revealed GDH to behave as a hexamer it is still unknown which forms of the protein are present in the biofilm-matrix. Future work involves resolution of the biofilm-matrix in Clear-Native PAGE gels in order to elucidate what structures are present in the biofilm-matrix. Since at high concentrations of GDH we were able to see high molecular forms, it would be interesting to know whether these structures could be present in the biofilm-matrix.

Fiber-forming proteins have been described to provide structural integrity in the biofilm of many bacterial species. Most of these fiber-forming can be defined as functional amyloid fibers in the context of the biofilm matrix (Erskine, MacPhee and Stanley-Wall, 2018). Some of these proteins possess specific machineries to control the expression, secretion and polymerization of subunits into amyloid fibers outside the cell such, an example of which is the well-known TasA fibers formed by *B. subtillis*, curli fibers of *E. coli* or Fap fibers in *Pseudomonas* sp. (Gophna *et al.*, 2001; Dueholm *et al.*, 2010; Romero *et al.*, 2010; Taglialegna, Lasa and Valle, 2016). Other amyloid structures are only built upon exposure to specific environmental triggers. An example of such

mechanism is the Bap fibers formed by *S. aureus.* The formation of Bap occurs when, after secretion, Bap is proteolytically processed resulting in N-terminal fragments that in the presence of acidic pH and low concentrations of calcium adopt a β-sheet-rich form that self-assembles into amyloid-like structures (Taglialegna *et al.*, 2016; Taglialegna, Lasa and Valle, 2016). While in TasA or Fap fibers polymerization is dependent on other proteins that act as fibrillation nucleators, recent studies revealed that in curli fibers eDNA, largely present in the biofilm matrix, can induce amyloid polymerization (Gallo *et al.*, 2015).

Enzyme filamentation has also been described in several enzymes and it can serve different purposes such as structural functions or even to regulate enzymatic activity (O'Connell *et al.*, 2012; Park and Horton, 2019). Interestingly, bovine-liver GDH has shown to form linear polymers that assemble into a helical structure upon binding of leucin, ADP, succinyl-coA or BCH to the allosteric sites (Josephs, 1970; Josephs and Borisy, 1972; Park and Horton, 2019). The NAD-dependent glutamate dehydrogenase from *Saccharomyces cerevisiae* has also shown to form filaments in *vivo* under nutrient starvation (Shen *et al.*, 2016). Whether *C. difficile* GDH has the ability to form filaments is unknown. While such structures were not observed in negative stain images, we do not know what environmental conditions could trigger filamentation or even if filamentation is dependent on higher protein concentration. Negatively stained GDH was imaged at a 0.2 mg/mL while high order forms could only be detected at 3 mg/mL. Future work involves a more profound study of the oligomeric states of GDH and how these conformations might change upon biofilm environmental conditions such as the acidic pH, and how it impacts on its activity (**Figure 13**).

Another goal of our study was to understand the role of enolase in *C. difficile* biofilms. Enolase is a glycolytic enzyme that catalyzes the dehydration of 2-phosphoglycerate to phosphoenolpyruvate. This enzyme is an abundant cytoplasmic protein that has other moonlight functions at the cell-surface (Paludo *et al.*, 2015). Enolase has been shown to function as an adhesin in many bacterial species; it binds to plasminogen, fibronectin, mucins and other proteins important in the development of infection (Henderson and Martin, 2011; C. Jeffery, 2018; C. J. Jeffery, 2018). In *S. aureus* enolase was recently shown to be present in the biofilm matrix and it was suggested that

it assembles at the cell-surface to form the extracellular matrix in a pH-dependent manner (Foulston *et al*., 2014). While the role of enolase in *S. aureus* biofilm is unknown, this enzyme was also shown to be present in the biofilm-matrix in *Candida albicans*. Moreover, in *C. albicans* extracellular enolase mediates the colonization of the small intestine mucosa (Silva *et al.,* 2014). These findings let us to choose enolase as an interesting target for study in the context of biofilm formation in *C. difficile*. The study of the role of enolase in the biofilm is complicated by the fact that *eno*, the enolase encoding gene, is essential and knock-out mutants are therefore impossible to create (Dembek *et al.*, 2015). In the present work we constructed a *C. difficile* conditional mutant strain with the use of a CRISPRi silencing system targeting *eno* (**Figure 12A**). As expected for an essential gene, a strain carrying the CRISPRi plasmid targeting *eno* showed a strong loss of viability in the presence of the Cas9 inducer, while in the absence of xylose the viability was the same as for the control strain (**Figure 12B**). The adhesin properties of other bacterial enolases leads us to hypothesize that this enzyme could have an important role in structuring the biofilm-matrix in *C. difficile*. Unfortunately, due to the lack of time, we weren't able to conclude the investigation of the role of enolase in *C. difficile* biofilms. Future work aims at confirming gene repression by immunoblotting with an anti-enolase antibody and at assessing the role of *eno* repression in biofilm formation. In any case, the development of a *C. difficile* conditional mutant strain for the *eno* gene was a crucial step to study the role of enolase in biofilms and it is, to our knowledge, the first *eno* mutant described for *C. difficile.*

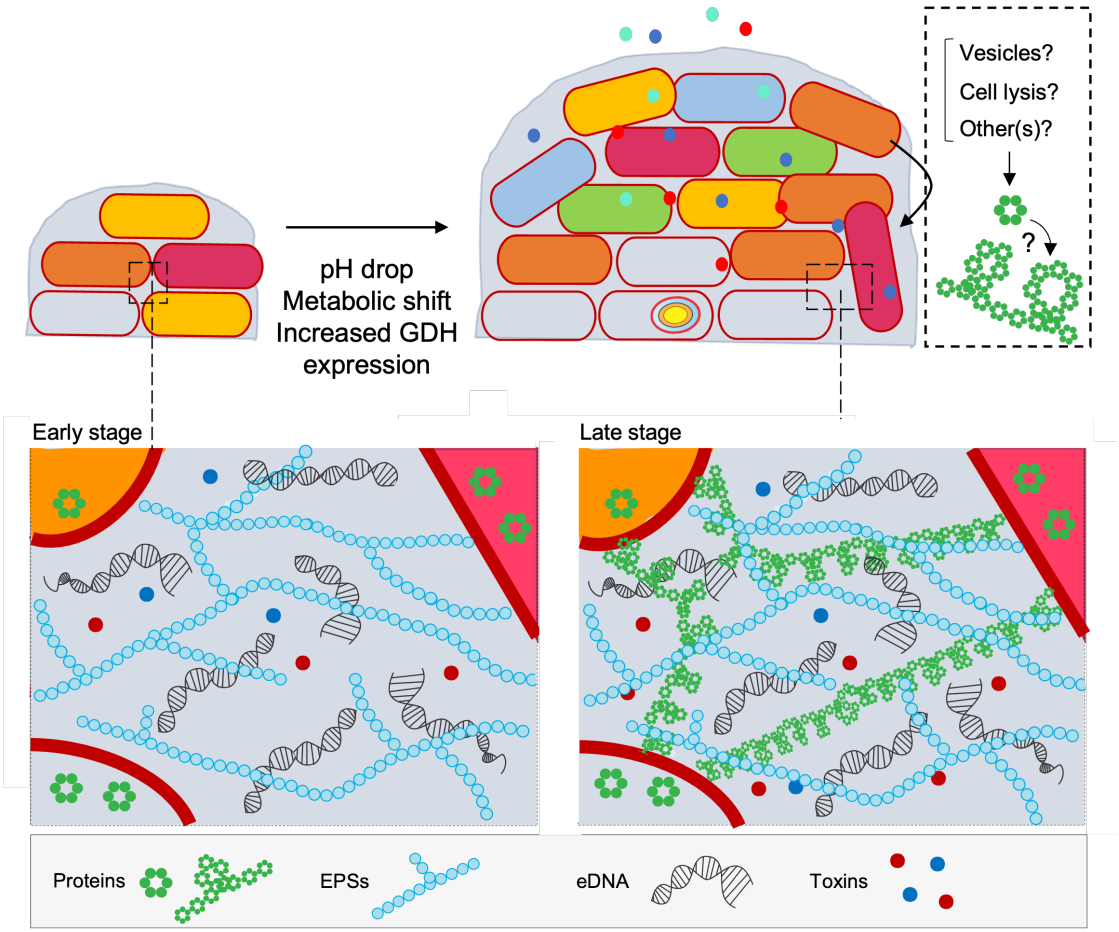

Figure 13. Model of *C. difficile* biofilm-matrix composition and role of biofilm-matrix proteins during biofilm development. The biofilm-matrix is mostly composed of proteins, eDNA, EPSs and in *C. dificile* can harbor toxins. Biofilm formation is accompanied by a drop in pH and characterized by a metabolic rearrangement that leads to the up-regulation of enzymes involved in pathways such as Stickland reactions, such as GDH. GDH is secreted to the extracellular medium through an unknown system which might include cell lysis, versicles or non-classical secretion systems. *C. difficile* GDH is able to form high-order aggregates in higher concentrations and other GDHs have shown to form filaments under specific conditions. The presence of such forms in the biofilm-matrix might be relevant as important structures. Based on previous works, eDNA might have an important role in early stage biofilms while proteins could be crucial in later stages by interacting with eDNA and other matrix components, thus conferring stability to the matrix. Matrix components (proteins, EPSs, eDNA, toxins) are not represented in scale.

In conclusion, our study characterized the biofilm matrix-associated proteins of a strong-biofilm producer clinical isolate from RT126, a livestock-associated ribotype. We report the biofilm matrix to be largely composed of cytoplasmic proteins associated with metabolism. We focused on the role of GDH on the biofilm formed by the reference strain 630. We demonstrated that GDH is present in the biofilm matrix, mostly in a catalytic inactive form and that biofilm formation is impaired in a *gluD* mutant strain. Moreover, extracellular complementation with a wild-type or a catalytic inactive allele of GDH restored the wild-type biofilm ability in the *gluD* mutant strain. We demonstrated that GDH behaves as an hexamer and presents high molecular forms, both of which are

catalytically active. While we weren't able to investigate the role of enolase on *C. difficile* biofilms, we developed a conditional mutant strain of enolase through the construction of a CRISPRi vector for silencing *eno* expression.

Overall, we suggest that rather than having a dedicated set of matrix proteins, *C. difficile* uses cytoplasmic proteins that moonlight at the cell surface to form the extracellular matrix of biofilms (**Figure 13**).

5. References

Abt, M.C., McKenney, P.T. and Pamer, E.G. (2016) '*Clostridium difficile* colitis: Pathogenesis and host defence', *Nature Reviews Microbiology*, 14(10), pp. 609–620.

Aktories, K., Schwan, C. and Jank, T. (2017) '*Clostridium difficile* Toxin Biology', *Annu. Rev. Microbiol*, 71(1), pp. 281–307.

Allegretti, J.R. *et al*. (2016) 'Recurrent *Clostridiu,m difficile* infection associates with distinct bile acid and microbiome profiles', *Alimentary Pharmacology and Therapeutics*, 43(11), pp. 1142–1153.

Amblee, V. and Jeffery, C.J. (2015) 'Physical features of intracellular proteins that moonlight on the cell surface', *PLoS ONE*, 10(6), pp. 1-16.

Ananthakrishnan, A.N. (2011) '*Clostridium difficile* infection: Epidemiology, risk factors and management', *Nature Reviews Gastroenterology and Hepatology*, 8(1), pp. 17–26.

Anderson, B.M. *et al*. (1993) 'Purification and characterization of *Clostridium difficile* glutamate dehydrogenase.', *Archives of Biochemestry and Biophysics*, 300(1), pp. 483–488.

Anjuwon-Foster, B.R. and Tamayo, R. (2017) 'A genetic switch controls the production of flagella and toxins in *Clostridium difficile'*, *PLoS Genetics*, 13(3), pp. 1-33.

Antunes, A. *et al.* (2012) 'Global transcriptional control by glucose andcarbon regulator CcpA in *Clostridium difficile'*, *Nucleic Acids Research*, 40(21), pp. 10701–10718.

Antunes, W. *et al*. (2018) 'Structure and assembly of a *Clostridioides difficile* spore polar appendage', *BioRxiv* [Preprint].

Arnaouteli, S. *et al.* (2021) '*Bacillus subtilis* biofilm formation and social interactions', *Nature Reviews Microbiology*, 19(9), pp. 600–614.

Awad, M.M. *et al*. (2015) '*Clostridium difficile* virulence factors: Insights into an anaerobic spore-forming pathogen', *Gut Microbes*, 5(5), pp. 579–593.

Baban, S.T. *et al.* (2013) 'The Role of Flagella in *Clostridium difficile* Pathogenesis: Comparison between a Non-Epidemic and an Epidemic Strain', *PLoS ONE*, 8(9), pp. 1-12.

Baghani, A. *et al.* (2020) 'High prevalence of *Clostridiodes diffiicle* PCR ribotypes 001 and 126 in Iran', *Scientific Reports*, 10(1), pp. 1-9.

Baktash, A. *et al.* (2018) 'Mechanistic insights in the success of fecal microbiota transplants for the treatment of *Clostridium difficile* infections', *Frontiers in Microbiology*, 9(1), pp. 1-9.

Barnhart, M.M. and Chapman, M.R. (2006) 'Curli biogenesis and function', *Annual Review of Microbiology*, 60(1), pp. 131–147.

Barreto, H.C. *et al.* (2020) 'Rampant loss of social traits during domestication of a Bacillus subtilis natural isolate', *Scientific Reports*, 10(1), pp. 1-16.

Benchling. 2018. Biology software. Benchling, San Francisco, CA

Bendtsen, J.D. *et al.* (2005) 'Non-classical protein secretion in bacteria', *BMC Microbiology*, 5(1), pp. 1-13.

Bolivar, J.M. *et al*. (2008) 'Immobilization-stabilization of a new recombinant glutamate dehydrogenase from *Thermus thermophilus'*, *Applied Microbiology and Biotechnology*, 80(1), pp. 49–58.

Bowen, W.H. *et al*. (2018) 'Oral Biofilms: Pathogens, Matrix, and Polymicrobial Interactions in Microenvironments', *Trends in Microbiology,* 26(3) pp. 229–242.

Brauer, M. *et al.* (2021) 'What's a Biofilm? - How the Choice of the Biofilm Model Impacts the Protein Inventory of *Clostridioides difficile'*, *Frontiers in Microbiology*, 12(1), pp. 1-42.

Brouwer, M.S.M. *et al*. (2013) 'Horizontal gene transfer converts non-toxigenic *Clostridium difficile* strains into toxin producers', *Nature Communications*, 4(1), pp. 1-6.

Brown, L. *et al.* (2017) 'YebC, a putative transcriptional factor involved in the regulation of the proteolytic system of *Lactobacillus*', *Scientific Reports*, 7(1), pp. 1-11.

Cao, Y. and Lin, H. (2021) 'Characterization and function of membrane vesicles in Gram-positive bacteria', *Applied Microbiology and Biotechnolog*y, 105(5), pp. 1795–1801.

Castro-Córdova, P. *et al*. (2021) 'Entry of spores into intestinal epithelial cells contributes to recurrence of *Clostridioides difficile* infection', *Nature Communications*, 12(1), pp. 1-18.

Commichau, F.M. *et al.* (2007) 'A regulatory protein-protein interaction governs glutamate biosynthesis in *Bacillus subtilis*: The glutamate dehydrogenase RocG moonlights in controlling the transcription factor GltC', *Molecular Microbiology*, 65(3), pp. 642–654.

Costerton, J.W., Stewart, P.S. and Greenberg, E.P. (1999) 'Bacterial biofilms: A common cause of persistent infections', *Science*, 284(1), pp. 1318–1322.

Czepiel, J. *et al.* (2019) 'Clostridium difficile infection: review', *European Journal of Clinical Microbiology and Infectious Diseases* , 38(1), pp. 1211-1221.

Dannheim, H. *et al.* (2017) '*Clostridioides difficile* 630Δ*erm* in silico and in vivo – quantitative growth and extensive polysaccharide secretion', *FEBS Open Bio*, 7(4), pp. 602–615.

Dapa, T. *et al.* (2013) 'Multiple factors modulate biofilm formation by the anaerobic pathogen *Clostridium difficile'*, *Journal of Bacteriology*, 195(3), pp. 545–555.

Das, T. *et al.* (2010) 'Role of extracellular DNA in initial bacterial adhesion and surface aggregation', *Applied and Environmental Microbiology*, 76(10), pp. 3405–3408.

Dawson, L.F. *et al.* (2012) 'Characterisation of *Clostridium difficile* Biofilm Formation, a Role for Spo0A', *PLoS ONE*, 7(12), pp. 1-13.

Dawson, L.F. *et al.* (2021) 'Extracellular DNA, cell surface proteins and c-di-GMP promote biofilm formation in *Clostridioides difficile'*, *Scientific Reports*, 11(1), pp. 1-21.

Deakin, L.J. *et al.* (2012) 'The *Clostridium difficile* spo0A gene is a persistence and transmission factor', *Infection and Immunity*, 80(8), pp. 2704–2711.

Dean, J.L.E. *et al.* (1994) 'The catalytic role of aspartate in the active site of glutamate dehydrogenase', *Biochem. J*, 301(1), pp. 13-16.

Dembek, M. *et al.* (2015) 'High-throughput analysis of gene essentiality and sporulation in *Clostridium difficile*', *mBio*, 6(2), pp. 1-13.

Dengler, V. *et al.* (2015) 'An electrostatic net model for the role of extracellular DNA in biofilm formation by *Staphylococcus aureus'*, *Journal of Bacteriology*, 197(24), pp. 3779–3787.

Donelli, G. *et al.* (2012) 'Biofilm-growing intestinal anaerobic bacteria', *FEMS Immunology and Medical Microbiology*, 65(2), pp. 318–325.

Dragoš, A. *et al.* (2018) 'Division of Labor during Biofilm Matrix Production', *Current Biology*, 28(12), pp. 1903-1913.

Dubois, T. *et al.* (2019) 'A microbiota-generated bile salt induces biofilm formation in *Clostridium difficile'*, *npj Biofilms and Microbiomes*, 5(1), pp. 1-12.

Dueholm, M.S. *et al.* (2010) 'Functional amyloid in *pseudomonas*', *Molecular Microbiology*, 77(4), pp. 1009–1020.

Edwards, A.N. and Mcbride, S.M. (2014) 'Initiation of sporulation in *Clostridium difficile*: A twist on the classic model', *FEMS Microbiology Letters*, 358(2), pp. 110–118.

Erskine, E., MacPhee, C.E. and Stanley-Wall, N.R. (2018) 'Functional Amyloid and Other Protein Fibers in the Biofilm Matrix', *Journal of Molecular Biology*, 430(20), pp. 3642–3656.

Escobar-Cortés, K., Barra-Carrasco, J. and Paredes-Sabja, D. (2013) 'Proteases and sonication specifically remove the exosporium layer of spores of *Clostridium difficile* strain', *Journal of Microbiological Methods*, 93(1), pp. 25–31.

Fawley, W.N. *et al.* (2007) 'Efficacy of Hospital Cleaning Agents and Germicides Against Epidemic *Clostridium difficile* Strains ', *Infection Control & Hospital Epidemiology*, 28(8), pp. 920–925.

Feehily, C. and Karatzas, K.A.G. (2013) 'Role of glutamate metabolism in bacterial responses towards acid and other stresses', *Journal of Applied Microbiology*, 114(1), pp. 11–24.

Finn, E., Andersson, F.L. and Madin-Warburton, M. (2021) 'Burden of *Clostridioides difficile* infection (CDI) - a systematic review of the epidemiology of primary and recurrent CDI', *BMC Infectious Diseases*, 21(1), pp. 1-11.

Flemming, H.C. *et al.* (2016) 'Biofilms: An emergent form of bacterial life', *Nature Reviews Microbiology*. Nature Publishing Group, 14(9), pp. 563–575.

Flemming, H.C. and Wingender, J. (2010) 'The biofilm matrix', *Nature Reviews Microbiology*, 8(9), pp. 623–633.

Foulston, L. *et al.* (2014) 'The extracellular matrix of *Staphylococcus aureus* biofilms comprises cytoplasmic proteins that associate with the cell surface in response to decreasing pH', *mBio*, 5(5), pp. 1-9.

Gallo, P.M. *et al.* (2015) 'Amyloid-DNA Composites of Bacterial Biofilms Stimulate Autoimmunity', *Immunity*, 42(6), pp. 1171–1184.

Gateau, C. *et al.* (2018) 'How to: diagnose infection caused by *Clostridium difficile'*, *Clinical Microbiology and Infection*, 24(5), pp. 463–468.

Girinathan, B.P. *et al.* (2016) 'Importance of glutamate dehydrogenase (GDH) in clostridium difficile colonization in vivo', *PLoS ONE*, 11(7), pp. 1-18.

Girinathan, B.P., Braun, S.E. and Govind, R. (2014) 'Clostridium difficile glutamate dehydrogenase is a secreted enzyme that confers resistance to H2O2', *Microbiology*, 160(1), pp. 47–55.

Gonzalez-Orta, M. *et al.* (2019) 'Are Many Patients Diagnosed with Healthcare-associated Clostridioides difficile Infections Colonized with the Infecting Strain on Admission?', *Clinical Infectious Diseases*, 69(10), pp. 1801–1804.

Gophna, U. *et al.* (2001) 'Curli fibers mediate internalization of Escherichia coli by eukaryotic cells', *Infection and Immunity*, 69(4), pp. 2659–2665.

Govind, R. and Dupuy, B. (2012) 'Secretion of Clostridium difficile toxins A and B requires the holin-like protein tcdE', *PLoS Pathogens*, 8(6), pp. 1-14.

Graf, A.C. *et al.* (2019) 'Virulence factors produced by staphylococcus aureus biofilms have a moonlighting function contributing to biofilm integrity', *Molecular and Cellular Proteomics*, 18(6), pp. 1036–1053.

Guery, B., Galperine, T. and Barbut, F. (2019) 'Clostridioides difficile: Diagnosis and treatments', *The BMJ*, 366(1), pp. 1-19.

Gupta, A. and Ananthakrishnan, A.N. (2021) 'Economic burden and cost-effectiveness of therapies for Clostridiodes difficile infection: a narrative review', *Therapeutic Advances in Gastroenterology*, 14(1), pp. 1-13.

Hall, I. C., & O'Toole, E. (1935). 'Intestinal flora in new-born infants with a description of a new pathogenic anaerobe, *bacillus difficilis*', *American Journal of Diseases of Children*, 1(1), pp. 390-402.

Heilmann, C. *et al.* (2005) 'The multifunctional *Staphylococcus aureus* autolysin Aaa mediates adherence to immobilized fibrinogen and fibronectin', *Infection and Immunity*, 73(8), pp. 4793–4802.

Henderson, B. and Martin, A. (2011) 'Bacterial virulence in the moonlight: Multitasking bacterial moonlighting proteins are virulence determinants in infectious disease', *Infection and Immunity*, 79(9), pp. 3476–3491.

Hennequin, C. *et al.* (2001) 'GroEL (Hsp60) of *Clostridium difficile* is involved in cell adherence*'*, *Microbiology*, 147(1), pp. 87-96.

Henriques, A.O. and Moran, C.P. (2007) 'Structure, assembly, and function of the spore surface layers', *Annual Review of Microbiology*, 61(1), pp. 555–588.

Høiby, N. *et al.* (2011) 'The clinical impact of bacterial biofilms', in *International Journal of Oral Science*, 3(1), pp. 55–65.

Hunt, J.J. and Ballard, J.D. (2013) 'Variations in Virulence and Molecular Biology among Emerging Strains *of Clostridium difficile'*, *Microbiology and Molecular Biology Reviews*, 77(4), pp. 567–581.

Ibáñez de Aldecoa, A.L., Zafra, O. and González-Pastor, J.E. (2017) 'Mechanisms and regulation of extracellular DNA release and its biological roles in microbial communities', *Frontiers in Microbiology*, 8(1), pp. 1-19.

Isidro, J. *et al.* (2017) 'Overview of *Clostridium difficile* Infection: Life Cycle, Epidemiology, Antimicrobial Resistance and Treatment', in *Clostridium Difficile - A Comprehensive Overview*. InTech.

Janoir, C. *et al.* (2007) 'Cwp84, a surface-associated protein of Clostridium difficile, is a cysteine protease with degrading activity on extracellular matrix proteins', *Journal of Bacteriology*, 189(20), pp. 7174–7180.

Janoir, C. (2016) 'Virulence factors of *Clostridium difficile* and their role during infection', *Anaerobe*, 37(1), pp. 13–24.

Jayaraman, V. *et al.* (2021) 'A counter-enzyme complex regulates glutamate metabolism in *Bacillus subtilis'*, *bioRxiv* [Preprint].

Jeffery, C. (2018) 'Intracellular proteins moonlighting as bacterial adhesion factors', *AIMS Microbiology*, 4(2), pp. 362–376.

Jeffery, C.J. (2003) 'Multifunctional proteins: Examples of gene sharing', *Annals of Medicine*, 35(1), pp. 28–35.

Jeffery, C.J. (2018) 'Protein moonlighting: What is it, and why is it important?', *Philosophical Transactions of the Royal Society B: Biological Sciences,* 373(1), pp. 1-8.

Johnson, S. *et al.* (2021) 'Clinical Practice Guideline by the Infectious Diseases Society of America (IDSA) and Society for Healthcare Epidemiology of America (SHEA): 2021 Focused Update Guidelines on Management of *Clostridioides difficile* Infection in Adults', *Clinical infectious diseases: an official publication of the Infectious Diseases Society of America*, 73(5), pp. 1029–1044.

Josephs, R. (1970) 'Electron Microscope Studies on Glutamic Dehydrogenase : Subunit Structure of Individual Molecules and Linear Associates', *J. Mol. Bio*, 55(1), pp. 147–153.

Josephs, R. and Borisy, G. (1972) 'Self-assembly of Glutamic Dehydrogenase into Ordered Superstructures: Multichain Tubes Formed by Association of Single Molecules', *J. Mol. Biol.*, 65(1), pp. 127–155.

Karasawa, T., Ikoma, S., Yamakawa, K., Ichi, S., & Kamura, N. (1995). 'A defined growth medium for Clostridium difficile', *Microbiology*, 141(1), pp. 371-375.

Karygianni, L. *et al.* (2020) 'Biofilm Matrixome: Extracellular Components in Structured Microbial Communities', *Trends in Microbiology*, 28(8), pp. 668–681.

Kavanaugh, J.S. *et al.* (2019) 'Identification of extracellular DNA-binding proteins in the biofilm matrix', *mBio*, 10(3), pp. 1-30.

Kelly, C.R. *et al.* (2021) 'ACG Clinical Guidelines: Prevention, Diagnosis, and Treatment of *Clostridioides difficile* Infections', *The American journal of gastroenterology*, 116(6), pp. 1124–1147.

Kim, H.J. *et al.* (2008) 'Defined spatial structure stabilizes a synthetic multispecies bacterial community', *Proceedings of the National Academy of Sciences of the United States of America*, 105(47), pp. 18188–18193.

Krutova, M. *et al.* (2018) 'The emergence of *Clostridium difficile* PCR ribotype 078 in piglets in the Czech Republic clusters with *Clostridium difficile* PCR ribotype 078 isolates from Germany, Japan and Taiwan', *International Journal of Medical Microbiology*, 308(7), pp. 770–775.

Kuehne, S.A. *et al.* (2010) 'The role of toxin A and toxin B in *Clostridium difficile* infection', *Nature*, 467(1), pp. 711–713.

Lanis, J.M. *et al.* (2013) '*Clostridium difficile* 027/BI/NAP1 Encodes a Hypertoxic and Antigenically Variable Form of TcdB', *PLoS Pathogens*, 9(8), pp. 1-11.

Larson, H., Prince, A. and Borriello, S. (1978) '*Clostridium difficile* and the aetiology of pseudomembranous colitis', 1(1), pp. 1063-1066.

Lawson, P.A. *et al.* (2016) 'Reclassification *of Clostridium difficile* as Clostridioides difficile (Hall and O'Toole 1935) Prévot 1938', *Anaerobe*, 40(1), pp. 95–99.

Lewis, K. (2010) 'Persister cells', *Annual Review of Microbiology*, 64, pp. 357–372.

Li, W. *et al.* (2020) 'Insights Into the Role of Extracellular DNA and Extracellular Proteins in Biofilm Formation of *Vibrio parahaemolyticus'*, *Frontiers in Microbiology*, 11(1), pp. 1-14.

Li, Y.H. and Tian, X. (2012) 'Quorum sensing and bacterial social interactions in biofilms', *Sensors*, 12(3), pp. 2519–2538.

Lim, S.C., Knight, D.R. and Riley, T. v. (2020) '*Clostridium difficile* and One Health', *Clinical Microbiology and Infection*, 26(7), pp. 857–863.

Lister, J.L. and Horswill, A.R. (2014) 'Staphylococcus aureus biofilms: Recent developments in biofilm dispersal', *Frontiers in Cellular and Infection Microbiology*, 4(1), pp. 1-9.

Louro, M. (2020) Characterization of biofilm formation in clinical isolates of *Clostridioides difficile*. I*TQB-NOVA.*

Louro, M. (2021) Characterization of *Clostridioides difficile biofilm*. *ITQB-NOVA.*

Mackin, K.E. *et al.* (2013) 'Spo0A differentially regulates toxin production in evolutionarily diverse strains of *Clostridium difficile'*, *PLoS ONE*, 8(11), pp. 1-16.

Maldarelli, G.A. *et al.* (2016) 'Type IV pili promote early biofilm formation by *Clostridium difficile'*, *Pathogens and Disease*, 74(6), pp. 1-10.

Mann, E.E. *et al.* (2009) 'Modulation of eDNA release and degradation affects *Staphylococcus aureus* biofilm maturation', *PLoS ONE*, 4(6), pp. 1-12.

Martin, J.S.H., Monaghan, T.M. and Wilcox, M.H. (2016) '*Clostridium difficile* infection: Epidemiology, diagnosis and understanding transmission', *Nature Reviews Gastroenterology and Hepatology*, 13(4), pp. 206–216.

Martínez-Meléndez, A. *et al.* (2022) 'An Update on *Clostridioides difficile* Binary Toxin', *Toxins*, 14(5), pp. 1-13.

Matamouros, S., England, P. and Dupuy, B. (2007) '*Clostridium difficile* toxin expression is inhibited by the novel regulator TcdC', *Molecular Microbiology*, 64(5), pp. 1274–1288.

Mckee, R.W. *et al.* (2018) 'Type IV Pili Promote *Clostridium difficile* Adherence and Persistence in a Mouse Model of Infection', *Infection and Immunity*, 86(5), pp. 1–13.

Mclean, J.E. *et al.* (2004) 'Inosine 5-monophosphate dehydrogenase binds nucleic acids *in vitro* and *in vivo'*, *Biochem. J*, 379(1), pp. 243-251.

McLoon, A.L. *et al.* (2011) 'Tracing the domestication of a biofilm-forming bacterium', *Journal of Bacteriology*, 193(8), pp. 2027–2034.

Mehner-Breitfeld, D. *et al.* (2018) 'Evidence for an adaptation of a phage-derived holin/endolysin system to toxin transport in *Clostridioides difficile'*, *Frontiers in Microbiology*, 9(1), pp. 1-12.

El Meouche, I. *et al.* (2013) 'Characterization of the SigD regulon of *C. difficile* and its positive control of toxin production through the regulation of tcdR', *PLoS ONE*, 8(12), pp. 1-17.

Meza-Torres, J. *et al.* (2021) 'Wolf in sheep's clothing: *Clostridioides difficile* biofilm as a reservoir for recurrent infections', *Microorganisms,* 9(9), pp. 1-35.

Modun, B. and Williams, P. (1999) 'The Staphylococcal Transferrin-Binding Protein Is a Cell Wall Glyceraldehyde-3-Phosphate Dehydrogenase', *Infection and Immunity*, 67(1), pp. 1086-1092.

Motta, J.P. *et al.* (2021) 'Gastrointestinal biofilms in health and disease', *Nature Reviews Gastroenterology and Hepatology*, 18(5), pp. 314–334.

Müh, U. *et al.* (2019) 'A Xylose-Inducible Expression System and a CRISPR Interference Plasmid for Targeted Knockdown of Gene Expression in *Clostridioides difficile*', *Journal of Bacteriology*, 201(14), pp. 1–12.

Mullany, P., Allan, E. and Roberts, A.P. (2015) 'Mobile genetic elements in *Clostridium difficile* and their role in genome function', *Research in Microbiology*, 166(4), pp. 361–367.

Munteanu, B., Braun, M. and Boonrod, K. (2012) 'Improvement of PCR reaction conditions for site-directed mutagenesis of big plasmids', *Journal of Zhejiang University: Science B*, 13(4), pp. 244–247.

Nadell, C.D., Drescher, K. and Foster, K.R. (2016) 'Spatial structure, cooperation and competition in biofilms', *Nature Reviews Microbiology*, 589(14), pp. 1-12.

Nazareth, C. *et al.* (2022) 'Epidemiology of *Clostridioides difficile* Infection in Portugal: A Retrospective, Observational Study of Hospitalized Patients', *Acta Medica Portuguesa*, 35(4), pp. 270–278.

Neumann-Schaal, M., Jahn, D. and Schmidt-Hohagen, K. (2019) 'Metabolism the difficile way: The key to the success of the pathogen *Clostridioides difficile'*, *Frontiers in Microbiology*, 10(1), pp. 1-9.

Ng, Y.K. *et al.* (2013) 'Expanding the Repertoire of Gene Tools for Precise Manipulation of the *Clostridium difficile* Genome: Allelic Exchange Using pyrE Alleles', *PLoS ONE*, 8(2), pp. 1-13.

Nobile, C.J. and Johnson, A.D. (2015) '*Candida albicans* Biofilms and Human Disease', *Annual Review of Microbiology*, 69(1), pp. 71–92.

Normington, C. *et al.* (2021) 'Biofilms harbour *Clostridioides difficile*, serving as a reservoir for recurrent infection', *npj Biofilms and Microbiomes*, 7(1), pp. 1-10.

O'Connell, J.D. *et al.* (2012) 'Dynamic reorganization of metabolic enzymes into intracellular bodies', *Annual Review of Cell and Developmental Biology*, 28(1), pp. 89–111.

Oliveira, T. *et al.* (2012) 'Crystal structure of NAD +-dependent *Peptoniphilus asaccharolyticus* glutamate dehydrogenase reveals determinants of cofactor specificity', *Journal of Structural Biology*, 177(2), pp. 543–552.

Olling, A. *et al.* (2012) 'Release of TcdA and TcdB from *Clostridium difficile* cdi 630 is not affected by functional inactivation of the tcdE gene', *Microbial Pathogenesis*, 52(1), pp. 92–100.

Paiva, A.M.O. *et al.* (2020) 'The C-terminal domain of *Clostridioides difficile* TcdC is exposed on the bacterial cell surface', *Journal of Bacteriology*, 202(22), pp. 1-37.

Paludo, G.P. *et al.* (2015) 'Systems biology approach reveals possible evolutionarily conserved moonlighting functions for enolase', *Computational Biology and Chemistry*, 58(1), pp. 1–8.

Paredes-Sabja, D. *et al.* (2012) '*Clostridium difficile* spore-macrophage interactions: Spore survival', *PLoS ONE*, 7(8), pp. 1-14.

Paredes-Sabja, D., Shen, A. and Sorg, J.A. (2014) '*Clostridium difficile* spore biology: Sporulation, germination, and spore structural proteins', *Trends in Microbiology*, 22(7), pp. 406–416.

Park, C.K. and Horton, N.C. (2019) 'Structures, functions, and mechanisms of filament forming enzymes: a renaissance of enzyme filamentation', *Biophysical Reviews*. Springer, 11(6), pp. 927–994.

Peng, N. *et al.* (2020) 'The exopolysaccharide-eDNA interaction modulates 3D architecture of *Bacillus subtilis* biofilm', *BMC Microbiology*, 20(1), pp. 1-12.

Percival, S.L. *et al.* (2011) 'Introduction to Biofilms', in *Biofilms and Veterinary Medicine*, 6(1), pp. 41–68.

Pereira, F.C. *et al.* (2013) 'The Spore Differentiation Pathway in the Enteric Pathogen *Clostridium difficile'*, *PLoS Genetics*, 9(10), pp. 1-19.

Pettit, L.J. *et al.* (2014) 'Functional genomics reveals that *Clostridium difficile* Spo0A coordinates sporulation, virulence and metabolism', *BMC Genomics*, 15(1), pp. 1-15.

Pizarro-Guajardo, M. *et al.* (2016) 'Ultrastructural variability of the exosporium layer of *Clostridium difficile* spores', *Applied and Environmental Microbiology*, 82(7), pp. 2202–2209.

Pizarro-Guajardo, M. *et al.* (2020) 'Characterization of Exosporium Layer Variability of *Clostridioides difficile* Spores in the Epidemically Relevant Strain R20291', *Frontiers in Microbiology*, 11(1), pp. 1-10.

Pizarro-Guajardo, M., Calderón-Romero, P. and Paredes-Sabja, D. (2016) 'Ultrastructural variability of the exosporium layer of *Clostridium difficile* spores from Sporulating Cultures and Biofilms', *Applied and Environmental Microbiology*, 82(19), pp. 5892–5898.

Plácido, D. *et al.* (2008) 'Auto-induction and purification of a *Bacillus subtilis* transglutaminase (Tgl) and its preliminary crystallographic characterization', *Protein Expression and Purification*, 59(1), pp. 1–8.

Poquet, I. *et al.* (2018) '*Clostridium difficile* Biofilm: Remodeling metabolism and cell surface to build a sparse and heterogeneously aggregated architecture', *Frontiers in Microbiology*, 9(1), pp. 1-20.

Purdy, D.,T. A. *et al.* (2002). 'Conjugative transfer of clostridial shuttle vectors from *Escherichia coli* to *Clostridium difficile* through circumvention of the restriction barrier', *Molecular Microbiology*, 46(2), pp. 439-52.

Putnam, E.E. *et al.* (2013) 'SpoIVA and sipl are *Clostridium difficile* spore morphogenetic proteins', *Journal of Bacteriology*, 195(6), pp. 1214–1225.

Rabin, N. *et al.* (2015) 'Biofilm formation mechanisms and targets for developing antibiofilm agents', *Future Medicinal Chemistry*, 7(4), pp. 493–512.

Rahmoun, L.A., Azrad, M. and Peretz, A. (2021) 'Antibiotic Resistance and Biofilm Production Capacity in *Clostridioides difficile'*, *Frontiers in Cellular and Infection Microbiology*, 11(1), pp. 1-10.

Ramos-Silva, P., Serrano, M. and Henriques, A.O. (2019) 'From Root to Tips: Sporulation Evolution and Specialization in *Bacillus subtilis* and the Intestinal Pathogen *Clostridioides difficile'*, *Molecular Biology and Evolution*, 36(12), pp. 2714–2736.

Recchi, C. *et al.* (2002) 'Signal-sequence-independent secretion of the staphylococcal nuclease in *Mycobacterium smegmatis*', *Microbiology*, 148(1), pp. 592-536

Rodriguez, C. *et al.* (2016) 'Clostridium difficile infection: Early history, diagnosis and molecular strain typing methods', *Microbial Pathogenesis*, 97(1), pp. 59–78.

Romero, D. *et al.* (2010) 'Amyloid fibers provide structural integrity *to Bacillus subtilis biofilms'*, *Proceedings of the National Academy of Sciences of the United States of America*, 107(5), pp. 2230–2234.

Roxas, B.A.P. *et al.* (2020) 'Phylogenomic analysis of *Clostridioides difficile* ribotype 106 strains reveals novel genetic islands and emergent phenotypes', *Scientific Reports*, 10(1), pp. 1-17.

Rupnik, M., Wilcox, M.H. and Gerding, D.N. (2009) '*Clostridium difficile* infection: New developments in epidemiology and pathogenesis', *Nature Reviews Microbiology*, 7(7), pp. 526–536.

Sangavai, C. and Chellapandi, P. (2017) 'Amino acid catabolism-directed biofuel production in *Clostridium sticklandii*: An insight into model-driven systems engineering', *Biotechnology Reports*, 16(1), pp. 32–43.

Santos, A. *et al.* (2016) 'Molecular and epidemiologic study of *Clostridium difficile* reveals unusual heterogeneity in clinical strains circulating in different regions in Portugal', *Clinical Microbiology and Infection*, 22(8), pp. 695–700.

Saujet, L. *et al.* (2013) 'Genome-Wide Analysis of Cell Type-Specific Gene Transcription during Spore Formation in *Clostridium difficile'*, *PLoS Genetics*, 9(10), pp. 1-28.

Schwan, C. *et al.* (2009) '*Clostridium difficile* toxin CDT induces formation of microtubule-based protrusions and increases adherence of bacteria', *PLoS Pathogens*, 5(10), pp. 1-14.

Semenyuk, E.G. *et al.* (2014) 'Spore formation and toxin production in *Clostridium difficile* biofilms', *PLoS ONE*, 9(1), pp. 1-14.

Semenyuk, E.G. *et al.* (2015) 'Analysis of bacterial communities during *Clostridium difficile* infection in the mouse', *Infection and Immunity*, 83(11), pp. 4383–4391.

Serrano, M. *et al.* (2016) 'A Recombination Directionality Factor Controls the Cell Type-Specific Activation of σK and the Fidelity of Spore Development in *Clostridium difficile*', *PLoS Genetics*, 12(9), pp. 1-34.

Shen, A. (2015) 'A Gut Odyssey: The Impact of the Microbiota on *Clostridium difficile* Spore Formation and Germination', *PLoS Pathogens*, 11(10), pp. 1-7.

Shen, Q.J. *et al.* (2016) 'Filamentation of Metabolic Enzymes in *Saccharomyces cerevisiae*', *Journal of Genetics and Genomics*, 43(6), pp. 393–404.

Silva, R.C. *et al.* (2014) 'Extracellular enolase of *Candida albicans* is involved in colonization of mammalian intestinal epithelium', *Frontiers in Cellular and Infection Microbiology*, 4(1), pp. 1-9.

Singh, T. *et al.* (2019) ' Updates in Treatment of Recurrent *Clostridium difficile Infection* ', *Journal of Clinical Medicine Research*, 11(7), pp. 465–471.

Slater, R.T. *et al.* (2019) '*Clostridioides difficile* LuxS mediates inter-bacterial interactions within biofilms', *Scientific Reports*, 9(1), pp. 1-15.

Smits, W.K. *et al.* (2016) '*Clostridium difficile* infection', *Nature Reviews Disease Primers*, 2(1), pp. 1–20.

Sonenshein, A. (2000) 'Control of sporulation initiation in *Bacillus subtilis*', *Current opinion in microbiology*, 3(1), pp. 561–566.

Sorg, J. A., & Sonenshein, A. L. (2010). 'Inhibiting the initiation of Clostridium difficile spore germination using analogs of chenodeoxycholic acid, a bile acid' *Journal of Bacteriology*, 192(19), pp. 4983–4990.

Sorg, J.A. and Sonenshein, A.L. (2008) 'Bile salts and glycine as cogerminants for *Clostridium difficile* spores', *Journal of Bacteriology*, 190(7), pp. 2505–2512.

Squire, M.M. and Riley, T. v. (2012) '*Clostridium difficile* Infection in Humans and Piglets: A "One Health" Opportunity', *Current topics in microbiology and immunology*, 365(1), pp. 299–314.

Stewart, P.S. (2002) 'Mechanisms of antibiotic resistance in bacterial biofilms', *Int. J. Med. Microbiol*, 292(1), pp. 107-113.

Taglialegna, A. *et al.* (2016) 'Staphylococcal Bap Proteins Build Amyloid Scaffold Biofilm Matrices in Response to Environmental Signals', *PLoS Pathogens*, 12(6), pp. 1-34.

Taglialegna, A., Lasa, I. and Valle, J. (2016) 'Amyloid structures as biofilm matrix scaffolds', *Journal of Bacteriology*, 198(19), pp. 2579–2588.

Tasteyre, A. *et al.* (2001) 'Role of FliC and FliD flagellar proteins of *Clostridium difficile* in adherence and gut colonization', *Infection and Immunity*, 69(12), pp. 7937–7940.

Thornton, C.S. *et al.* (2018) 'Epidemiological and genomic characterization of community-acquired Clostridium difficile infections', *BMC Infectious Diseases*, 18(1), pp. 1-9.

Tremblay, Y.D. and Dupuy, B. (2022) 'The blueprint for building a biofilm the *Clostridioides difficile* way', *Current Opinion in Microbiology*, 66(1), pp. 39–45.

Tremblay, Y.D.N. *et al.* (2021) 'Metabolic adaption to extracellular pyruvate triggers biofilm formation in *Clostridioides difficile'*, *ISME Journal*, 15(12), pp. 3623–3635.

Tsai, B.Y. *et al.* (2016) 'Zoonotic potential of the Clostridium difficile RT078 family in Taiwan', *Anaerobe*, 41(1), pp. 125–130.

Tunio, S.A. *et al.* (2010) 'The moonlighting protein fructose-1, 6-bisphosphate aldolase of *Neisseria meningitidis*: Surface localization and role in host cell adhesion', *Molecular Microbiology*, 76(3), pp. 605–615.

Turnbull, L. *et al.* (2016) 'Explosive cell lysis as a mechanism for the biogenesis of bacterial membrane vesicles and biofilms', *Nature Communications*, 7(1), pp. 1-13.

Valiente, E., Cairns, M.D. and Wren, B.W. (2014) 'The *Clostridium difficile* PCR ribotype 027 lineage: A pathogen on the move', *Clinical Microbiology and Infection*, 20(5), pp. 396–404.

Vestby, L.K. *et al.* (2020) 'Bacterial biofilm and its role in the pathogenesis of disease', *Antibiotics*, 9(2), pp. 1-29.

de Vos, W.M. (2015) 'Microbial biofilms and the human intestinal microbiome', *npj Biofilms and Microbiomes*, 1(1), pp. 1-3.

Waligora, A.J. *et al.* (2001) 'Characterization of a cell surface protein of *Clostridium difficile* with adhesive properties', *Infection and Immunity*, 69(4), pp. 2144–2153.

Whitchurch, C.B. *et al.* (2002) 'Extracellular DNA Required for Bacterial Biofilm Formation', *Science*, 295P(1), pp. 1487.

Wilson, K.H., Sheagren, J.N. and Freter, R. (1985) 'Population Dynamics of Ingested *Clostridium difficile* in the Gastrointestinal Tract of the Syrian Hamster*'*, *The Journal of Infectious Diseases*, 151(2), pp. 365-361.

Wittig, I., Karas, M. and Schägger, H. (2007) 'High resolution clear native electrophoresis for in-gel functional assays and fluorescence studies of membrane protein complexes', *Molecular and Cellular Proteomics*, 6(7), pp. 1215–1225.

Wydau-Dematteis, S. *et al.* (2018) 'Cwp19 is a novel lytic transglycosylase involved in stationary-phase autolysis resulting in toxin release in *Clostridium difficile*', *mBio*, 9(3), pp. 1-19.

Yang, C.K. *et al.* (2011) 'Nonclassical protein secretion by bacillus subtilis in the stationary phase is not due to cell lysis', *Journal of Bacteriology*, 193(20), pp. 5607–5615.

Yutin, N. and Galperin, M.Y. (2013) 'A genomic update on clostridial phylogeny: Gram-negative spore formers and other misplaced clostridia', *Environmental Microbiology*, 15(10), pp. 2631–2641.

Zhang, L.J. *et al.* (2019) 'The first isolation of *Clostridium difficile* RT078/ ST11 from pigs in China', *PLoS ONE*, 14(2), pp. 1-11.

Zhang, W.Z. *et al.* (2020) 'The molecular characters and antibiotic resistance of *Clostridioides difficile* from economic animals in China', *BMC Microbiology*, 20(1), pp. 1-7.

Zhao, L. *et al.* (2017) 'Multimer recognition and secretion by the non-classical secretion pathway in *Bacillus subtilis'*, *Scientific Reports*, 7(1), pp. 1-18.

Zhu, D., Sorg, J.A. and Sun, X. (2018) '*Clostridioides difficile* biology: Sporulation, germination, and corresponding therapies for *C. difficile* infection', *Frontiers in Cellular and Infection Microbiology*, 8(1), pp. 1-10.

References

6. Appendix

Appendix 1. Bacterial strains used in this study

Strains	Relevant properties	Origin/Reference
E. coli		
DH5α	F– Φ80l*acZ*ΔM15 Δ(*lacZYAargF*) *U169 recA1 endA1 hsdR17* (rK–, mK+) *phoA supE44 λ– thi-1 gyrA96 relA1*	Bethesda Research laboratories
HB101	*supE44 aa14 galK2 lacY1 D(gpt-proA)* 62 *rpsL20* (StrR) *xyl-5 mtl-1 recA13 Δ*(*mcrC-mrr) hsdSB*(rB-mB-) RP4, $Amp^RKm^RTc^R$	El Meouche *et al., 2013*
BL21	F- *ompT gal dcm Ion hsdSB* (*rB-mB-)* λ (DE3 [*lacI lac UV5-T7p07 ind1 sam7 nin5]*) [*malB*+]K-12 (λS)	Novagen
AHCD207	HB101 (pRP4)/pMTL-YN3, Amp^RCm^R	Laboratory stock
AHCD203	HB101 (pRP4)/pMTL-YN1, Amp^RCm^R	Laboratory stock
AHCD1442	HB101 (pRP4) /pIR2, Amp^RCm^R	This work
AHCD1443	HB101 (pRP4) / pIR3, Amp^RCm^R	“
AHCD1442	HB101 (pRP4) / pIA33, Amp^RCm^R	“
AHCD1444	BL21 (DE3) / pIR4, Amp^R	‘’
AHCD1445	BL21(DE3) / pIR5, Amp^R	‘’
C. difficile		
AHCD1190	630Δ*erm*	Laboratory stock
CD1800	Epidemic strain (RT126) classified as high biofilm producer	Louro, 2021
AHCD772	630Δ*erm*Δ*pyrE*	Heap *et al.,* 2012.
AHCD1772	630Δ*erm*Δ*pyrE*Δ*gluD*	This study
AHCD1773	630Δ*erm*Δ*gluD*	“
AHCD1774	630Δ*erm* pIA33, $Thia^R$	“
AHCD1775	630Δ*erm* pIR3, $Thia^R$	“

Appendix 2. Growth media

Culture Media	Composition (for 100 mL)
LB	1 g tryptone; 0.5 g yeast extract; 0.5 g NaCl (pH 7.0)
BHI	3.7 g BHI (Oxoid)
BHISG-DOC	3.7 g BHI; 300 µL L-cystein hydrochloride (1.27 M); 10 mL of D- glucose (1 M); 240 µL sodium deoxycholate (100 mM)
70:30	6.3 g bactopeptone; 0.35 g protease peptone; 1.11 g BHI; 0.15 g yeast extract; 0.07 g (NH4)2SO4; 0.11 g Tris-base; 0.1 g of L-cystein hydrochloride
CDMM	Amino acids (5x): Casamino acids, 10 mg/mL; L-tryptophan, 0.5 mg/mL; L-cysteine, 0.5 mg/mL
	Salts (10x): Na_2HPO_4, 5 mg/mL; $NaHCO_3$, 5 mg/mL; KH_2PO4, 0.9 mg/mL; NaCl (0.9 mg/mL)
	Glucose (20x): D-glucose, 10 mg/mL
	Trace salts (50x): $(NH_4)SO_4$, 0.04 mg/mL; $CaCl_2H_2O$, 0.026 mg/mL; $MgCl_2.6H_2O$, 0.02 mg/mL; $MnCl_2.4H_2O$, 0.01 mg/mL; $CoCl_2.6H_2O$, 0.001 mg/mL
	Iron (100x): $FeSO4.7H2O$, 0.004 mg/mL
	Vitamins: D- biotin (1000x), 0.001 mg/mL; Calcium D-panthothenate (1000x), 0.001 mg/mL; Pyridoxine (1000x), 0.001 mg/mL
Auto-induction	100 mL LB; 1x 5052; 1x NPS (0.5 M $(NH_4)2SO4$, 1 M KH_2PO_4 , 1 M Na_2HPO_4 , pH 6.75); 1 mM $MgSO_4$

Appendix 3. Solutions used in this work

Solutions	Composition
Coomassie solution	0.5 g/mL Coomassie Brilliant Blue R-250; 80% absolute ethanol; 20% acetic acid
Destaining solution	30% absolute ethanol; 10% acetic acid
Loading buffer 10x	50 mL: Tris-HCl; 7 mL β-mercaptoethanol; 20 g SDS; 0.2 g bromophenol blue; remaining volume made up of glycerol 86%
Non-denaturing loading buffer 10 x	10 mL: 1 M Tris-HCl, pH 6.8; 0.04 g bromophenol blue; remaining volume made up of glycerol 86%
Non-denaturing loading buffer 2x (for Clear-Native PAGE gels)	37 mM Tris; 10% glycerol 86%; 0.05% bromophenol blue;
PBS 10x	137 mM NaCl; 2.7 mM KCl; 4.3 mM Na_2HPO_4; 1.4 mM KH_2PO_4
PBS-Tween	100 mL PBS 1x; 0.01 mL Tween 20
PBS-Tween (blocking solution)	900 µL ddH_2O; 100 µL PBS;1 µL Tween 20
Gel buffer 3x	150 mM BisTris (pH 7)
AB mix	48% Acrylamide; 1.5% Bisacrylamide
Anode buffer 5x	250 mM BisTris
Cathode buffer	50 mM Tricine; 15 mM BisTris; 0.02% DDM; 0.05% DOC (pH 7)
Resolving gel 12.5%	41% distilled water; 25.4% 4x lower Tris buffer; 12.6% bis- acrylamide; 0.1% SDS; 0.1% APS; 0.005% TEMED
Resolving gel 15%	35% distilled water;25% 4x lower Tris buffer; 37.67% bis- acrylamide; 0.1% SDS; 0.1% APS; 0.005% TEMED
Stacking gel	61.2% distilled water; 25.5% 4x upper Tris buffer; 10.2% bis- acrylamide; 0.1%SDS; 0.1% APS; 0.1% TEMED
Stacking gel 3.5% (for non-SDS-polyacrylamide gels)	65% distilled water; 25% 0.5 M Tris, pH 6.8; 8.52% bis-acrylamide; 0.1% APS; 0.1% TEMED
Resolving gel 7.5% (for non-SDS-polyacrylamide gels)	55% distilled water; 25% 1.5 M Tris, pH 8.8; 18.7% bis-acrylamide; 0.1% APS; 0.005% TEMED
Resolving gel 5% (for Clear-Native PAGE gels)	1.592 mL distilled water; 940 µL Gel buffer 3x; 8.5 µL DDM 10%; 280 µL AB Mix; 13 µL APS 10%; 2.5 µL TEMED
Resolving gel 15% (for Clear-Native PAGE gels)	560 mL distilled water; 940 µL Gel buffer 3x; 8.5 µL DDM 10%; 853 µL AB Mix; 464 µL glycerol 87%; 13 µL APS 10%; 2.5 µL TEMED
Stacking gel (for Clear- Native PAGE gels)	870 µL distilled water; 500 µL Gel buffer 3x; 2.3 µL DDM 10%; 125 µL AB Mix; 13 µL APS 10%; 2.5 µL TEMED
Electroblotting buffer (for nitrocellulose membrane)	14.4 g/L glycine; 3.02 g/L Tris base; 10 % EtOH
Electroblotting buffer (for PVDF membrane)	0.192 M glycine; 0.025 M Tris, pH 8.3; 20% methanol (pH 8.3)
French press buffer	10 mM imidazole; 20 mM Phosphate; 1 mM PMSF (pH 7.4)
Start buffer	10 mM imidazole; 20 mM Phosphte; 0.5 M NaCl (pH 7.4)
Tris-glycine buffer 5x	1.5% Tris base; 7.21% Glycine
STET buffer	8% sucrose; 0.5% Triton X-100 (v/v); 50 mM EDTA; 10 mM of Tris-HCl (pH 8.0)
Orange G loading buffer 10x	2-5% ficoll -400; 11 mM EDTA; 3.3 mM Tris-HCl; 0.017% SDS; 0.15% Orange G (pH 8.0)
RF1 buffer	12 mg/mL RbCl; 9.9 mg/mL $MnCl_2$; 11% glycerol; 3% KAcl, pH 7.46 (pH 5.8)
RF2 buffer	1.2 mg/mL RbCl; 8.3 mg/mL $CaCl_2$; 10% glycerol; 2% MOPS 0.5 M (pH 6.8)

Appendix 4. List of plasmids used in this study.

Plasmid	Relevant properties	Origin/Reference
pET-16b	Protein expression vector (Amp^R)	Novagen
pMTL-YN3	Plasmid for mutant construction using ACE, $Thia^R$	Ng *et al.,* 2013
pMTL-YN1	Plasmid Δ*pyrE* reversion ACE, $Thia^R$	"
pIA33	P*xyl*::dCas9-opt P*gdh*::sgRNA-rfp, $Thia^R$	Müh et al., 2019
pIR2	pMTL-YN3 containing homology regions for Δ*gluD* construction, $Thia^R$	This work
pIR3	P*xyl*::dCas9-opt P*gdh*::sgRNA-*eno,* $Thia^R$	"
pIR4	pET-16b carrying *his$_6$-gdh,* Amp^R	"
pIR5	pET-16b carrying *his$_6$-gdh^{D147S},* Amp^R	"

Appendix 5. List of primers used in this study.

Primers	Sequence (5' to 3')*
gluD_151F	CGGGATCCTCAATTGGAAGGGTTTGC
gluD_2069R	ATCTTAGTACCATCCTCCTGACATTTGAAAGC
gluD_2075F	GGATGGTACTAAGATTTACTC
gluD_2691R	CCGCTCGAGCAAACGTATATCTTAACC
gluD_127F	GGTTAATCAAATTGTAGAGAGATTG
gluD_2694R	CAAACATATCTTCTTGCCTTCC
pyrE-vef-Fw	CAATAATTTTATAACATTAACATGG
pyrE-vef-Rev	GTGTTACTTAAAAAATGTAAAT
sgRNA2	GGGTGGCCAGTTTAGCATTTACTCCACCTGTTTTAGAGCTAGAAATAGCA AGTTAAAATAAGGCTAGTCCGTTATCAACTTGAAAAAGTGGCACCGAGT CGGTGC
ReversesgRNA	ATAAGAATGCGGCCGCGCGATCGCATAAAAATAAGAAGCCTGCAAATGC AGGCTTCTTATTTTTATAAAAAAAGCACCGACTCGGTGCCACTTTTTCAA GTTG
pET16b-gdhF	CATGCCATGGTCAGGAAAAGATGTAAATGTC
pET16b-gdhR	CCG CTC GAG TTA ATG ATG ATG ATG ATG ATG GTA CCA TCC TCT TAA TTT CAT AGC
GDHAspSer_F	GACGTTCCTGCACCA**AGC**GTAAATACTAATGGTC
GDHAspSer_R	GACCATTAGTATTTAC**GCT**TGGTGCAGGAACG

*Native or introduced restriction sites are underlined; base substitutions are shown in bold.

Appendix 6. List of identified matrix proteins.

Protein	MW (kDa)	Signal peptide	Moonlight protein
3-hydroxybutyryl-CoA dehydrogenase	30.68	Sec/SPII	
6-phosphofructokinase	34.24	No	×
ABC transporter, substrate-binding protein (cluster 10, nitrate/sulfonate/bicarbonate)	36.38	Sec/SPII	
ABC transporter, substrate-binding protein (cluster 15, trp?)	35.99	Sec/SPII	
Acetaldehyde dehydrogenase / Alcohol dehydrogenase	96.81	No	×
Acetyl-CoA acetyltransferase	40.85	No	
Aspartate aminotransferase (AspB-4)	44.79	No	
ATP-dependent Clp protease, ATP-binding subunit ClpC	91.25	No	
Chaperone protein ClpB (ATP-dependent unfoldase)	97.64	No	
Chaperone protein DnaK	66.55	No	×
D-proline reductase, 45 kDa subunit / D-proline reductase, 23 kDa subunit	67.63	No	
Electron-bifurcating caffeyl-CoA reductase-Etf complex, electron transfer flavoprotein subunit alpha	37.15	No	
Enolase	46.1	No	×
Formate--tetrahydrofolate ligase	59.95	No	
Fructose-bisphosphate aldolase class II	32.91	No	×
Glucose-6-phosphate isomerase	50.85	No	×
Heat shock protein 60 kDa family chaperone GroEL	57.81	No	×
Hydroxyproline dehydratase putative	44.23	No	
hypothetical protein - SlpA	77.22	Sec/SPI	
Inosine-5'-monophosphate dehydrogenase / CBS domain	54.78	No	×
Iron-sulfur cluster assembly protein SufB	33.29	No	
NAD-specific glutamate dehydrogenase	46.02	No	×
Oligopeptide ABC transporter, substrate-binding protein OppA	58.2	Sec/SPII	
Phosphoglycerate kinase	43.03	No	×
Phosphoglycerate mutase	24.42	No	×
Phosphoribosylamine--glycine ligase	45.78	No	
Probable transcriptional regulatory protein YebC	26.03	No	
Pyruvate kinase / Phosphohistidine swiveling domain	63.18	No	×
Pyruvate-flavodoxin oxidoreductase	128.89	No	
Ribonucleotide reductase of class II (coenzyme B12-dependent)	83.36	No	×
Rubrerythrin	20.62	No	
Spermidine/putrescine import ABC transporter ATP-binding protein PotA	39.77	No	
Translation elongation factor Tu	2.52	No	×
Translation elongation factor Tu	24.38	No	×
Translation elongation factor Tu	14.52	No	×
Triosephosphate isomerase	27.21	No	×